BOND BEHAVIOR OF NSM FRP STRIPS IN CONCRETE UNDER SUSTAINED LOADING

Mohamed Reda Ali Elewa Emara

Universitat de Girona

Doctoral Thesis

Bond Behavior of NSM FRP Strips in Concrete under Sustained Loading

Mohamed Reda Ali Elewa Emara

2018

Universitat de Girona

Escola Politècnica Superior

Doctoral Thesis

Bond Behavior of NSM FRP Strips in Concrete under Sustained Loading

Mohamed Reda Ali Elewa Emara

2018

Doctoral Program in Technology

Supervisors

Prof. Lluís Torres Llinàs
University of Girona

Dr. Cristina Barris Peña
University of Girona

Dr. Marta Baena Muñoz
University of Girona

Thesis submitted to the University of Girona in partial fulfillment for the degree of Doctor of Philosophy

Mohamed Reda Ali Elewa Emara

Bond Behavior of NSM FRP Strips in Concrete under Sustained Loading

Doctoral Thesis, 2018

Doctoral Program in Technology

Supervisors: Prof. Lluís Torres Llinàs
Dr. Cristina Barris Peña
Dr. Marta Baena Muñoz

University of Girona

AMADE Research Group

Escola Politècnica Superior

Department of Mechanical Engineering and Industrial Construction

Carrer Universitat de Girona, 4

17003, Girona

IN THE NAME OF ALLAH

To my family; my parents, my wife and my daughters.

Acknowledgement

I would like to express my gratitude to my supervisors, Prof. Lluís Torres Llinàs, Dr. Marta Baena Muñoz and Dr. Cristina Barris Peña, for the indefatigable help and for the key contributions that have allowed the development of the present thesis. I also would like to thank the help received from Prof. Joaquim Barros during my short research stay in the University of Minho, Guimarães, Portugal.

I would also like to acknowledge the support from Marie Curie Initial Training Network, Endure.

Of course, I am grateful to all members of the research group AMADE of the University of Girona for the help and nice moments that I have received from each one.

I would also like to thank my family for the support they provided me through my entire life and in particular, I must acknowledge my parents, my wife and my two daughters for their support.

Funding

The period of research has been funded by the FP7 Marie Curie Actions of the European Commission (FP7-PEOPLE-2013-ITN-Contract 316716).

List of publications

- Emara, M., Torres, L., Baena, M., Barris, C., and Moawad, M., "Effect of sustained loading and environmental conditions on the creep behavior of an epoxy adhesive for concrete structures strengthened with CFRP laminates", Composites Part B: Engineering, vol. 129C (2017), pp. 88-96, https://doi.org/10.1016/j.compositesb.2017.07.026.

- Emara, M., Torres, L., Baena, M., Barris, C., and Cahis, X., "Bond response of NSM CFRP strips in concrete under sustained loading and different temperature and humidity conditions", Composite Structures, vol. 192C (2018), pp. 1-7, https://doi.org/10.1016/j.compstruct.2018.02.048.

- Emara, M., Barris, C., Baena, M., Torres, L., and Barros, J., "Bond behavior of NSM CFRP laminates in concrete under sustained loading", submitted to Construction and Building Materials Journal on 11 November, 2017.

- Emara, M., Torres, L., Barris, C., Baena, M., and Moawad, M., "Bond Behavior of NSM FRP strips in Concrete under Sustained Loading", in the 19th International Conference on Composite Structures (ICCS19), 5-9 September 2016 in Porto, Portugal.

- Emara, M., Torres, L., Baena, M., Barris, C., Moawad, M., and Sevillano, E., "Creep of an epoxy adhesive for Near Surface Mounted Fiber Reinforced Polymers strengthening of Reinforced Concrete beams under different environmental conditions", in the 7th International Conference on Structures (ACHE), A Coruña, Spain, 20-22 June 2017.

- Emara, M, Baena, M, Torres, L, Barris, C, Moawad, M, and Perera, R. Effect of Sustained Load and Environmental Conditions on the Bond between NSM FRP Strips and Concrete, in the 8th International Conference on Advanced Composites in Construction (ACIC), Sheffield, UK, 5-7 September 2017.

- Emara, M., Baena, M., Barris, C., Torres, L., and Moawad, M., 2017. Time-dependent bond behavior between NSM CFRP strips and concrete, in the

Fourth Conference on Smart Monitoring,. Assessment and Rehabilitation of Civil Structures (SMAR). 13-15 September, Zürich, Switzerland.

- Emara, M., Barris, C., Baena, M., Moawad, M., Torres, L., and Perrera, R., Residual capacity of concrete strengthened with NSM CFRP strips subjected to sustained loading, in the 20th International Conference on Composite Structures (ICCS-20), Paris, France, 4-7 September 2017.

Universitat de Girona

To whom it might concern,

Dr. Lluís Torres Llinàs, Professor at the *Universitat de Girona* of the Department of *Enginyeria Mecànica i de la Construcció Industrial*, Dr. Cristina Barris Peña, lecturer at the *Universitat de Girona* of the Department of *Enginyeria Mecànica i de la Construcció Industrial*, and Dr. Marta Baena Muñoz, lecturer at the *Universitat de Girona* of the Department of *Enginyeria Mecànica i de la Construcció Industrial*,

CERTIFY that,
The study entitled *Bond Behavior of NSM FRP Strips in Concrete under Sustained Loading* has been carried out under their supervision by Mohamed Reda Ali Elewa Emara and that it fulfills the requirements to aim for the *International Mention*,

Girona, February2018,

Dr. Lluís Torres Llinàs
Universitat de Girona, Spain

Dr. Cristina Barris Peña
Universitat de Girona, Spain

Dr. Marta Baena Muñoz
Universitat de Girona, Spain

List of Figures

List of Tables

Contents

Abstract

There is a general trend towards the rehabilitation and strengthening of existing Reinforced Concrete (RC) structures to the detriment of projects addressed to new constructions. The use of Fiber Reinforced Polymers (FRP) reinforcement for the rehabilitation and strengthening of RC structures has received considerable attention in the last decades. FRP reinforcement provides several advantages over the traditional steel plates and rebars, such as the high strength-to-weight ratio and corrosion resistance.

The Near-Surface Mounted (NSM) FRP strengthening technique, in which FRP reinforcement is bonded into grooves cut in the concrete cover, has been recently introduced in many projects and has attracted the researchers' attention due to several advantages it provides over the traditional plate bonding (Externally Bonded [EB]) technique with FRP. This interest is justified by the fact that in FRP strengthening of RC structures a proper bond between FRP reinforcement and concrete is a fundamental requirement to ensure the composite action development between both materials and to allow the stress transfer between them during the loading process. Therefore, bond has a major influence on the load carrying capacity as well as on the failure mode of the strengthened member.

A large number of research programs focused on the short-term bond behavior of NSM FRP in concrete have been carried out in the last years. However, the growing interest on NSM FRP technique requires gaining further knowledge also about the long-term behavior of RC strengthened through NSM FRP reinforcement systems, where little work has been done so far. Additionally, materials involved in the NSM strengthening system (concrete, adhesive and FRP) may be vulnerable to time-dependent effects when simultaneously subjected to sustained loading, being epoxy adhesives the most sensitive components, which, in turn can produce a significant effect in the overall behavior of the NSM system over time.

This work has the aim of contributing to a better knowledge, as well as providing reliable data of the long-term bond behavior of the NSM FRP reinforcement systems. To this end, a study on the time-dependent bond-slip response of the NSM Carbon

FRP (CFRP) strips in concrete when subjected to sustained loading and different environmental conditions has been performed.

In this study, two experimental campaigns have been carried out. In the first campaign, four test series have been performed to investigate the tensile creep behavior of epoxy adhesive specimens when subjected to different levels of sustained loading and different temperature and humidity conditions. In the second campaign, the long-term bond behavior, in terms of bond strength and bond-slip response, of NSM CFRP strips in concrete has been investigated, both analytically and experimentally, to further extend the knowledge in this particular research domain. In this respect, five series of single shear pull-out concrete blocks strengthened with NSM CFRP strips subjected to sustained loading have been tested. Different sustained load levels, bonded lengths, groove widths, temperature and humidity levels have been considered. The experimental long-term results of both campaigns have been reported and discussed. In addition, a simplified methodology to analytically simulate the time-dependent bond-slip response of NSM CFRP strips in concrete has been presented. The experimental data have been compared to predictions obtained with the proposed methodology.

Resum

Hi ha una tendència cada vegada més generalitzada cap a la rehabilitació de les estructures existents de formigó armat en detriment dels projectes de noves construccions. És en aquest camp en el que en les últimes dècades ha despertat un especial interès la utilització de Polímers Reforçats amb Fibres (FRP, de l'anglès Fiber Reinforced Polymer), fonamentalment a causa dels avantatges que aquest tipus de reforç ofereix en comparació amb les tradicionals xapes o barres d'acer, entre els que destaquen l'elevada ràtio resistència-pes i la resistència a la corrosió.

Cada vegada són més els projectes que apliquen la tècnica de reforç amb FRP inserits en el recobriment del formigó (NSM, de l'anglès Near-Surface Mounted), així com els treballs d'investigació sobre el tema, com a conseqüència dels seus avantatges en comparació amb el reforç extern (EB, de l'anglès Externally Bonded) amb FRP. L'existència d'un bon comportament adherent entre reforç FRP i formigó és clau per a la utilització amb èxit de les tècniques de reforç. És aquesta adherència l'encarregada de la transmissió d'esforços entre ambdós materials durant el procés de càrrega, i per això es considera que el comportament adherent té una importància vital tant en la capacitat com en el mode de ruptura de l'element reforçat.

Durant els últims anys s'han portat a terme nombrosos treballs d'investigació sobre el comportament adherent instantani dels reforços NSM FRP amb formigó. No obstant això, l'interès creixent sobre la tècnica NSM FRP demana la generació de més coneixement sobre el seu comportament a llarg termini, camp en el que s'han realitzat molt pocs treballs fins al moment. Convé recordar, a més, que els materials involucrats en la tècnica de reforç NSM (formigó, adhesiu i FRP) poden ser vulnerables als efectes diferits quan es troben exposats de manera simultània als efectes de càrregues mantingudes, essent els adhesius epoxídics el component més sensible. Com a conseqüència, el comportament a llarg termini del sistema de reforç NSM FRP es por veure significativament afectat.

El principal objectiu d'aquest treball és el de contribuir a la millora del coneixement del comportament adherent a llarg termini dels sistemes de reforç NSM FRP, així com proporcionar-ne dades experimentals contrastades. Amb aquesta finalitat s'ha realitzat un estudi de la resposta adherència-lliscament a llarg termini de laminats

de NSM FRP de carboni (CFRP) amb formigó sotmesos a càrregues mantingudes i diferents condicions ambientals.

En el present estudi s'han portat a terme dues campanyes experimentals. En la primera s'han realitzat quatre sèries d'assajos per a estudiar la fluència amb càrregues de tracció d'un adhesiu epoxídic sotmès a la combinació de diferents càrregues mantingudes i diferents condicions de temperatura i humitat. En la segona campanya s'ha realitzat un estudi del comportament adherent a llarg termini, en termes de la resposta adherència-lliscament, de laminats NSM CFRP amb formigó, tant a nivell experimental com analític, amb la finalitat d'ampliar en coneixement en aquets camp. En aquest sentit, s'han executat cinc sèries d'assajos de pull-out a tallant simple, amb càrrega mantinguda, en els que el formigó estava reforçat amb làmines de NSM CFRP. Com a paràmetres d'estudi s'han considerat diferents valors de la càrrega mantinguda, longitud adherent, amplada de ranura, temperatura i humitat. Els resultats experimentals a llarg termini d'ambdues campanyes s'han presentat i analitzat, havent-se observat que els canvis en els paràmetres estudiats van tenir un efecte rellevant en la resposta a llarg termini. Addicionalment, s'ha presentat una metodologia simplificada per a la simulació analítica del comportament adherent de la resposta adherència-lliscament a llarg termini dels laminats NSM FRP amb formigó. La metodologia proposada s'ha comprovat mitjançant la comparació de les dades experimentals amb les prediccions obtingudes analíticament.

Resumen

Cada vez es más generalizada la tendencia hacia la rehabilitación y refuerzo de las estructuras existentes de hormigón armado en detrimento de los proyectos de nuevas construcciones. Es en este campo en el que en las últimas décadas ha suscitado un especial interés el uso de refuerzo de Polímeros Reforzados con Fibras (FRP, del inglés Fiber Reinforced Polymer), debido fundamentalmente a las ventajas que este tipo de refuerzo ofrece en comparación con las tradicionales chapas o barras de acero, entre las que cabe destacar su elevada relación resistencia-peso y su resistencia a la corrosión.

Cada vez son más los proyectos que aplican la técnica de refuerzo con FRP inserido en el recubrimiento del hormigón (NSM, del inglés Near-Surface Mounted), así como los trabajos de investigación a este respecto, debido a sus ventajas en comparación con el refuerzo externo (EB, del inglés Externally Bonded) con FRP. La existencia de un buen comportamiento adherente entre refuerzo FRP y hormigón es clave para el exitoso uso de cualquiera de las dos técnicas de refuerzo. Es esta adherencia la encargada de la transmisión de esfuerzos entre ambos materiales durante el proceso de carga, y por ello se considera que el comportamiento adherente tiene vital importancia tanto en la capacidad como en el modo de fallo del elemento reforzado.

Durante los últimos años se han llevado a cabo numerosos trabajos de investigación sobre el comportamiento adherente instantáneo de los refuerzos NSM FRP en hormigón. Sin embargo, el interés creciente sobre la técnica NSM FRP demanda la generación de más conocimiento sobre su comportamiento a largo plazo, campo en el que se han realizado escasos trabajos hasta el momento. Cabe recordar, además, que los materiales involucrados en la técnica de refuerzo NSM (hormigón, adhesivo y FRP) pueden ser vulnerables a los efectos diferidos cuando son expuestos de manera simultánea a cargas mantenidas, siendo los adhesivos epoxi el componente más sensible. Como consecuencia, el comportamiento a largo plazo del sistema de refuerzo NSM FRP se puede ver significativamente afectado.

El principal objetivo de este trabajo es el de contribuir a un mejor conocimiento del comportamiento adherente a largo plazo de los sistemas de refuerzo NSM FRP, así

como proporcionar datos experimentales contrastados sobre el mismo. Para ello se ha realizado un estudio de la respuesta adherencia-deslizamiento a largo plazo de laminados de NSM FRP de carbono (CFRP) en hormigón bajo cargas mantenidas y diferentes condiciones ambientales.

En el presente estudio se han llevado a cabo dos campañas experimentales. En la primera de ellas se han realizado cuatro series de ensayos para estudiar la fluencia bajo cargas de tracción de un adhesivo epoxi cuando éste es sometido a la combinación de diferentes cargas mantenidas y diferentes condiciones de temperatura y humedad. En la segunda campaña se ha realizado un estudio del comportamiento adherente a largo plazo, en términos de respuesta adherencia-deslizamiento, de laminados NSM CFRP en hormigón, tanto a nivel experimental como a nivel analítico, con el fin de ampliar el conocimiento en este campo. En este sentido, se han ejecutado cinco series de ensayos de pull-out a cortante simple bajo carga mantenida en los que el hormigón estaba reforzado con láminas NSM CFRP. Como parámetros de estudio, se han considerado diferentes valores de carga mantenida, longitud adherente, ancho de ranura, temperatura y humedad. Los resultados experimentales a largo plazo de ambas campañas se han presentado y analizado, observándose que los cambios en los parámetros estudiados tuvieron un efecto relevante en la respuesta a largo plazo. Adicionalmente, se ha presentado una metodología simplificada para la simulación analítica de la respuesta adherencia-deslizamiento a largo plazo de los laminados NSM CFRP en hormigón. La metodología propuesta se ha comprobado mediante la comparación de los datos experimentales con las predicciones obtenidas analíticamente.

1 Introduction and objectives

1.1 Introduction

Reinforced Concrete (RC) structures, which can be found all over the world, are vulnerable to several factors that can affect their service life, cause deterioration, or simply can make the bearing capacity of the structure not to be enough for resisting the service loads. Some factors are natural, such as accidental loading (earthquakes, wind and blast, etc.) or environmental conditions (temperature, humidity, etc.), and some others are related to the design process, such as changing the structural system or increasing the service load. Nowadays, there is a general trend towards rehabilitation of structures instead of new construction [1, 2]. In order to preserve the existing RC structures, and consequently increase its service life, strengthening is often needed. In that sense, Fiber Reinforced Polymer (FRP) materials play an important role in preserving RC structures due to the advantages they provide over other traditional materials. FRP materials are lightweight, noncorrosive, and exhibit high tensile strength. These materials are available in several forms, sizes, shapes and surface patterns, and can be used in a wide range of structures and in areas with limited access where traditional techniques would be difficult to implement [3–7]. However, the brittle failure and in some cases low modulus of elasticity, in addition to the low resistance to transverse loads are the main disadvantages of FRP materials.

Existing RC structures can be strengthened using FRP materials through two main common techniques: Externally Bonded (EB) technique, in which the FRP element is bonded to the outer surface of the strengthened member, and Near Surface Mounted (NSM) technique, in which the FRP reinforcement is inserted into a groove cut in the concrete cover of the RC member.

In recent years, there has been an increasing interest in the NSM technique due to its potential advantages over the EB one, such as: (i) minimum installation time, (ii) no requirement of surface preparation except groove cutting, (iii) lower proneness to debonding failure, and (iv) lesser exposure to mechanical damage, fire and vandalism as the FRP reinforcement is protected by the concrete cover [8, 9].

Whatever the strengthening technique is used, FRP reinforcements must be connected to the concrete by means of a load bearing material (epoxy adhesives, cement mortar, etc.), whose main function is to transfer the bond stresses between reinforcing material and concrete. Bond controls the composite action development between FRP and concrete [9, 10], and therefore it is considered as one of the main parameters affecting the success and efficiency of the strengthening system.

So far numerous studies have been carried out on the short-term bond behavior of NSM FRP reinforcement systems, while a few have dealt with their long-term bond performance. The long-term behavior of the strengthening system, mainly that of the adhesive (whose viscoelastic behavior is generally ignored in the actual analytical models), under different conditions may affect bond and load carrying capacity over time, and therefore could be the cause of unexpected deformations, redistribution of stresses or even a premature failure.

The scarcity of experimental information and the uncertainty associated with the durability and long-term structural performance of FRP reinforcement as strengthening solutions is recognized as being one of the primary impediments to a broader adoption of these materials in civil infrastructure applications. Therefore, to contribute to solve this deficiency, a study investigating the structural bond of NSM FRP RC strengthened elements when subjected to various environmental conditioning regimes under the effect of sustained loading is completely needed. To this end, long-term behavior of the constituents of a FRP strengthening joint (FRP, adhesive, concrete), bond behavior of the joint, as well as long-term bond-slip response of strengthened elements is of major interest.

1.2 Objectives

The effect on the FRP RC strengthened structures of environmental conditions with different moisture and temperature regimes, combined with the presence of sustained loading during the life-span of the structure, is regarded as an area of incomplete knowledge. Understanding and clarifying how the structure is affected by these type of external actions is a main requirement for an improved design of FRP strengthened members. The main objective of the present thesis is to study the long-term bond behavior , in terms of bond strength and bond-slip response, of the NSM Carbon FRP (CFRP) strips in concrete when subjected to sustained loading and different environmental conditions, being the sustained loading level, bonded length, groove width, temperature and humidity the main parameters of the study. In order to achieve this aim, the following tasks have been undertaken:

1. Review the experimental and analytical research carried out on both short-term and long-term bond behavior of NSM FRP reinforcement in concrete and the composing materials (FRP and adhesives) to gain a better understanding of the bond-slip behavior and the role of the different variables involved in that behavior.

2. Experimental investigation of creep behavior of the epoxy adhesive when subjected to different levels of sustained loading at different environmental conditions of temperature and humidity.

3. Experimental investigation of the effect of sustained load level, bonded length, groove width, temperature and humidity level on the time-dependent bond-slip response of NSM CFRP strips in concrete using direct pull-out tests. Based on experimental results, the influence of the different variables on time-dependent bond-slip response of NSM CFRP strips in concrete should be defined.

4. Development of an analytical model suitable for constitutive modeling of bond mechanism of NSM strips in elements subjected to long-term loading with the reference to the obtained experimental results.

1.3 Thesis layout

In order to achieve the aim of the current study, the thesis is structured as follows:

In Chapter 2, a detailed review of the works carried out on the study of both short-term and long-term bond behavior of NSM FRP reinforcement in concrete available in the bibliography is given. First, a detailed description of FRP materials, including their types, constituent materials, manufacturing processes and mechanical properties, is given and followed by a description of the two main common methodologies for RC strengthening with FRP materials (EB and NSM). Then, a complete review of experimental programs on short-term bond behavior of NSM FRP is presented. Special attention is given to the main parameters governing the bond behavior, test methods, test setups, test specimens and available bond models that simulate the bond behavior. After that, a review of the available works concerning the behavior of materials composing NSM system under sustained loading and environmental conditions is presented. Finally, a complete review of the experimental and analytical works on the bond behavior under sustained loading and environmental conditions for both EB and NSM systems is presented.

In Chapter 3, an experimental program to study the tensile creep behavior of the adhesive used, when subjected to different levels of sustained loading and different conditions of temperature and humidity, is presented. Finally the experimental results are presented.

In chapter 4, a detailed description of the experimental program on the time-dependent bond-slip response of NSM CFRP strips in concrete is presented, giving details of test setup and conditions, based on the analysis done in Chapter 2. On the other hand, materials involved in the presented program need to be fully characterized, including both their short-term and long-term behavior, and this is done in this chapter. Finally the experimental results are presented

In Chapter 5, a simplified analytical model to simulate the time-dependent bond-slip response of NSM CFRP strips in concrete is developed and described. The proposed model is checked through the comparison with the experimental data previously presented in Chapter 4.

Finally, the thesis is concluded in Chapter 6 in addition to some suggestions for future work.

2 Literature Review

2.1 Introduction

Concrete is the most common construction material due to its numerous advantages, such as, for example, tailored strength, high durability, fire resistance, and excellent relationship between performance and cost. But service life of concrete structures is affected by different factors, such as age, loads or environmental conditions which make rehabilitation and strengthening essential issues [11, 12]. To that end, the development of new materials and techniques for construction, repairing, rehabilitation, and strengthening of concrete structures taking advantage of emerging technologies is of major importance [13, 14].

2.2 Fiber Reinforced Polymers (FRP)

Polymer composite materials, which can be defined as a combination of two or more materials on a macroscopic scale to form a useful third material [15], are being widely used in the field of civil engineering, as well as in many other fields, due to several advantages they provide. Some applications of the polymer composites materials in different fields are presented in Table 2.1. Several properties can be enhanced or affected by forming a polymer composite material such as: strength, stiffness, corrosion resistance, weight, fatigue life, temperature-dependent behavior and time-dependent behavior [15].

Nowadays, the use of Fiber Reinforced Polymer (FRP) materials, the most common polymer composite material used in construction and civil engineering applications, as an alternative to steel has increased either for internal reinforcement or for strengthening purposes of concrete structures [16, 17]. FRP materials provide several advantages over conventional steel, among them: (i) their high ratio of tensile strength to self-weight (the strength of FRP reinforcement can be 10 to 15 times higher than that of steel, meanwhile, its weight is 5 times lower) (ii) their reduced weight results in the ease of handling and in a reduction of the dead load added on the structure, (iii) their corrosion resistance provides high durability when subjected to aggressive environments, (iv) they provide a low coefficient of

thermal expansion, (v) they can be used in a wide range of structures due to their electromagnetic neutrality and high cutability, and (vi) they can be available in several sizes and shapes [18]. On the other hand, the brittle failure and in some cases low modulus of elasticity, in addition to the low resistance to transverse loads can be considered as drawbacks of the FRP materials [19].

Table 2.1: Some applications of polymer composites [20].

Application area	Examples
Aerospace	Space structures, satellite antenna, rocket motor cases, high pressure fuel tanks, nose cones, launch tubes
Aircraft	Fairings, access doors, stiffeners, floor beams, entire wings, wing skins, wing spars, radomes, vertical and horizontal stabilizers, helicopter blades, landing gear doors, seats, interior panels
Chemical	Pipes, tanks, hoppers, valves, pumps, impellers
Construction	Bridges and walkways including decks, handrails, cables, frames, grating
Domestic	Interior and exterior panels, chairs, tables, baths, shower units, ladders
Electrical	Panels, housing, switch gear, insulators, connectors
Leisure	Tennis racquets, ski poles, golf clubs, protective helmets, fishing rods, playground equipment, bicycle frames
Marine	Hulls, decks, masts, engine shrouds, interior panels
Medical	Prostheses, wheel chairs, orthofies, medical equipment
Transportation	Body panels, dashboards, frames, cabs, spoilers, front end, bumpers, leaf springs, drive shafts

Fibers and matrix are the two major components forming the FRP material; the fibers provide strength and stiffness, and the matrix (resin) mainly provides the transfer of stresses and strains between the fibers [7]. Therefore, FRP composites are manufactured by embedding continuous high strength fibers in a polymer (resin) matrix (see Figure 2.1).

Because FRPs are composed of two distinct materials, FRP properties depend primarily on those of the individual constituents. It is thus instructive to examine the

role and properties of each of the component materials, the fibers and the matrix, separately, before discussing the properties of the FRP composite as a whole.

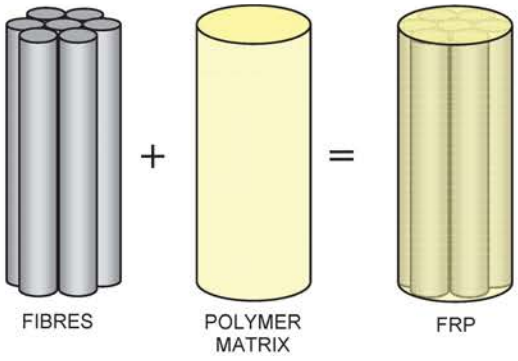

Figure 2.1: Basic material components of FRP composite [21].

2.2.1 Fibers

The main role of fibers is to provide the strength and stiffness of the FRP in order to resist the major portion of the load acting on the composite system. Therefore, fibers are the main component that forms the backbone of the FRP materials, and their properties influence the FRP overall properties. Fibers are generally selected to have high stiffness, high ultimate strength, high elastic modulus, convenient elongation at tensile rupture, low variation of strength between individual fibers, reduced number of defects, stability during handling, durability and acceptable cost [21].

The fiber volume fraction in FRP materials usually ranges from 30 to 75%. Besides, mechanical properties (strength and stiffness) of commercially available fibers cover a large spectrum. As a result, the properties of the resulting composite have a considerable variation [22]. For structural engineering applications, fibers are characterized by extremely large length-to-diameter ratios and by extremely small diameters (as small as 5-10 microns). The molecular structure of the material is aligned along the length of the fibers giving them high tensile strength [21]. A scanning electron micrograph showing microscopic carbon fibres used in FRP fabrication is shown in Figure 2.2.

Many different types of fibers are available for use, all of them having their own advantages and disadvantages. Based on the fiber type used, the most used FRP composites are classified into four groups: Carbon FRP (CFRP), Glass FRP (GFRP), Aramid FRP (AFRP) and Basalt FRP (BFRP). The properties and characteristics of these fibers are presented in the subsequent sections.

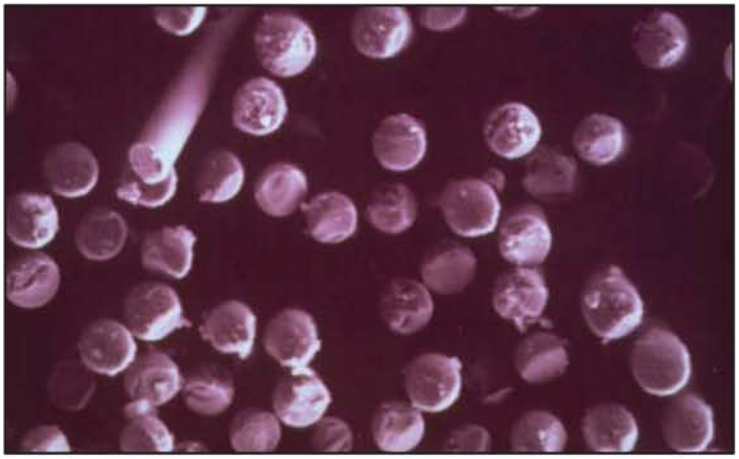

Figure 2.2: Scanning electron micrograph showing microscopic carbon fibers used in FRP fabrication [21].

2.2.1.1 Carbon fibers

Several advantages have made carbon fibers widely used in composite materials, among them their high stiffness and strength combined with low density and intermediate cost. In addition, carbon fibers have high fatigue strength and a very low coefficient of linear thermal expansion and, in some cases, even negative thermal expansion [7, 20]. Carbon fibers are chemically inert and not susceptible to corrosion or oxidation at temperatures below 400°C. Moreover, carbon fibers possess a high modulus of elasticity, 200-600 GPa, and their ultimate elongation varies from 0.3-2.5%. The main disadvantage of the carbon fiber is being electrically conductive and, therefore, might initiate galvanic corrosion when in direct contact with steel [23].

2.2.1.2 Glass fibers

Glass fibers are the most common type of all reinforcing fibers used in FRP materials. Glass is an amorphous material composed of a silica network [24]. The main advantages of glass fibers include low cost, high tensile strength, chemical resistance, and high temperature resistance. Additionally, they provide low tensile modulus, sensitivity to abrasion while handling, relatively low fatigue resistance, and brittleness [7]. Glass fibers are sensitive to moisture, stress corrosion at high stress levels, and also may have problems with relaxation; these drawbacks can be overcome with the correct choice of matrix which protects the fibers [23].

2.2.1.3 Aramid fibers

Aramid fibers are a synthetic organic polymer fibers (an aromatic polyamide) produced by spinning a solid fiber from a liquid chemical blend. Aramid fibres are characterized by high strength, moderate elastic modulus, and low density. Its tensile strength-to-weight ratio is 43% lighter than that of glass fibers and approximately 20% lighter than most carbon fibers. In addition to high strength, the fibers also offer better resistance to abrasion and impact, as well as chemical and thermal degradation [7, 20]. Major drawbacks of these fibers include degradation when exposed to ultraviolet light and the fact that they are very difficult to cut and special tooling and techniques are required. In addition, FRPs manufactured from aramid fibres have low compressive and shear strengths as a consequence of the unique anisotropic properties of the fibres [21, 22].

2.2.1.4 Basalt fibers

Basalt fibers are a unique product derived from volcanic material deposits. Basalt is an inert rock, found in abundant quantities, and has excellent strength, durability, and thermal properties. Basalt fibers are manufactured from basalt rock in a single-melt process and are better than glass fibers in terms of thermal stability, heat and sound insulation properties, vibration resistance, as well as durability. Basalt fibers offer an excellent economic alternative to other high-temperature-resistant fibers and are typically utilized in heat shields, composite reinforcements, and thermal and acoustic barriers [7]. The difficult heating process of the crushed basalt in furnaces and the difficult quality control of the fibres are the main drawbacks of BFRP [18].

2.2.2 Matrix

The most obvious role of a matrix is to act as a binder that holds together the reinforcement fibers. However, other primary functions of the matrix (or resin) within the FRP composite material can be also defined:

- to transfer stresses between individual fibers
- to provide a barrier against the environment
- to separate and disperse fibers within the composite
- to protect the surface of the fibers from mechanical abrasion

While fibers provide the strength and stiffness of an FRP, the matrix influences the inter-laminar shear as well as the in-plane shear properties of the material [7]. The ability to manufacture the composite depends strongly on the matrix's physical and thermal characteristics such as viscosity, melting point, and curing temperature [22].

The most common and used type of matrices are the organic ones, also known as resins or polymers, which consist of long-chain molecules of hydrogen and carbon atoms held together by primary or covalent bonds. Depending on the arrangement of hydrocarbon chains, different molecular configurations and hence different properties are obtained [20]. Polymers can be classified under two types, thermoplastics and thermosets, according to the effect of heat on their properties [7, 21]. Both types have certain advantages and disadvantages as presented in Table 2.2.

Almost exclusively, thermosets are currently used in structural engineering applications. These polymers generally have good thermal stability at service temperatures, good chemical resistance, and display low creep and relaxation properties in comparison with most thermoplastics [21]. In general, the three most common thermosetting resins currently used, to manufacture FRPs used in infrastructure applications, are: polyester, vinylester, and epoxy. A brief description of each resin is presented in Table 2.3 and in the following sections.

Table 2.2: Some advantages and disadvantages of using thermoset and thermoplastic matrices [24].

Application	Property	Thermoplastic matrix	Thermoset matrix
Matrix	Formulation	More simple	Complex
	Melt viscosity	Rather high	Low
	Fiber impregnation	Very difficult	Comparably easy
	Cost	Low to high	Low to medium
Composite	Processing cycle	Short to long	Very long
	Processing temperature and pressure	High	Moderate
	Size of products	Small to medium	Can be very long
	Resistance to solvents	Poor to good	Good
	Damage tolerance	Fair to good	Poor to excellent
	Resistance to creep	Not known	Good
	Toughness	High	Low
	Ease of application	Less labor intensive	Labor intensive

Table 2.3: Comparison of resins [7].

Type	Advantages	Disadvantages
Polyesters	Easy to use	Only moderate mechanical properties
	Lowest cost of resins available	High styrene emissions in open molds
		High cure shrinkage
		Limited range of working times
Vinylester	Very high chemical/ environmental resistance	Post-cure generally required for high properties
	Higher mechanical properties than polyesters	High styrene content
	High mechanical and thermal properties	Higher cost than polyesters
		High cure shrinkage
Epoxies	High water resistance	More expensive than vinylesters
	Long working times available	Corrosive handling
	Temperature resistance up to 140°C wet/ 220°C dry	Critical mixing
	Low cure shrinkage	

2.2.2.1 Polyester

Polyester resins are the most economical and widely used resin types in the manufacture of FRP components for infrastructure applications, especially in the marine industry. Nearly half a million tons of this material are used annually in the United States in composite applications [7]. Polyester resins can be formulated to obtain a wide range of properties ranging from soft and ductile to hard and brittle. Their advantages include low viscosity, low cost, and fast curing time. In addition, polyester resins have been considered the least toxic thermoset resin. The most significant disadvantage of polyesters is their high volumetric shrinkage [7, 22].

2.2.2.2 Vinylester

Vinylester resins are more flexible and have higher fracture toughness than cured polyester resins. The handling, mechanical and chemical characteristics of vinylesters are similar to polyesters, and for this reason, they are often identified as a class of polyesters. Some advantages of the vinylesters, which may justify their higher cost, include better chemical and corrosion resistance, hydrolytic stability, and better physical properties, such as tensile strength as well as impact and fatigue resistance. It has been shown that a 0.5 to 1.5 mm thick layer of a vinylester resin matrix can provide an excellent permeation barrier to resist blistering in marine laminates [7, 22].

2.2.2.3 Epoxy

Epoxy resins are a broad family of materials that provide better mechanical and chemical performances as compared to other organic resins. Aerospace applications use epoxy resins almost exclusively, except when high temperature performance is a key factor. For structural applications, epoxies are often used in wet lay-up applications of FRP plates and sheets because of their ability to cure well at room temperature and owing to their outstanding adhesion characteristics. Epoxies generally outperform most other resin types in terms of mechanical properties and resistance to environmental degradation. Despite their high cost, long curing time, and handling difficulties, they are being used because of their many advantages, such as [7, 21, 22]:

- wide range of material properties
- minimum or no volatile emissions and low shrinkage during curing
- excellent resistance to chemical degradation
- very good adhesion to a wide range of fibers and fillers

2.2.3 FRP composites manufacturing and products

Among a wide variety of techniques by which FRP components can be manufactured, three techniques are of immediate interest to the structural engineering: (i) pultrusion, which is used for manufacturing FRP composites with uniform cross-sectional shape such as FRP bars, rods, tendons, plates, and structural sections, (ii) wet lay-up, which is often used in structural rehabilitation applications where FRP sheets or fabrics are bonded to the exterior of RC, steel, aluminum, or timber members, and (iii) filament winding, which is an automated process in which raw fibers are drawn off spools, through a resin bath, and wound onto a rotating mandrel [21].

In a FRP composite, the fibers may be placed in one direction (unidirectional) or may be woven or bonded in many directions (bi or multi-directional). Unidirectional composites are commonly employed for strengthening purposes. FRP composites can be produced in different shapes such as rebars, strips/laminates, plates, and profiles, as shown in Figure 2.3.

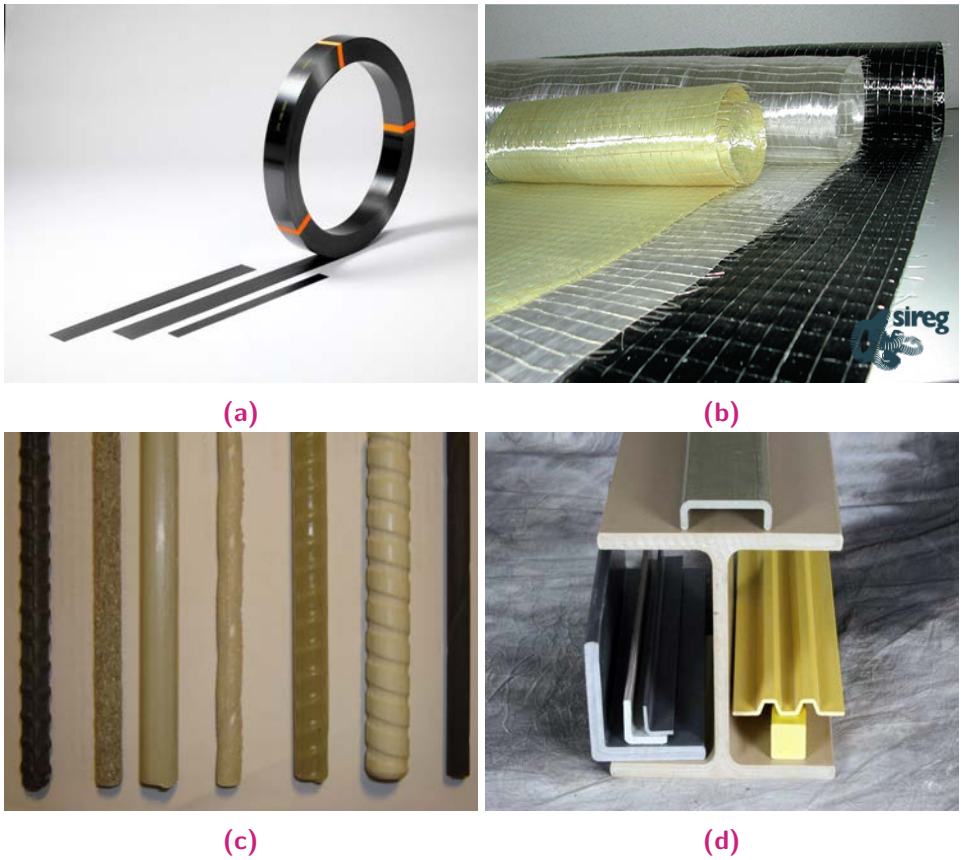

Figure 2.3: Different shapes of FRP composites; (a) Strips/laminates, (b) Sheets, (c) Bars and (d) Profiles.

FRP bars are mainly used either as internal reinforcement for RC structures or as NSM reinforcement for strengthening applications. A wide range of FRP bars is available in the market having several classifications based on different features such as type of fiber, cross sectional shape, surface texture and surface treatment. On the other hand, both FRP sheets and strips/laminates are mainly used for strengthening and rehabilitation of existing structures. The sheets are generally supplied in form of rolls as shown in Figure 2.3b. In the case of laminates and strips, the presence of the polymeric matrix provides stiffness to them (see 2.3a). Usually, the strips have thicknesses of about 1.0-1.5 mm, whereas the thickness of the sheets is about 10 times smaller. The advantages of the sheets are their high versatility and portability, while the main drawback is that it is difficult to determine a priori the amount of epoxy required to be applied on the reinforcement.

Among various FRP shapes and cross sections available, strips (jointly with bars) are the most usual reinforcement shape used for NSM reinforcement systems, since the reinforcement must be placed into a relatively narrow groove in the concrete cover. FRP strips are least prone to debonding from the concrete substrate [25]. Besides, the use of narrow strips maximizes the surface area to sectional area ratio for a given

volume and thus minimizes the risk of debonding [9]. In case of using FRP strips, the normal stresses accompanying the tangential stresses in the adhesive act against both sides of the strip into the concrete substrate, thus effectively confining the strip and improving bond performance. On the contrary, when round FRP bars are used, the normal stresses act outward in all directions, eventually causing the epoxy cover to split when the tensile strength of the adhesive is reached [26]. Higher local bond strength has been provided by NSM reinforcement with FRP strips compared to that provided by both NSM reinforcement with FRP rods and EB systems [27, 28].

2.2.4 Mechanical properties of FRPs

The mechanical properties of FRPs depend on a number of factors: the relative proportions between fibers and matrix; the mechanical properties of the constituent materials (fiber, matrix and any additives); the orientation of the fibers; and the manufacturing process. For this reason, it is not possible to give unique values of FRPs mechanical properties [21]. A comparison between the behavior under tension of different FRP materials is shown in Figure 2.4, where their typical linear elastic stress-strain behavior until rupture is shown. These materials do not possess the ductility that steels have, and their brittleness may limit the ductile behavior of RC members strengthened with FRP composites, thus limiting the stress redistribution [4].

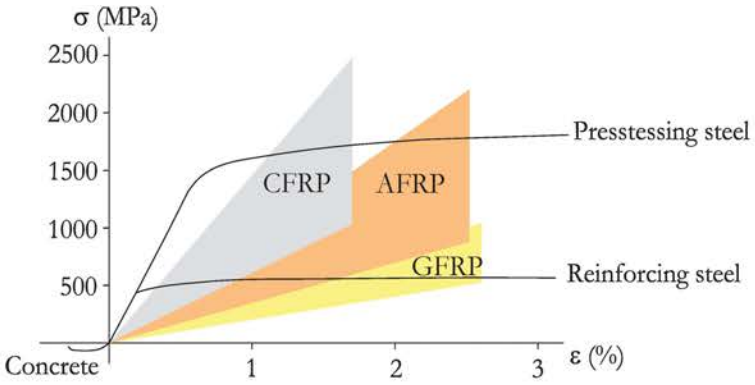

Figure 2.4: Typical stress-strain relationships for FRP and steel bars [19].

In comparison to conventional steel, FRP materials usually present significantly higher tensile strengths and lower moduli of elasticity, specially in the case of GFRP reinforcement. The modulus of elasticity of FRPs remains practically constant up to the failure point [29].

Some properties of different commercially available FRP materials (glass, carbon, and aramid FRPs) are given in Table 2.4, while a qualitative comparison of the three main types of FRPs is shown in Table 2.5.

Table 2.4: Mechanical properties of FRP materials [19].

FRP types	Unit	GFRP	CFRP	AFRP
Fiber content	%	50-80	65-75	60-70
Density	kg/m^3	1600-2000	1600-1900	1050-1250
Tensile modulus	GPa	25-55	120-250	40-125
Tensile strength	MPa	400-1800	1200-2250	1000-1800

Table 2.5: A qualitative comparison of the three main types of FRPs [21].

Criteria	GFRP	CFRP	AFRP
Tensile strength	Very Good	Very Good	Very Good
Modulus of elasticity	Adequate	Very Good	Good
Long term behavior	Adequate	Very Good	Good
Fatigue behavior	Adequate	Excellent	Good
Bulk density	Adequate	Good	Excellent
Alkaline Resistance	Adequate	Very Good	Good
Price	Very Good	Adequate	Adequate

For unidirectional FRP materials, the strength is dependent on whether the applied load is tensile or compressive. The response of an FRP material in tension is largely dependent on the failure strains of the two component materials. When loaded in compression, the FRP's ultimate strength is less than that achieved in tension, and depends on many factors such as the fiber type, the matrix properties, and the matrix-fiber interface strength. The ultimate compressive strength of FRPs can be reached due to fiber micro-buckling, transverse tensile failure in the matrix, or shear failure. Axial compressive strengths for uniaxial FRP materials loaded in the fiber direction are typically about 55%, 20%, and 78% of the axial tensile strength for glass, aramid, and carbon FRPs, respectively [21].

Most unidirectional FRP materials used in civil engineering applications show good fatigue behavior in comparison with steel. Research related to the fatigue behavior of FRP composites is ongoing, but the following general comments can be made. Carbon FRPs display outstanding fatigue behavior. This has been attributed to the fact that carbon fibers have a very high stiffness, which limits the strains experienced by the matrix component, and prevents matrix cracking and breakdown of the matrix-fiber interfacial bond, thus preventing failure. Tensile fatigue tests conducted on unidirectional carbon/epoxy FRP strands have indicated that CFRP can sustain much greater mean stresses and stress amplitudes than steel. Glass fibers are considerably less stiff, hence glass FRP matrices experience larger strains during load cycling

which lead to more matrix cracking that can eventually lead to failure. Finally, aramid fibers have stiffness values that are intermediate between glass and carbon, and therefore, we might expect that they display intermediate fatigue behavior. However, aramid fibers themselves are innately sensitive to fatigue damage through a process called de-fibrillation, which can lead eventually to fatigue failure. Figure 2.5 shows typical fatigue life curves for carbon and glass FRPs, where the superior fatigue behavior of carbon FRPs is evident [21].

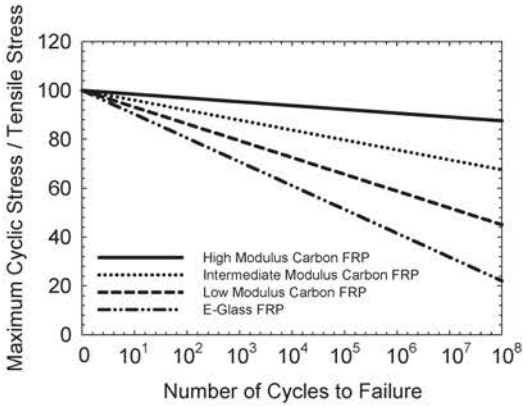

Figure 2.5: Fatigue-life curves for FRPs with different fiber types [21].

Although carbon, glass, and aramid fibers display comparatively little creep behavior under most ambient conditions, the visco-elastic of FRP matrix materials (they display properties of both elastic solids and viscous fluids) may results in creep of FRP materials under sustained load. The amount of creep exhibited by a particular FRP material will depend primarily on the fiber volume fraction and the orientation of the fibers with respect to the applied loads. In addition, both temperature and moisture can have significant effects on the creep behavior of polymers. However, for most unidirectional FRP materials used in civil engineering applications creep is not normally a significant concern, provided that the sustained stress in the FRP is limited. Thus, most available standards conservatively recommended that the sustained stress levels in unidirectional FRP structural components should be limited to a certain percentage of the FRP's design ultimate strength [21]. Some types of fibers (glass in particular) are susceptible to creep rupture (sometimes called stress-corrosion) failure mode. In this mode of failure, the fibers fracture under sustained load levels that are much lesser than the failure stress of the composite observed under static testing. Because of the susceptibility of glass fibers, and hence GFRPs, to creep rupture, stress levels in glass FRPs are often severely limited under sustained loads to less than 20 or 25% of the static tensile strength [21].

2.2.5 Adhesives used with FRP in strengthening applications

Adhesives play an important role for most industries, for both structural and non-structural use. They are responsible for holding materials together and provide the following general advantages [30]:

- Increased speed of production
- Wider selection of materials combinations to suit production cost
- Local stress concentrations can be avoided
- Improved fatigue resistance when compared to welded structures

Five theories to describe mechanisms of adhesion are available: (i) Mechanical adhesion theory in which surfaces are held together by mechanical interlocking as a result of the penetration of adhesives into pores, cavities, voids and other surface irregularities on the surface of the substrate; (ii) Electrostatic adhesion theory in which the adhesion takes place due to electrostatic effects between the adhesive and the adherend; (iii) Diffusion adhesion theory in which the adhesion is developed through the interdiffusion of molecules in between the adhesive and the adherend (the molecules of both materials are mobile and soluble in each other); (iv) Wetting adhesion theory (also known as dispersive adhesion) which proposes that adhesion results from molecular contact between two materials and the surface forces that develop through the attraction between molecules of different charge (the Van der Waals forces) and (v) Chemical adhesion theory in which the adhesion is attributed to the formation of an adhesion bond to surface chemical forces. Hydrogen, covalent, and ionic bonds formed between the adhesive and the adherends are stronger than the dispersion attractive forces [31, 32].

Although a bonded joint is preferably loaded in shear, the adhesive layer can be subjected to various forces, based on the bonded joint design, such as tension, compression, shear, cleavage and peel (see Figure 2.6) [30].

Structural adhesives are a common type of adhesives that are used for bonding several materials, such as metals, glass, ceramics, concrete, plastics and composites, providing a load-bearing joint [30]. Epoxy based and cement based adhesives are the most widely accepted structural adhesives used for strengthening RC structures with FRP [9].

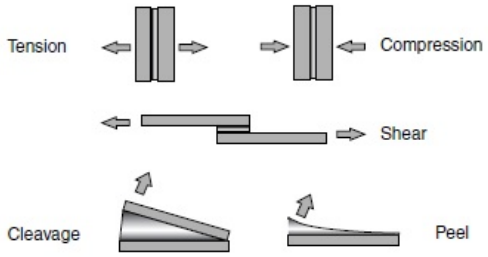

Figure 2.6: Different forces acting on a bonded joint [30].

Epoxy adhesives were first used in 1930 in Germany, USA and Switzerland [30]. They are based on polymeric materials and exhibit properties that are characteristic for polymers, as for example the change from relatively hard to elastic glass-like behavior to relatively rubbery behavior at a certain temperature. This phenomenon takes place at what is called as glass transition temperature (T_g). Being T_g a very important material property that depends on the polymer, typical values for T_g in epoxies normally vary between 45°C and 200°C [30].

Although epoxy based adhesives have a wide range of mechanical and physical properties that make them the most efficient bonding material in building industry, their main drawback is that their properties can be affected when subjected to relatively low and high temperatures [9, 30]. In those cases, cement based adhesives can provide lower material cost and better resistance to high temperature. However, bond tests of NSM reinforcement have identified limitations for using cement based adhesives due to their low bond strength [33].

2.2.6 Applications of FRPs in Civil Engineering

FRP composites are durable and lightweight and consequently they can fulfil many of the requirements of structural materials for civil engineering. Moreover, in addition to the easiness of use and the mechanical properties that FRP materials provide over other conventional materials, their tremendous variety in types, shapes and properties allow them to be effectively used in enormous variety of applications in structural engineering and construction applications such as FRP structures, FRP reinforced concrete, and repair and rehabilitations of structures (see Figure 2.7).

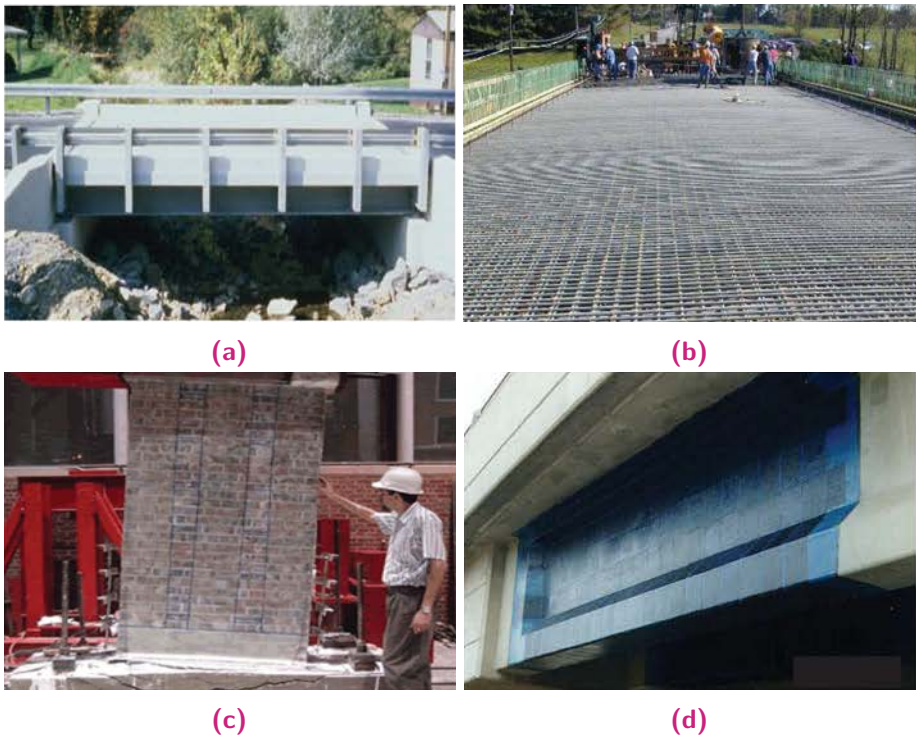

Figure 2.7: Applications of FRPs in Civil Engineering (a) A short-span FRP road bridge, (b) GFRP reinforcing bars placed in a concrete bridge deck, (c) Strengthening of clay brick masonry wall with EB GFRP sheets, and (d) Strengthening of RC bridge girder with CFRP sheets [21].

2.3 Concrete strengthening techniques with FRPs

As previously mentioned in this chapter, the use of FRPs for strengthening RC structures has been proven to be an efficient methodology due to their unique properties when compared to steel and other building materials. Two main techniques have become common in the FRP strengthening systems; namely the EB and the NSM (see Figure 2.8). A brief description of each technique is presented in the following paragraphs.

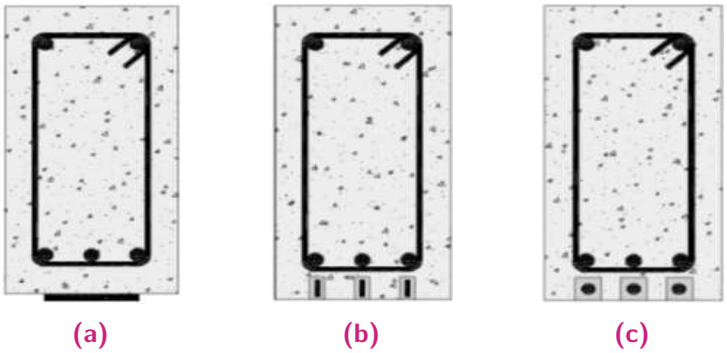

Figure 2.8: Concrete strengthening with FRPs (a) EB (b) NSM strips and (c) NSM bars [34].

2.3.1 Externally Bonded (EB) technique

Externally Bonded (EB) reinforcement is one of the most widely used concrete strengthening techniques in which the FRP reinforcement, either sheets or plates, is applied to the external tensile surface of the member to be strengthened by means of epoxy adhesives [35–42]. In order to efficiently transfer the loads from the strengthened member to the installed FRPs, the concrete surface should be roughened and cleaned and a sufficient concrete cover in good conditions should be provided to ensure a proper bonding between FRPs and substrate.

The use of FRPs in the EB technique results in different systems, being the wet lay-up (or cured in-situ) and prefabricated (or precured) the most common ones. In wet lay-up system, the surface of the strengthened member is coated with a primer layer and then the FRPs are installed using an adhesive. Finally, a paint layer is applied as a protective layer. In prefabricated system, the FRPs are embedded in the adhesive and then applied to the surface of the strengthened member through the use of adhesives [1]. The application of each system (i.e. wet lay-up and prefabricated) depends on the structure to be strengthened; for example, the wet lay-up system, due to the high flexibility of the FRP sheets, can be used to strengthen plane as well as convex surfaces, whereas prefabricated strips are generally best suited for plane and straight surfaces. Some examples of strengthening with EB technique are shown in Figure 2.9.

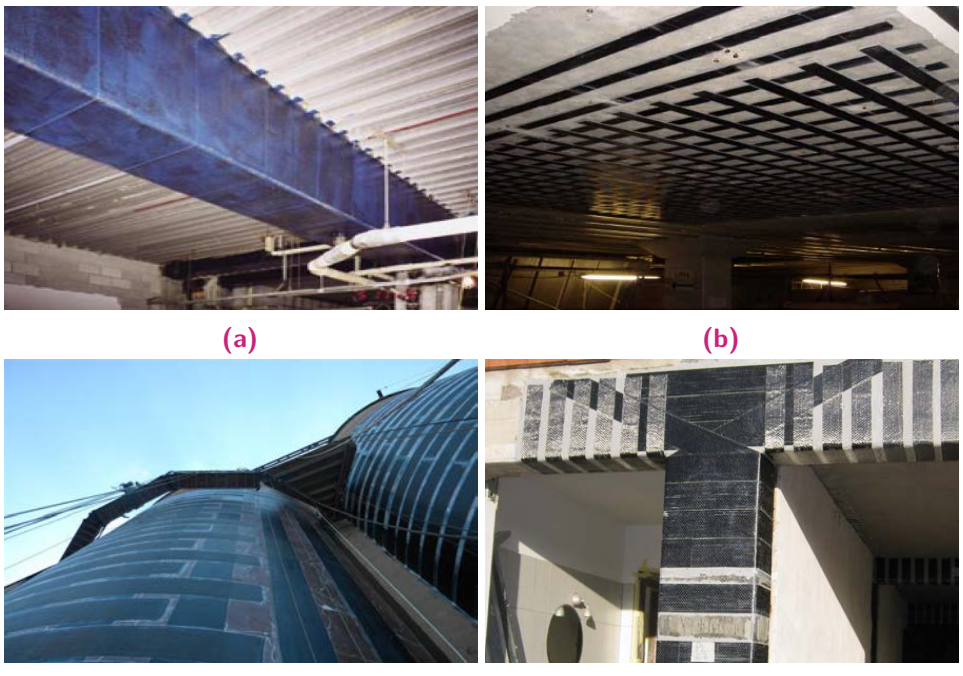

Figure 2.9: EB applications (a) Beam strengthening, (b) Slab strengthening, (c) Silos strengthening, (d) Beam-column connection.

Although the EB system has many practical advantages, debonding of the plate from concrete may lead to a brittle failure of the RC element strengthened in flexure. Such a mode of failure not only reduces the strengthening potential of EB plates but is also not recommendable from the point of view of structural safety [43].

2.3.2 Near Surface Mounted (NSM) technique

The NSM FRP strengthening technique appeared as an alternative to the EB in the early 2000s. In fact, in the 1940s it started to be used in Europe for the strengthening of RC structures with steel. In the NSM, the FRP reinforcement is inserted into pre-cut grooves opened in the concrete cover, and fixed with adhesive. The NSM application involves the following steps [44]:

1. Opening grooves in the concrete cover using a saw cut machine
2. Cleaning the grooves with compressed air
3. Cleaning the FRP with an appropriate cleaner (e.g., acetone)
4. Preparing the adhesive according to the supplier's recommendations
5. Filling the grooves and, if possible, cover the lateral faces of the FRP with the adhesive
6. Inserting the FRP into the grooves, and slightly press it to force the adhesive to flow between the FRP and the grooves' borders. This phase requires a special care in order to assure that the grooves are completely filled with adhesive. When this is not the case, the formation of voids might occur
7. Removing the adhesive in excess and leveling the surface
8. Respecting the adhesive curing time defined by the supplier

In most existing NSM FRP field applications, CFRP reinforcement has been used to strengthen concrete structures, whilst GFRP reinforcement has been mainly used to strengthen masonry and timber structures [9]. Limited applications were found regarding AFRP [45], while BFRP is an economic alternative to CFRP and GFRP in some applications [18]. The properties and characteristics of these fibers are presented in the subsequent sections. Some examples of NSM technique in the strengthening are shown in Figure 2.10.

Figure 2.10: NSM applications (a) Strengthening of parking garage decks [46] and (b) Strengthening of bridge in Sweden [23].

GFRP and CFRP materials are usually used as NSM reinforcement. When the FRP to be used has a square or round cross-section, the FRP is named to be bar, whereas strip is used to refer to FRP with rectangular cross-section whose width is significantly larger than the thickness.

Schematic drawings of bar and strip NSM reinforcement are shown in Figure 2.11. Due to the final cross-section geometry of the grooves, square and rectangular reinforcements explore it better than round ones, since a uniform adhesive thickness is achieved. Additionally, when round bars are used, the normal stresses (perpendicular to the reinforcement) accompanying the tangential bond stresses (parallel to the reinforcement) tend to split the epoxy cover, while when square or rectangular bars are used, they act mainly towards the groove, lateral to concrete. If choices are to be made between square and rectangular (strip) reinforcement, rectangular ones have shown to be more efficient since they maximize the ratio of surface to cross-sectional area, which minimizes the bond stresses associated with a given tensile force in the FRP [9, 44, 47]. The main disadvantage of rectangular reinforcement is the need for a deeper groove to provide the same reinforcing area.

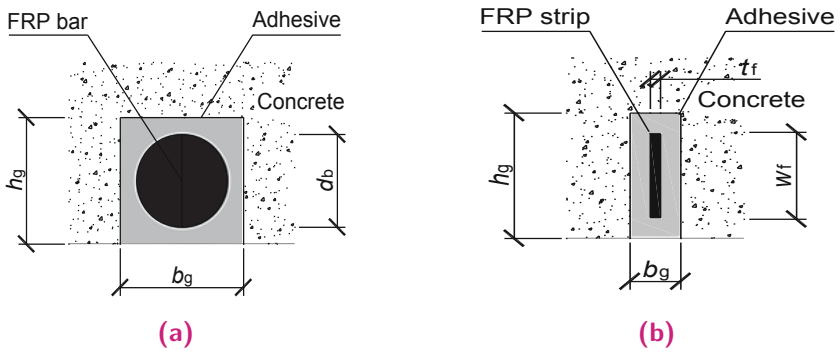

Figure 2.11: NSM systems using FRP (a) bar and (b) strip [44].

2.3.2.1 Prestressed NSM-FRP Strengthened RC

Prestressing of NSM FRP laminates in RC structures is an innovative application that combines benefits from both external prestressing and passive bonded FRP laminate systems, allowing laminates to be used more efficiently as a greater portion of their tensile capacity is promised [48](see Figure 2.12). Prestressed NSM laminates may be used for flexural strengthening, shear strengthening as well as confinement of RC members [34, 49–53]. FRP laminates provide several advantages when used in prestressing and post-tensioning strengthening applications. The benefits of prestressing FRP laminates are [48]:

- Improving serviceability and reducing deflections
- Reducing crack widths and delaying the onset of cracking
- Relieving internal steel reinforcement strains
- Resisting fatigue failure
- Resulting in the yield of internal steel rebars at a higher proportion of the ultimate load
- Providing more efficient use of the concrete and the FRP
- Opposing stresses due to both dead and live loads
- Reducing the risk of premature failure
- Increasing the ultimate capacity

- Increasing shear capacity by the longitudinal stresses induced

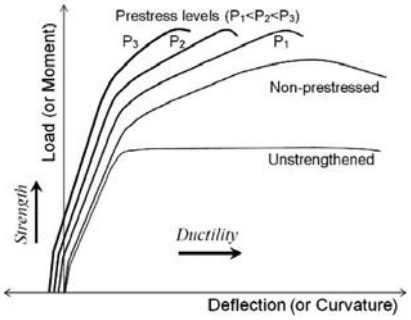

Figure 2.12: Typical load-deflection curves for beams strengthened with prestressed and non-prestressed FRP laminates [34].

One of the main drawbacks of prestressing CFRP laminates is the reduction in their strain capacity. Because FRP materials exhibit linear elastic behavior up to failure, a portion of their strain capacity is used at prestressing. Therefore, fiber fracture will take place at a lower deflection when compared with non prestressed strengthened members [54].

Three main techniques have been proposed for prestressing FRP laminates: (i) cambered beam systems; (ii) systems that tension the FRP laminate against an independent external reaction frame; and (iii) systems that tension the FRP laminate against the strengthened beam itself [48]. The differences between the three techniques are summarized in Table 2.6.

Table 2.6: Characteristics of FRP prestressing system for field application [48].

Characteristics	Cambered prestressing system	Prestressing against an independent beam	Prestressing against a strengthened beam
Specialized equipment	Large hydraulic jacks to lift up the girder	Vehicle to provide prestressing bed	Very little specialized equipment
Flexibility	Can be applied to beams of any length, dimension	Limited by the strengthening system	Can be applied to beams of any length, dimension
Accessibility	Requires jacking location; impractical over a water course or structures far above ground level; close traffic below bridge	Requires access for the external mechanism, vehicle and crews	Requires access for light equipment and crew; access from above is feasible
Achievable prestress level	Low; little control over profile	High, dependent upon anchor; can be controlled; profile can be customized	
Quantity of FRP material	Much more materials used than with other methods	FRP material can be used efficiently	
Anchorages	None	Lateral post-tensioning	Essential part of the system
On-site labor	Moderate	Moderate, high if lateral post-tensioning used	

2.3.3 Comparison between EB and NSM techniques

Despite of the the wide number of applications of the EB technique, it has some practical limitations. The main limitation is that, in general, the bond between

the concrete and the FRP usually prevents the FRP sheet from developing its full tensile strength, this resulting in premature debonding failures [43, 55, 56]. As a result, strain limits need to be imposed in the design procedure. Moreover, since the EB FRP reinforcement system is located on the external face of the elements, FRP and epoxy adhesive are exposed to environmental effects, fire and vandalism acts. Besides, the reinforcing performance of FRP materials can be negatively affected due to freeze/thaw cycles [57].

Using the NSM technique has the ability to partially solve the aforementioned drawbacks due to several advantage it provides, such as [2, 9, 44, 47, 58]:

- NSM reinforcement is less prone to debond from the concrete substrate
- In structural behavior of flexure and shear strengthened RC beams, the same amount of NSM reinforcement provides higher load bearing capacity and higher deflection up to failure compared to EB, mainly because of the larger bond surface and the improved anchorage capacity of the FRPs
- NSM reinforcement can be more easily anchored into adjacent members to resist end peeling and debonding failures. This advantage is particularly attractive for the strengthening of members in which the maximum moments may occur at their ends, such as flexural strengthening of beams and columns in RC frames
- The surface preparation is limited to the cutting of grooves resulting in reduction in the amount of installation work
- Unlike EB, NSM reinforcement can be pre-stressed without anchorage
- The energy required to remove NSM is in many cases much larger than that for EB laminates
- The aesthetic of the strengthened structure is virtually unchanged
- NSM provides a significant decrease of harm resulting from fire, mechanical damages and other effects
- It is suitable to strengthen the negative moment regions of beams and slabs

Moreover, the tensile strength of the FRP materials is better exploited by the NSM technique with much higher utilization factors than those attained in EB systems. This indicates that the use of NSM FRP as a strengthening technique may represent

an interesting alternative to EB plates. However, the installation process in the case of NSM systems is a crucial aspect for its effectiveness: the bonding of strips/bars in grooves by epoxy is more sensitive to detailing of the application and to the curing process of the adhesive than in the case of EB systems [59].

An experimental comparison of the effectiveness of NSM and EB techniques for the flexural and shear strengthening of RC beams can be found in [60]. In this study, the effectiveness was determined in terms of deformation capacity and load-carrying capacity. According to experimental results, NSM showed to be more efficient for flexural strengthening than EB, with the differences in effectiveness reducing as the longitudinal equivalent reinforcement ratio increased. In the case of shear strengthening, NSM was the most effective strengthening technique when CFRP reinforcement was used, being it also the easiest and the fastest to apply. An important observation is that failure modes of beams strengthened with NSM technique were not as brittle as the ones observed in beams strengthened with EB technique.

Shear behavior of RC beams strengthened with NSM CFRP strips, both alone and in combination with EB CFRP strips, was studied in [61]. Experimental results showed an increase in shear stiffness and strength of beams strengthened with a combination of NSM and EB systems when compared to that of beams strengthened only with NSM. The general conclusion of this study was that combining both NSM and EB strips provided better resistance to the applied load and better redistribution of the total stress.

Another comparison of the effectiveness of FRP reinforcement in the NSM and EB strengthening techniques can be found in [59]. According to experimental results, the tensile strength of the FRP materials was better exploited by the NSM technique with much higher utilization factors (36-100%) than those attained in EB systems (approximately 15%), thus indicating that the NSM technique may represent an interesting alternative to EB plates. The NSM technique also allowed higher efficiency factors to be attained against lower axial stiffness.

Besides, bond capacities of NSM and EB using FRP plates were experimentally studied in [62] and, according to the results, NSM was found to develop bond strengths that were 1.5 times those attained in EB. Nonetheless, the scarce knowledge is the main limitation of NSM reinforcement.

A summary of some characteristics and aspects of EB and NSM systems is shown in Table 2.7.

Table 2.7: Characteristics and aspects of EB and NSM [2].

	EB		NSM
	Laminates	Sheets	
Shape	Rectangular strips	Thin uni-directional or bi-directional fabrics	Rectangular strips or laminates
Dimensions: Thickness Width	 1-2 mm 50-150 mm	 0.1-0.5 mm 200-600 mm	 1-10 mm 10-30 mm
Application aspects	For flat surfaces	Easy to apply on curved surfaces	For flat surfaces
	Thixotopic adhesive for bonding	Low viscosity resin from bonding and impregnation	Depends on the distance to steel reinforcement
	Not more than one layer recommended	Multiple layers can be used more than 10 possible	A slot need to be swan up in the concrete cover
	Stiffness of laminate and the use of thixotropic adhesive allow for certain surface unevenness	Unevenness needs to be leveled out	The slot needs careful cleaning before bonding
	Simple in use	Need well documented quality systems	Bonded with a thixotropic adhesive
	Quality guaranteed from factory	Can easily be combined with finishing systems, such as plaster and paint	Possible to use cement mortar for bonding
	Suitable for strengthening in bending	Suitable for strengthening in shear and bending	Suitable for strengthening in bending
	Need to be protected against fire	Needs to be protected against fire	Minor protection against fire
			Protected against impact and vandalism

2.4 Failure modes and mechanisms for NSM FRP

In this section, the possible failure modes of NSM FRP strengthened elements, both at structural and at local level, are listed and analyzed.

2.4.1 Failure modes at structural level

According to the literature, the following failure modes were observed in the case RC members strengthened NSM FRP system:

Crushing of concrete in compression before yielding of the reinforcing steel: in this failure mode, the concrete reaches its crushing strain prior to the yield of the longitudinal steel reinforcement because of over reinforcement. This type of failure is brittle and undesirable [7].

Yielding of the steel in tension followed by concrete crushing: this failure occurs when the area of FRP is sufficient to generate more tension force than the concrete can generate in compression after yielding of steel. In this situation, the under-reinforced section is transformed to an over-reinforced one. Besides, it is entirely dependent on the geometry of the member and on both internal and external reinforcement details. This failure mode is preferable as it provides the greatest warning of failure and leads to a ductile failure, with all materials being used up to their capacity [7].

FRP rupture before yielding of steel: in this failure mode, the FRP reaches its tensile strength when long bonded lengths are combined with low FRP reinforcement ratio. Due to the fact that FRP strips provide lower cross-sectional area when compared with bars, FRP rupture is more likely to occur for the NSM strips than the NSM bars [63]. Despite FRP rupture represents the most economical use of the FRP material, it is the least desirable from design perspective due to its sudden and violent manner. Structures strengthened with prestressed FRP more frequently fail by fiber tensile rupture because after prestressing the FRP a portion of its strain capacity is used [1].

Yielding of the steel in tension followed by FRP rupture: this failure allows for the full utilization of steel reinforcement and provides some ductility. Even after yielding of steel, the contribution of the FRP reinforcement provides some flexural rigidity. Since the FRP behavior is linearly elastic, this failure mode is brittle as compared to typical under-reinforced RC beams [7].

FRP debonding: this failure can be observed in both shear and flexural strengthening applications, and may occur when the designed strengthening system cannot reach its full capacity due to the propagation of shear and/or flexural cracks or due to the concentration of stresses near the ends of the FRP [64]. This type of failure is very brittle, sudden and clearly undesirable [7, 65]

Shear/tension delamination of the concrete cover: also known as delamination of concrete cover. this failure mode can occur if the force in the FRP cannot be sustained by the substrate. Such behavior is generally sudden and undesirable. This failure mode can be prevented by limiting the maximum stress allowed on the FRP [7].

Splitting of the adhesive cover: this failure mode may occur due to high stresses, either radial stresses for bars or shear stresses for strips, that cause the failure in the adhesive adjacent to the FRP-adhesive interface, resulting in splitting of the adhesive around the FRP reinforcement [9]. This failure mode is undesirable.

In practical design situations, to increase the probability of failure in the concrete before bond failure or tensile rupture of the FRP, the ultimate strain in the FRP is typically limited to a value of 70% of the manufactures' guaranteed ultimate tensile strain [6]. In addition, concrete crushing and internal steel yielding, internal steel yielding and FRP rupture or internal steel yielding and FRP debonding are the expected failure modes when the strengthening system is well designed, being, concrete crushing combined with steel yielding the preferred mode of failure because it provides the greatest warning of failure. [6, 64].

2.4.2 Failure modes at local level

From the existing studies on the NSM FRP bond behavior, four distinct local failure modes, which at the end lead to the previously mentioned failure modes at structural level, have been identified (see Figure 2.13):

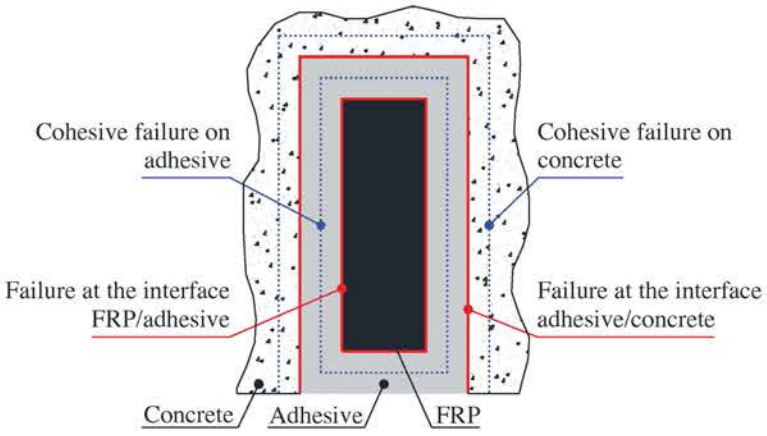

Figure 2.13: Four possible failure modes associated with debonding phenomenon [64].

Bond failure at FRP-epoxy interface: this failure mode may occur, as pure interfacial failure, depending on the adhesive properties, FRP surface characteristics,

bonded length and the confinement in the transversal direction. The pure interfacial failure mode is critical when the degree of surface deformation is not enough to provide an appropriate mechanical interlocking between FRP reinforcement and epoxy adhesive. In this case the bond resistance relies primarily on the adhesion between materials [9].

Cohesive shear failure in the epoxy layer: this failure mode occurs when the shear strength of the epoxy is exceeded, and depends mainly on the adhesive properties and the degree of transverse confinement. This local failure mode was observed for NSM strips with a roughened surface [66].

Bond failure at concrete-epoxy interface: this failure mode occurs as pure interfacial failure between epoxy and concrete substrate. This failure mode is typical in pre-cast grooves and, in general, in grooves with smooth surface and depends on concrete and adhesive properties, bonded length and the confinement in the transversal direction [9, 64].

Cohesive shear failure in the concrete: this failure mode may occur depending on the degree of concrete confinement and its mechanical properties. This failure mode has rarely been found in bond tests, but it has been observed in bending tests either at the strengthened region [67] or at bar cut-off point [63].

2.5 Bond between FRPs and concrete

Bond behavior between FRP and concrete is a fundamental property of the FRP strengthening techniques. Bond is considered the key factor that controls the success and the efficiency of the strengthening system as it is responsible of the composite action development between FRP and concrete. Besides, for RC strengthened members, bond behavior influences the ultimate capacity of the element, as well as its serviceability behavior in terms of crack width and crack spacing [9, 10, 64, 68].

2.5.1 Factors affecting bond behavior of NSM

Bond in NSM FRP strengthened elements may be influenced by the mechanical properties of the involved materials (adhesive, FRP and concrete), as well as by the geometry of the strengthening system (FRP dimensions, groove geometry and groove location, among others) [9, 64, 69–72]. Additionally, the type of load and its period of application, along with the environmental conditions can interact with the aforementioned factors.

2.5.1.1 Concrete strength

Literature review on experimental programs reveals that concrete strength had no effect on the ultimate failure load when the failure mode was not cohesive within concrete [73, 74]; in contrast, it plays a critical role on the bond properties between the NSM FRP reinforcement and concrete in the case of specimens with short bonded length [75].

The bond behavior of NSM FRP system was investigated through beam tests carried out on RC beams strengthened with NSM CFRP laminates using different bonded lengths (40 mm, 60 mm and 80 mm) and concrete strengths of 35 MPa, 45 MPa and 70 MPa [27, 76]. Results revealed that the concrete strength had practically a marginal influence, for the bonded lengths used, on the bond strength of NSM strip and concrete.

In the work carried out in [77], the effect of concrete strength on the bond between NSM CFRP strips and concrete was studied through pull-out tests performed on concrete blocks strengthened with NSM CFRP strips; the concrete strength used varied from 30 MPa to 65 MPa, while the bonded length ranged from 100 mm to 350 mm. The experimental results showed that the failure load increased with the increase in the concrete strength.

The experimental results reported in [78] indicated that changing the concrete strength from 22 MPa to 42.2 MPa had no effect on the load capacity of the specimens tested when epoxy splitting or bar-epoxy interface failure took place.

2.5.1.2 Bonded length

Several studies were carried out to investigate the effect of the bonded length on the behavior of concrete strengthened with NSM technique. Most of them reported that increasing the bonded length increased the ultimate pull-out load [10, 27, 33, 67, 76, 79–83] as well as the debonding resistance of the strengthened system [62, 63]; however, results presented in [77] showed that there is a limit in this increasing with failure load plateauing for bonded lengths larger than the effective one, after which any increase in the bonded length did not affect the load carrying capacity of the system. Moreover, the average bond strength decreased, due to the non-uniform distribution of the bond stresses along the bonded length.

2.5.1.3 Groove dimensions and surface configuration

Several studies investigated the effect of groove size on the bond performance in the case of concrete strengthened with NSM system to consequently determine optimized groove dimensions.

The effect of groove size on the bond of NSM system using round GFRP bars and rectangular preformed groove was investigated and reported in [33, 67]. The results obtained showed that the bond capacity increased with increasing the groove size. Based on this study the groove size was recommended to lie between 1.5 to 2 times the bar diameter. Increasing the groove width changed the failure mode from cohesive failure in the epoxy to be in the concrete surrounding the groove. Further increase in the groove width caused splitting failure at the epoxy concrete interface.

Experimental results reported in [84] showed that increasing the groove depth from 12 to 16 and 20 mm increased the slip from 0.25 to 0.74 and to 1.09 mm, respectively, and the average bond strength increased from 7.4 MPa to 10.3 MPa and to 11.1 MPa, respectively. For round cross-sectional bars, it was reported that the ultimate load increased with the increase of the groove size. Also if the failure was by concrete splitting, the average bond strength increased [33].

Based on the experimental results [85], an adhesive thickness of 1 mm to 2 mm in case of CFRP strips was proposed. Other researchers [47] suggested a minimal groove size of 3 times the strip thickness and 1.5 times the strip height, and for round cross-sectional bars they suggested a minimal groove size of 1.5 times the bar diameter, as shown in Figure 2.14.

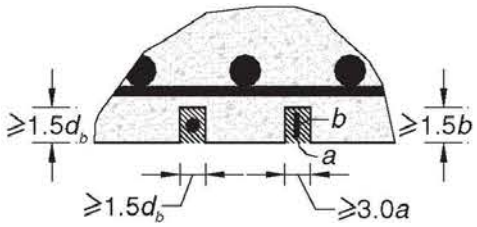

Figure 2.14: Minimum dimensions of groove [47].

Experimental results reported in [86] showed that increasing the groove size for specimens with epoxy adhesives had no influence on the failure load while the failure load decreased with increasing the groove size for specimens with cement adhesives due to higher shrinkage of cement in bigger grooves.

Results presented in [69] showed that increasing the groove width to depth ratio, for a given groove depth, caused an increase in bond strength. Besides, increasing the groove dimensions caused a moderate increase in the local bond strength of the NSM strengthened joint. Authors recommended the use of square grooves with groove size to bar diameter ratio (k) equal to 2.

Moreover, the minimal groove width was defined to be 1.5 to 2 times the bar diameter for bars with either plain or deformed surface, and the minimal groove depth was proposed to be 3 mm larger than the bar diameter [9]. On the other hand, results reported in [74] stated that the groove width to nominal rod diameter ratio ranging between 1.7 and 2.5 appeared to be optimal.

The experimental results reported in [82] revealed that increasing groove width increased the failure load regardless of FRP properties and the surface treatment. The percentage of increase was small (approximately 8.85%) either due to bar-epoxy interface failure in the case of NSM CFRP bars or epoxy splitting in the case of NSM GFRP bars.

The groove surface coating is dependent on the groove manufacturing process, getting rough surfaces when groove is cut after concrete curing and smooth surfaces when the groove is obtained by installing plastic strips with desired dimensions at the bottom of the mold before casting [67]. Rough surfaces not only are considered to be more realistic, but also provide better bond characteristics as smooth surface is more prone to failure in the concrete-adhesive interface [64].

2.5.1.4 Groove filling material

The two main groove fillers are the epoxy based and the cement based adhesives. Several studies have investigated the effect of groove filling material on the bond of NSM FRP strengthened elements, showing that epoxy adhesives provide better mechanical performance as groove filling materials [9, 80, 86].

The experimental program presented in [80] showed that specimens with epoxy filled grooves had higher bond failure loads than the cement filled ones. The authors attributed this to the higher tensile strength of epoxy that delayed the formation of the longitudinal splitting crack in the cover allowing the normal pressure between FRP reinforcement and surrounding material to be fully developed. Furthermore, experimental results reported in [86] showed that specimens with cement adhesives showed a failure load of about 40% to 56% of the failure load provided by specimens with epoxy adhesives.

Experimental results reported in [87] showed that the maximum bond stress of concrete strengthened with NSM CFRP strips was independent of the type of the applied adhesive. On the other hand, the adhesive type and its properties were found to have a great influence on the bond characteristics in case of NSM FRP bars [82, 88].

The use of cement based adhesives, with relatively low shear strength, resulted in a reduction in the adhesion capacity to the FRP; in addition, their shrinkage needs to be controlled [33]. Besides, in the case of application of cyclic loading, the cementitious adhesives are not recommended. However, they can be used under static load conditions [89]. On the other hand, the use of cement based adhesives can be advantageous concerning fire and environmental protection. Moreover, epoxy adhesives are expensive and should be carefully applied considering health and environmental aspects [18].

2.5.1.5 FRP reinforcement characteristics

FRP characteristics, such as fiber type and area (which provide the reinforcement stiffness), cross-sectional shape and surface configuration, influence the bond of NSM FRP system [70] and may be considered as a key parameters in the bond-slip law. Besides, the geometrical properties of FRPs, as the ratio between perimeter and cross-sectional area, have an important role in the bond-slip response of the connection and the maximum pull-out load [90].

Experimental results, such as those reported in [59, 78, 86, 91], showed that the ultimate capacity of NSM FRP system is dependent on the fiber type and its surface pattern. The lowest load carrying capacity was obtained when BFRP bars with sand coated surface were used, while smooth CFRP bars provided the highest load carrying capacity, and a moderate range of load carrying capacity was observed in case of NSM reinforcement with spirally wounded GFRP bars. The failure modes observed were debonding at the epoxy-concrete interface and debonding at the bar-epoxy interface for BFRP and GFRP bars, respectively, while a combination of debonding at the epoxy-concrete interface and detachment of a concrete layer was observed in the case of CFRP bars. Different failure modes were observed and reported in [82, 83], according to the fibers used; in this sense, bar-epoxy interface failure was found in specimens with NSM CFRP bars, while epoxy splitting and bar damage was observed in specimens with NSM GFRP bars.

FRP reinforcement provides several surface treatments such as plain, sand blasted, sand coated, ribbed and spirally wounded surface patterns. The surface condition

of the FRP rods influences the bond strength, with deformed rods appearing to be more efficient than sand blasted rods, from the standpoint of the bond properties [10, 67].

In the study reported in [80], the effect of the surface configuration of CFRP bars on the bond properties of NSM FRP reinforcement strengthening systems was investigated. According to experimental results, CFRP ribbed and CFRP spirally wounded bars were the preferable types for NSM FRP reinforcement.

The effect of FRP bars surface configuration and surface treatment on the bond strength of NSM FRP bars in concrete was studied and reported in [71]. Experimental results showed that the highest pull out force was recorded in the case of ribbed CFRP round bars, due to the increase in the mechanical interlocking force allowing the specimens to resist more pull-out force. On the other hand, specimens with sand coated displayed less pullout force than the ribbed ones but higher than the roughened bars. Different failure modes were observed for each surface configuration. Epoxy splitting accompanied by cracks in the concrete cover along the bonded length was observed for the sand coated specimen. However, cohesive failure in the epoxy cover and concrete cover along the bonded length was observed for the specimens with ribbed bars. Specimen with roughened bars failed due to epoxy splitting and breakage of concrete cover.

Another experimental study reported in [92] investigated the effect of surface treatment on the bond of CFRP rods in concrete. Results were compared to those of steel bars showing that the bond between smooth CFRP rods and concrete was significantly lower than the bond between smooth steel bar and concrete due to the low roughness of the smooth CFRP rods in comparison with the roughness of steel. On the other hand, the ultimate bond strength of both machined and sanded CFRP rods could reach twice that of ribbed steel bars. Moreover, the residual friction between the CFRP rods and the concrete remained equal to or greater than that found for ribbed steel bar.

Experimental results reported in [93] revealed that the bond strength between FRP reinforcement and concrete was mainly influenced by the axial stiffness and the surface texture of the NSM FRP systems. It was observed that the experimental failure load increased as the axial stiffness increased until a certain value, and that for the NSM FRP systems characterized by similar axial stiffness, the ribbed surface allowed the transfer of higher loads compared to the sand-coating treatment.

Results of the study reported in [94] showed that smooth CFRP bars, with no surface treatment, developed a bond law similar to that of GFRP bars. Moreover, CFRP strips developed larger slip in the bond-slip relationship, when compared with CFRP

bars of similar modulus of elasticity and smooth surface, leading to a more ductile global response in terms of load-displacement relationship. This can be explained by the larger bond perimeter and the higher confinement provided by the surrounding concrete in the case of the strips.

The cross-sectional shape of FRP reinforcement is an additional parameter influencing the bond between FRP reinforcement and concrete. FRP reinforcement can be manufactured either in the shape of bars or strips. As indicated previously FRP bars can be available in circular, rectangular, square or oval cross-section, while FRP strips have a rectangular cross-section with a large aspect ratio. In the case of FRP bars, square bars seem to be the most effective shape for NSM reinforcement, in comparison to circular bars, due to its cross-sectional area to perimeter ratio [72]. Furthermore, FRP strips were found to be more effective, compared to FRP bars in NSM reinforcement [23, 95], and strip cross sectional area was found to have a great effect in increasing the pull-out force [71]. The pull-out load significantly increased with the increase of the strip height, due to the more confinement provided with increasing the groove depth; this additional confinement was confirmed by the splitting failure (Figure 2.15) [77]. The increase in the strip thickness from 1.2 to 2.4 mm resulted in an increase in the pull-out load, not only due to a larger bond surface but also due to a larger cross-sectional area (that reduces the deformation capacity).

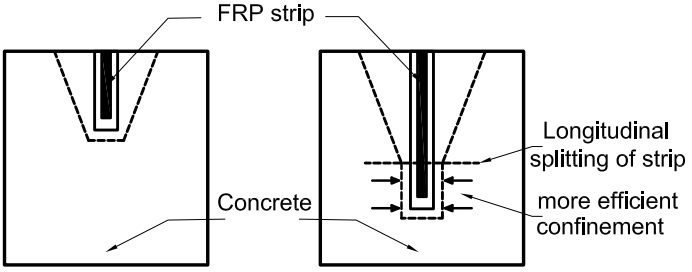

Figure 2.15: Change of the failure plan with increasing the strip height.

2.5.2 NSM bond test methods

Pull-out tests are typically used to determine bond capacities and concrete splitting resistance along the reinforcement. Direct pull-out test and beam pull-out test (Figure 2.16) are considered the most common types of bond tests. Despite the availability of different test setups in the literature for each of the two bond tests [96], the presence of a standard configuration for both tests is critical aspect in the analysis of bond in NSM systems. It is worth mentioning that the strengthening technology is related with evaluation of the quality of the concrete cover and that specimens produced in the laboratory may have mechanical properties that differ

from those provided in real strengthening situations [97]. In this section, the tests of elements made only of a new concrete are discussed.

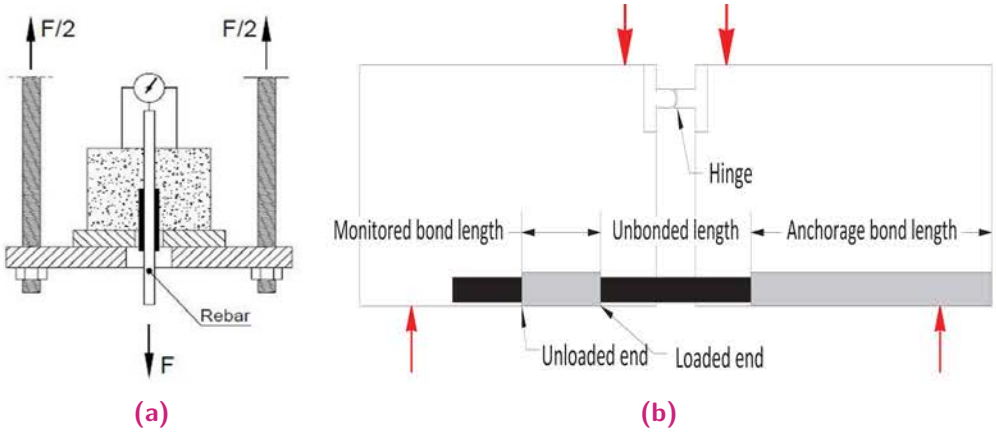

Figure 2.16: Schematic representation of pull-out tests (a) Direct pull-out test (b) Beam pull-out test [18].

2.5.2.1 Beam test

In the case of beam tests, specimens consist of one or two prismatic blocks. If one block is used, it has usually a hinge at the compression flange in the middle of the span (see Figure 2.17). If two blocks are used, they are joined by a hinge in the compressed flange and by the tested reinforcement in the tension side (see Figure 2.16b). In this setup, the overall length of NSM reinforcement can be divided into three lengths; the monitored bonded length, which is the studied bonded length, symmetrically to this we can find the anchorage bonded length, where the tensile forces from the reinforcement are reacted, and finally, the unbounded length, that is located in the middle of the span separating the previously mentioned lengths. In order to ensure the failure in the monitored bonded length, the anchorage bonded length has to be longer than the monitored one or additional confinement has to be provided. The slip of the reinforcement at both the loaded and unloaded ends, as well as the deflection of the beam, can be measured using LVDTs. Strains in the reinforcement can be measured along the bonded length or at the unbonded length to evaluate the bond stress-strain behavior. Beam tests can be carried out either in displacement or in force controlled modes. However, the displacement controlled mode is recommended if the post-peak behavior is to be observed [18].

The bond of NSM system was investigated and reported in [67] through testing unreinforced concrete beam specimens. In order to provide a larger tension area to prevent flexural cracking, an inverted T-shaped cross section was selected. The distribution of the internal forces was controlled through hinge placed at the top and

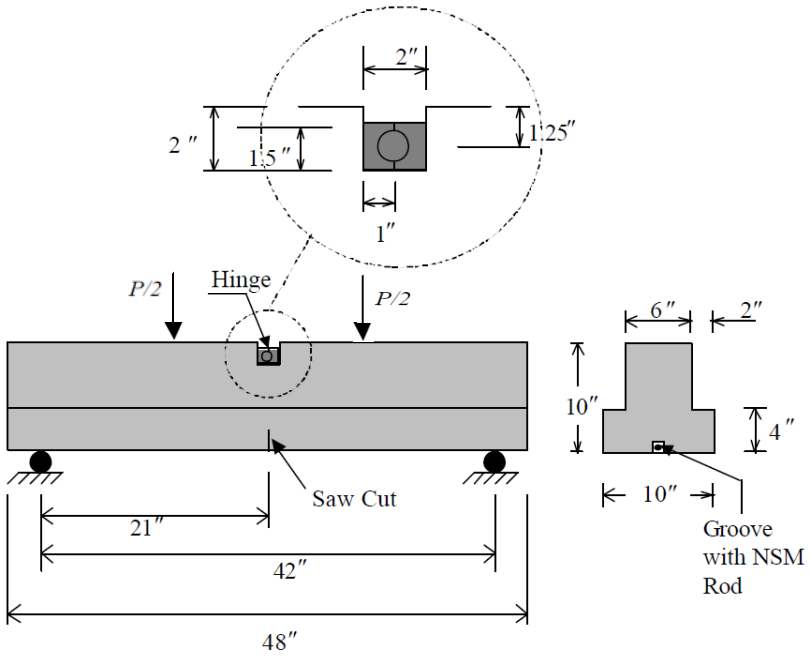

Figure 2.17: Test specimen configuration and test setup for beam pull-out test using one block [67] (units in inches).

a saw cut at the bottom of the specimen (see Figure 2.17). In this setup, the FRP element used for strengthening was located on the tension side of the beam bonded to the specimens in two regions, one at each side of the saw cut; one part was the test region, in which the bonded length was achieved by letting the remaining length unbonded, while the FRP was fully bonded to the other side to ensure that the failure would occur in the test region. The distance from the starting point of the bonded length to the closest support of the beam should be adopted according to the used bonded length. Internal cracks in the epoxy paste, perpendicular to the direction of the principal tensile stresses, were observed in all the specimens after failure.

Beam pull-out tests were carried out to study the effect of the bonded length and the concrete strength on the bond behavior of NSM CFRP strips [27]. a two blocks specimen with a rectangular cross section was used (see Figure 2.18). Besides, a steel hinge was provided at the upper part and CFRP laminate was bonded to one block along the bonded length forming the test region, while it was fully bonded to the other concrete block, again to ensure the occurrence of the failure in the test region. The failure occurred at concrete-adhesive and adhesive-laminate interfaces, with the formation of cracks in the epoxy paste.

In the work reported in [98], beam pull-out tests were performed to study the bond between CFRP laminates and concrete for both EB and NSM FRP reinforcement using simply supported beams with different spans (see Figure 2.19). Single and double CFRP strips were used as NSM reinforcement and beams were tested under

four point loading. Results showed that the debonding strain was affected by the location of the CFRP bonded length as well as of the bending and shear regions.

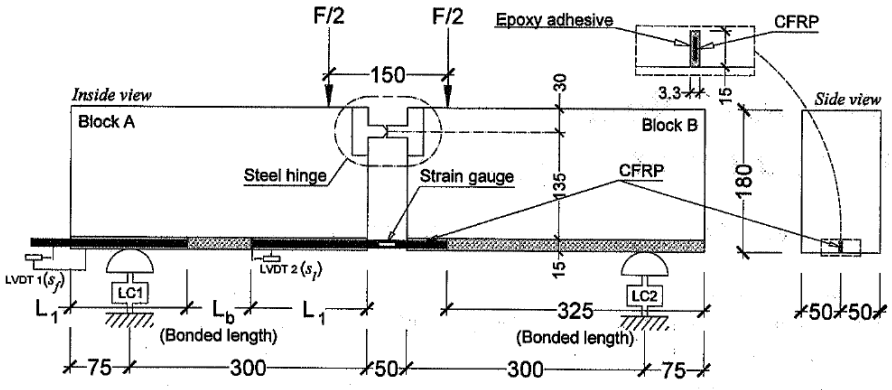

Figure 2.18: Test specimen configuration and test setup used by Sena Cruz and Barros [27] (units in mm).

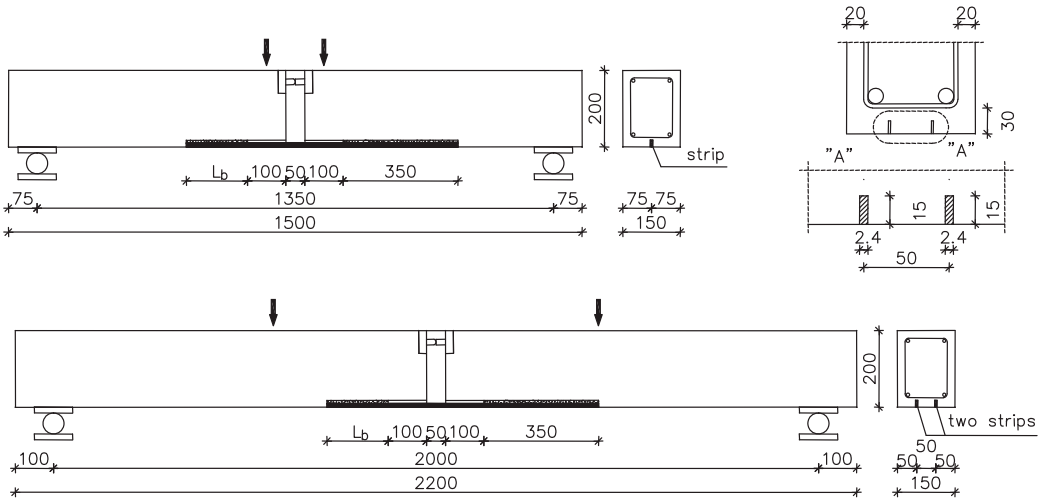

Figure 2.19: Scheme of NSM strengthened beams with single and double CFRP strips [98] (units in mm).

Although beam pull-out tests are more representative for bond behavior of real members, as the effect of member curvature (deflection) can be considered [58, 67], they also have some practical disadvantages such as [10, 64, 95]: (i) relatively large specimens are required, making the specimens to be expensive specially if long bonded lengths are tested; (ii) it is difficult to conduct the test in slip-control mode; and (iii) it is difficult to visually inspect the behavior of the joint during loading, especially the initiation and propagation of cracks.

2.5.2.2 Direct pull-out test

Unlike beam pull-out tests, in which almost the same configuration is typically used, the direct pull-out test has many different and variable configurations.

In order to develop a bond test method for NSM, direct double shear pull-out tests were carried out and reported in [99]. The tested specimens were concrete blocks (152 mm x 152 mm x 203 mm), with two grooves cut in two opposite faces. CFRP sand blasted rods were glued to the concrete by means of a two-component epoxy adhesive. A tensile force was applied to the CFRP rods, while the concrete block was restrained by means of a steel frame (see Figure 2.20). One disadvantage of this test setup is the flexural effect, which may affect both bond behavior and the ultimate load. This flexural effect may be introduced due to a small eccentricity between grooves or rods in the two opposite sides. Besides, being the groove too close to the edge of the concrete block, it may cause edge failure for short bonded length [33].

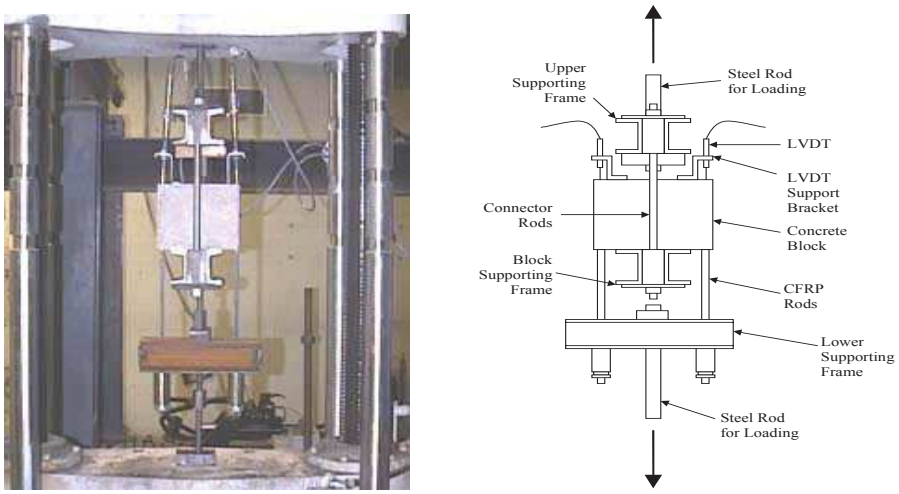

Figure 2.20: Pull-out test setup used by Yan et al. [99].

In order to overcome the drawbacks of conventional single shear specimens (this consisting in a concrete block in which the FRP reinforcement is glued to one side of the specimen), a C-shaped concrete specimen with a square groove in the middle to introduce the FRP bar (see Figure 2.21) was proposed [33]. The proposed C-shaped specimen provided the following advantages; (i) it was possible to measure both loaded and unloaded end slips; (ii) it overcome the eccentricity problems; and (iii) confinement to the FRP reinforcement was provided. On the other hand, the following disadvantages were observed; (i) the proposed specimen had to be designed for each groove depth to ensure that the NSM bar was placed in the center of gravity of the concrete block; (ii) it was not suitable for studying the edge effect, (iii) it was hard to have a proper view of the failure surface; and (iv) it is difficult to

have access to cut the groove and glue the FRP bar/strip. Even so, this configuration was also used in other studies [82, 86, 100].

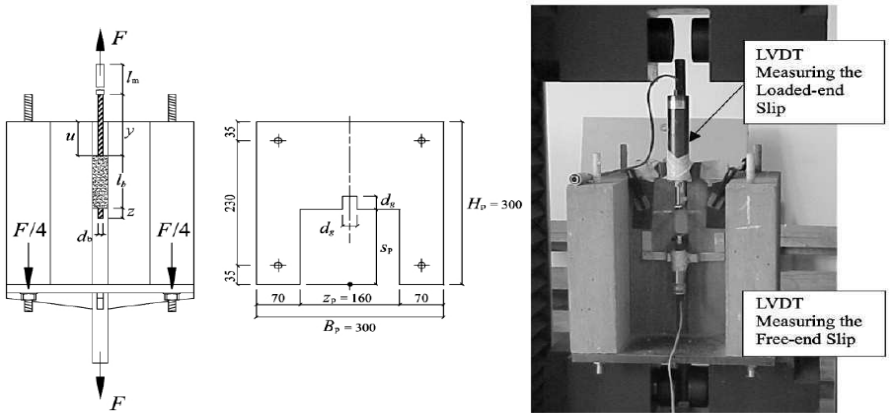

Figure 2.21: C-shaped pull-out specimen [33] (units in mm).

Another alternative specimen to overcome the eccentricity problems was proposed in [101]. The authors performed single shear pull-out tests to L-shaped specimens which provided a proper view of the failure surface with the possibility of measuring both the loaded and unloaded end slips (see Figure 2.22). On the other hand, the problem of specimen size and manipulation was still present.

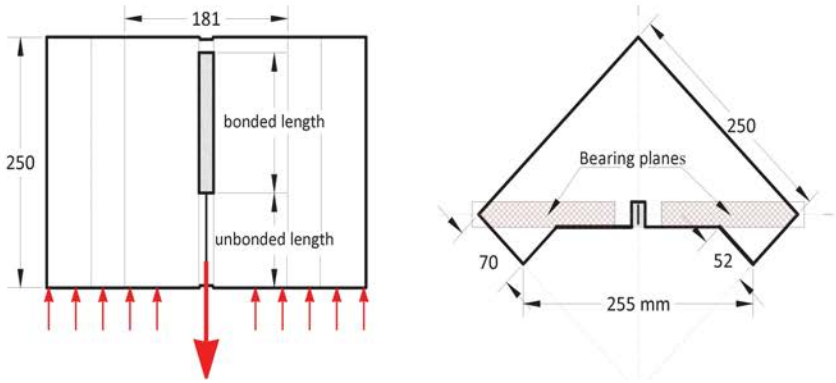

Figure 2.22: L-shaped pull-out specimen [101] (units in mm).

Single shear pull-out tests in which the concrete block was under compression were performed and reported in [81]. In order to interrupt compressive stresses generated between the loading plate and the lateral bar surface, foam sheets were placed parallel to the test bar as a compression field breakers (see Figure 2.23); this made the FRP bar to be subjected to direct tension and therefore provide a better simulation of the normal conditions in the tension zone in flexural beams. Another modification was the presence of strengthening in the tension side of the specimen by means of EB CFRP sheets terminated at a transverse distance of 50 mm from the bar axis, so as to avoid interference with the shear stress-state normally developing along the anchored NSM bar. The modified specimen might overcome the drawbacks of the conventionally eccentric pullout specimens but required additional care, time,

effort and cost. In addition to the reduction in lateral concrete cover, the lack of concrete confinement resulted in relatively low bond stresses.

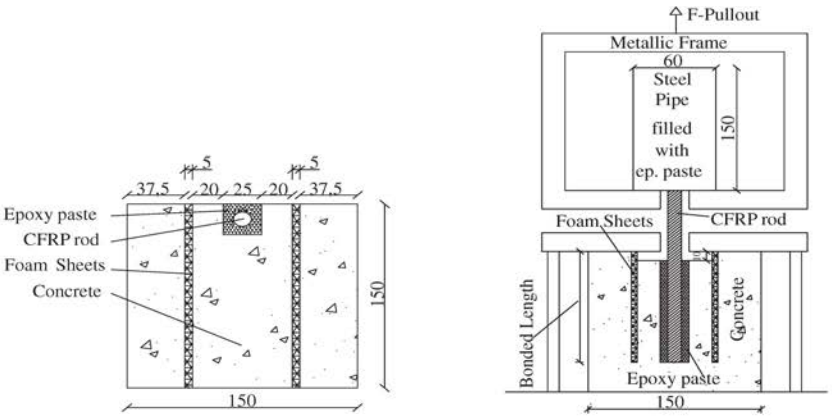

Figure 2.23: Schematic of test specimen and test setup by Novidis et al. [81].

In some experimental studies such as those reported in [91, 93], pull-out tests were carried out including two different test setups: single shear test and double shear test (see Figure 2.24). Concrete blocks of 200 mm x 160 mm cross-sectional area and 400 mm depth were tested under single shear pull-out test, while concrete blocks of 150 mm x 150 mm cross-sectional area and 400 mm depth were assigned for the double shear pull-out test. One or two steel bars were embedded in the concrete prisms to allow anchorage and application of load. The bonded length of CFRP rods/strips was 300 mm and started 50 mm apart of the loaded end to avoid local premature failure of concrete. Again the alignment and eccentricity of double shear pull-out test specimen were the main problems, in addition to the size of the specimens that made it hard to be manipulated. In both test setups used in this study, single shear setup and double shear setup, the embedded steel rod may have an influence on the bond strength.

Figure 2.24: Test setups a) Double-shear b) Single-shear [91].

Irrespective the test setup to be single or double shear pull-out test, the specimens can be subjected to either tension or compression stresses (see Figure 2.25). The failure load is expected to be higher for concrete specimens subjected to compression stresses due to concrete confinement. The effect of this confinement can be avoided by starting the bonded length leaving a suitable unbounded distance from the top of concrete [64, 77, 81].

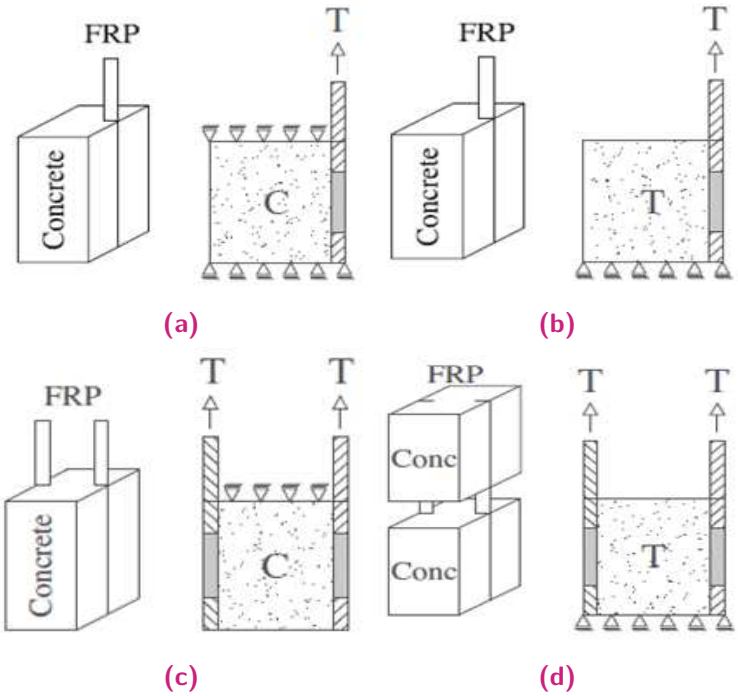

Figure 2.25: DPT configurations: single-shear test(a) compression and (b) tension; double-shear test (c) compression and (d) tension.(C: compression; T: tension) [64].

In compression direct pull-out tests, concrete cohesive failure is generally observed, described by a concrete layer attached to the composite element (FRP/adhesive) after failure. For the case of tension tests, the concrete cohesive failure is characterized by a wedge of concrete starting from the unloaded end of the connection to its loaded end [64].

To summarize, it is clear that different test types, configurations, and setups are available to study the bond behavior of NSM FRP reinforcement systems, each having advantages and disadvantages. The suitable test type, setup and specimen configuration should be selected carefully, depending on the test conditions and parameters to be studied, as they may have an influence on the output results [102]. Although the beam pull-out test is said to be more representative of real conditions and suitable for long bonded lengths, its setup is more complicated, requires more effort in experimental work and additionally it is difficult to inspect the tested zone during the tests; it also has the difficulty of carrying out the test under displacement-control mode. Direct pull-out test is a suitable alternative to avoid

disadvantages of beam pull-out tests, with the advantages of a more manageable specimen size, reduced material use, less expensive, and the ability to perform a high number of tests. However, it has disadvantages such as possible eccentricity of the reinforcement and difficulties with gripping of the reinforcement at load application end [18]. Direct pull-out tests can be divided into two main types: single-shear pull-out test, in which one concrete block is used and the FRP bar/laminate is bonded to one face of the specimen having the advantage of simple preparation; and double-shear pull-out test, in which one or two concrete blocks are used and the FRP bar/laminate are bonded to two opposite faces of the specimen. Although double-shear pull-out test is considered a way to overcome the eccentricity of the reinforcement in single-shear pull-out test, it has the following disadvantages; (i) small eccentricity between grooves of placement of reinforcement in the opposite faces may cause flexural effects on the bond behavior; (ii) measurements should be taken in both reinforcements; and (iii) the capacity of the connection may be affected due to the embedded steel bars.

2.6 NSM FRP bond models

Several bond models have been proposed to simulate and predict the bond behavior of the NSM FRP reinforcement system. A number of the existing NSM bond models are based on local bond-slip curves derived empirically from bond tests [67]. Some of them were derived based on experimental data from direct pull-out tests [66, 103], whilst others were based on results obtained from beam tests [67, 104]. In addition, finite element models have also been built by several researchers [63, 79, 80].

A closed-form analytical solution to predict the interfacial shear stresses for NSM FRP strips was introduced by Hassan and Rizkalla [63]. The proposed model was based on the combined shear-bending model developed by Malek et al. [105] for EB FRP plates. The model was modified to account for the double bonded area of NSM strips and the continuous reduction in flexural stiffness due to cracking of the concrete. The main assumptions for this model were that the shear and bending stresses could be investigated separately and the debonding was assumed to occur due to high shear stress concentration. The model was developed considering the equilibrium of an infinitesimal portion of the strengthened concrete beam as shown in Figure 2.26. The model was validated by comparing the predicted values with experimental test results.

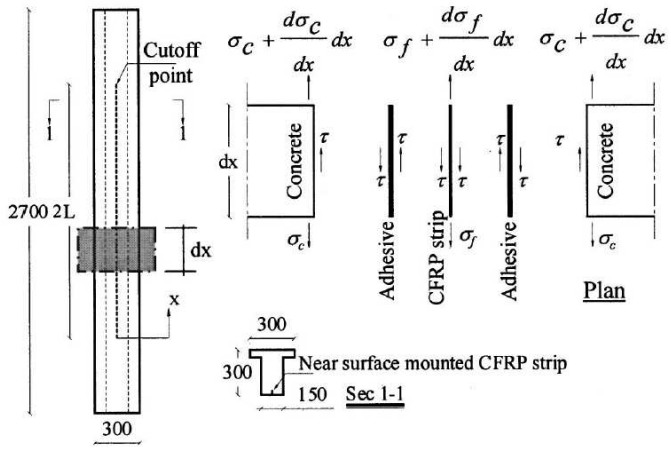

Figure 2.26: Infinitesimal portion of NSM strengthened concrete beam modeled by Hassan and Rizkalla [63].

The aforementioned closed-form analytical solution reads:

$$\tau = \frac{t_f}{2}\left[\frac{n\,P\,L_0\,y_{eff}}{2\,I_{eff}}\,\omega\,e^{-\omega X} + \frac{n\,P\,y_{eff}}{2\,I_{eff}}\right] \tag{2.1}$$

where τ is the shear stress, t_f is the thickness of FRP strip, n is the ratio between the modulus of elasticity of FRP to that of concrete, P is the applied concentrated load, L_0 is the unbonded length of the FRP strip, y_{eff} is the distance from the FRP strip to the neutral axis of the section, I_{eff} is the effective moment of inertia of the section and ω is expressed by Equation 2.2,

$$\omega^2 = \frac{2\,G_a}{t_a\,t_f\,E_f} \tag{2.2}$$

where G_a and t_a are the shear modulus and thickness of adhesive, respectively, and E_f and t_f are the elasticity modulus and thickness of FRP strip, respectively.

Kanakubo et al. [106] introduced new formulas for predicting the bond strength between FRP laminates and concrete, differentiating whether the bonded length was longer or shorter than the effective bonded length. For each case, the proposed formula was developed by solving the second differential equation of bond problem using Equivalent Bond Stress Block (EBSB), which was defined such that the bond stress distribution had the same area with the actual bond stress distribution. The bond stress was assumed as a constant value throughout the bonded region.

Hassan and Rizkalla [79] proposed an analytical bond model to evaluate the development length of NSM FRP bars, assuming linear elastic behavior for concrete, adhesive and FRP. The main philosophy of the proposed approach was to provide rules to preclude significant amount of plasticity in the concrete and adhesive surrounding the NSM FRP bar. Constant bond stress distribution was assumed along

the anchorage length, and transfer of stresses from deformed NSM FRP bar to the concrete was assumed to be mainly through the mechanical interlocking of the lugs to the surrounding adhesive. The proposed model was validated by comparing the predicted values with results obtained from both experimental and nonlinear finite element modeling.

A model to predict the debonding resistance of NSM joint was introduced by Seracino et al. [77]. The was optimized using a nonlinear regression analysis. The debonding failure load (P_{IC}) could be estimated through the following formula:

$$P_{IC} = \alpha\,\beta\,\sqrt{f_c}\,d_p^{1.36}\,b_p^{0.21} \;\leq\; f_{rupt}\,d_p\,b_p \tag{2.3}$$

where α is a factor equal to 0.19 and 0.16 for the mean and characteristic values, respectively; β= 1 in the case of bonded length (L_b) more than or equal to 200 mm and β= L_b/200 for L_b less than 200 mm; and f_c is the concrete compressive strength. The adhesive properties were not considered in the proposed model.

In the work reported in [103], a closed form analytical expression was presented to estimate the debonding resistance of adhesively bonded plate to concrete joint. The model was a function of geometric and materials properties and was derived using the idealized linear softening bond-slip model shown in Figure 2.27. This model did not take into account the the properties of the adhesive assuming that the adhesive was sufficiently strong and stiff.

The model assumed a bond failure initiated by intermediate cracks with a bond failure plane located at concrete-epoxy interface (see Figure 2.28). The confinement effect of the concrete cover, the concrete strength and the axial stiffness of the plate were the main parameters considered in that model. The model can be applied to any bonded plating technique and plate material. The debonding failure load (P_{IC}) can be calculated according to the following equations:

$$P_{IC} = \sqrt{\tau_{max}\,\delta_{max}}\,\sqrt{L_p\,(EA)_p} \tag{2.4}$$

$$\tau_{max} = (0.802 + 0.078\,\varphi)\,f_c^{0.6} \tag{2.5}$$

$$\delta_{max} = \frac{0.0976\,\varphi_f^{0.526}}{0.802 + 0.078\,\varphi_f} \tag{2.6}$$

$$\varphi_f = \frac{d_f}{b_f} \tag{2.7}$$

where τ_{max} is the maximum bond stress (MPa), δ_{max} is the maximum slip (mm), L_p is the perimeter of the failure plan (mm), $(EA)_p$ is the axial stiffness of FRP plate (N), d_f and b_f are the lengths of the failure planes perpendicular and parallel to the concrete surface (mm), respectively, and f_c is the concrete compressive strength (MPa).

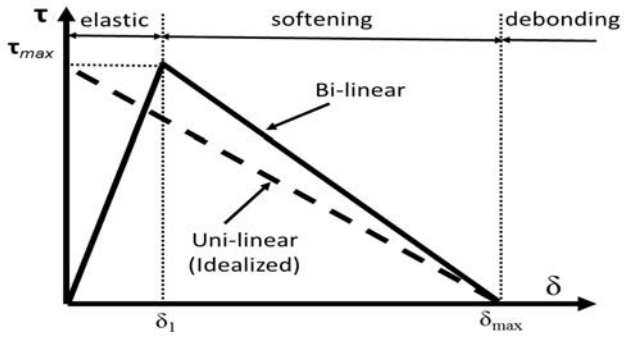

Figure 2.27: Bond-slip model of plate to concrete joint [103].

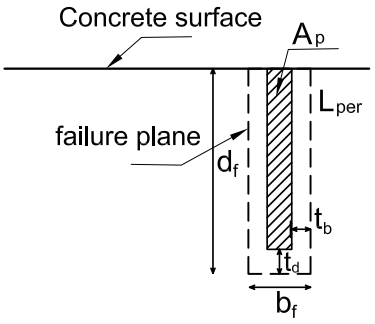

Figure 2.28: Failure plane assumed by Seracino et al. [103].

Ali et al. [107] developed a mathematical model, as well as design equations, to predict the intermediate crack debonding capacities of NSM plates. The mathematical model previously proposed by Yuan et al. [108] for EB plates was reformed for NSM plates. The fundamental equation governing the bond of NSM strip in concrete was solved using the two different interface bond characteristics shown in Figure 2.27: the bilinear bond-slip model and the simplified unilinear bond-slip model. The developed model showed good agreement with the experimental data.

Zhang et al. [109] proposed a bond strength model for NSM CFRP strips bonded to concrete, applicable to cases where debonding occurs due to cohesive failure in the surrounding concrete. The bond strength (P_U) was calculated using the following formula:

$$P_U = \sqrt{2G_f\, E_f\, A_f\, C_{failure}} \;\leq\; P_t \quad where \quad L_b \geq L_e \tag{2.8}$$

$$P_U = \beta_L \sqrt{2G_f\, E_f\, A_f\, C_{failure}} \leq P_t \quad where \quad L_b < L_e \tag{2.9}$$

$$G_f = 0.4\,\gamma^{0.422}\, f_c^{0.619} \tag{2.10}$$

where G_f is the interfacial fracture energy (N/mm), L_b and L_e are the provided and the effective bonded lengths (mm), respectively, E_f and A_f are the modulus of elasticity (MPa) and the cross sectional area (mm^2) of CFRP strip, respectively, $C_{failure}$ is the groove perimeter (mm), β_L is a reduction factor, P_t is the tensile capacity of the CFRP strip (kN), γ is the groove height to width ratio and f_c is the concrete compressive strength (MPa).

Another model, based on the fracture energy equation, for NSM CFRP strips-to-concrete bonded joint was developed and reported in [110]. The bond-slip model was based on the results of a 3D finite element parametric study. The bond-slip relationship was proposed to be in the following form:

$$\tau = A(\frac{2B - s}{B})^2\, sin(\frac{\pi}{2}\frac{2B - s}{B}) \qquad where \quad s \leq 2B \tag{2.11}$$

$$\tau_{max} = 1.15\,\gamma^{0.138}\, f_c^{0.613} \tag{2.12}$$

$$A = 0.72\,\gamma^{0.138}\, f_c^{0.613} \tag{2.13}$$

$$B = 0.37\,\gamma^{0.284}\, f_c^{0.006} \tag{2.14}$$

where τ is the bond stress (MPa), s is the slip (mm), τ_{max} is the maximum bond stress (MPa), γ is the groove height to width ratio and f_c is the concrete compressive strength (MPa).

2.6.1 Maximum local bond stress

In this section, different formulas to calculate the maximum local bond stress, in the case of NSM FRP system, are presented.

Hassan and Rizkalla [63] proposed a formula to determine the maximum local bond stress for NSM FRP strip considering cohesive shear failure in the concrete. Based on the assumption that the epoxy adhesive and the CFRP strips have larger shear strength and adhesion properties compared to concrete and assuming also that the failure of NSM CFRP strips was governed by the shear strength of the concrete, the maximum local bond stress (τ_{max}) could be determined by the following expression:

$$\tau_{max} = \frac{f'_c\, f_{ct}}{f'_c + f_{ct}} \tag{2.15}$$

where f'_c and f_{ct} are the concrete compressive strength and tensile strength (MPa), respectively.

Assuming that the failure of NSM CFRP strip system was due to cohesive shear failure in the epoxy layer, Blaschko [66] proposed the following formulation:

$$\tau_{max} = 0.2\sqrt[4]{a'_e}\,\tau_{af} \tag{2.16}$$

where τ_{max} is the maximum local bond stress (MPa), τ_{af} is the shear strength of the epoxy (MPa), and a'_e is the distance between the symmetry axis of the groove and the edge of the concrete block (mm).

It should be noted that the two previously mentioned formulas give very different results as they related the local bond strength according to two different parameters and assumed two different failure modes. In addition, De Lorenzis and Teng [9] reported the following differences between the two formulas: (i) in Blaschko's model, the experimental data was obtained from pull-out bond tests, while those of Hassan and Rizkalla were from flexural tests on RC beams reinforced with bars of different length and (ii) Blaschko's model was calibrated using pull-out test experimental results, while Hassan and Rizkalla derived their model based on Mohr's circle for the pure shear stress state.

In the analytical study by Ali et al. [107], the maximum local bond stress (τ_f) was calculated as follows [77, 103]:

$$\tau_f = 0.54\sqrt{f_c}\, b_p^{0.4}\, t_p^{0.3} \tag{2.17}$$

where f_c is the concrete compressive strength (MPa), b_p and t_p are the width and the thickness (mm) of the CFRP laminate, respectively.

2.6.2 Effective bonded length, development length and anchorage length

The effective or critical bonded length can be defined as the bonded length at which the maximum stress can be attained by a bonded joint, and beyond which a further increase in bonded length does not increase the load carrying capacity of the system [9, 111]. Besides, the development length is the bonded length required to achieve the design strength of the FRP reinforcement in a critical section [6]. Finally, the anchorage length is the shortest bonded length required for FRP reinforcement to resist a given load.

Hassan and Rizkalla [79] proposed the following formulas to estimate the development length of NSM FRP bar in concrete. The minimum development length required for NSM FRP bar to avoid concrete splitting failure could be calculated as:

$$L_d = G_1 \frac{d}{4} \frac{f_{frp}}{\mu f_a} \tag{2.18}$$

while the minimum development length required for NSM FRP bar to avoid epoxy splitting failure can be expressed as:

$$L_d = G_2 \frac{d}{4} \frac{f_{frp}}{\mu f_a} \tag{2.19}$$

where L_d is the development length (mm) required to develop a stress of f_{frp} in the FRP bar (MPa), G_1 and G_2 are coefficients determined from FE analysis, d is the FRP bar diameter (mm), μ is the friction coefficient, f_{ct} and f_a are the tensile strengths of concrete and adhesive (MPa), respectively.

De Lorenzis et al. [80] computed the development length for NSM round bars in case of saw cut grooves. Values predicted with the model were often found to be impractically high. Therefore, the author suggested a better calibration of the post peak local bond-slip, as a significant scatter and irregular behavior were observed in case of splitting failure.

For NSM CFRP strips having a cross section of 1.4 mm $\times$ 10 mm, Sena-Cruz and Barros [104] estimated the development bonded length to be in the range between 80 and 90 mm (less than 10 times the strip height). Moreover, in the case of using CFRP strips having a cross section of 1.2 mm $\times$ 25 mm, Blaschko [66, 85] found that the full development tensile capacity of NSM strip in concrete was achieved experimentally with a bonded length equal to 150 mm, which was approximately 7.5 times the strip height.

According to the analytical work carried out by Seracino et al. [103], the effective (critical) bonded length could be estimated as follows:

$$L_C = \frac{\pi}{2\lambda} \tag{2.20}$$

$$\lambda^2 = \frac{\tau_{max}\, L_p}{\delta_{max}\, (EA)_p} \tag{2.21}$$

$$\tau_{max} = (0.802 + 0.078\,\varphi)\, f_c^{0.6} \tag{2.22}$$

$$\delta_{max} = \frac{0.0976\,\varphi_f^{0.526}}{0.802 + 0.078\,\varphi_f} \tag{2.23}$$

$$\varphi_f = \frac{d_f}{b_f} \tag{2.24}$$

where τ_{max} and δ_{max} are the maximum bond stress (MPa) and the maximum slip (mm), respectively, L_p is the perimeter of the failure plan (mm), $(EA)_p$ is the axial stiffness of FRP plate (N), d_f and b_f are the lengths of the failure planes perpendicular and parallel to the concrete surface (mm), respectively, and f_c is the concrete compressive strength (MPa).

The development length of EB systems can be computed based on several guidelines. ACI 440-2R-08 [6] proposed:

$$L_d = \frac{A_f\, f_{fd}}{\rho_f\, \tau_{avg}} \tag{2.25}$$

where A_f and f_{fd} are the FRP cross-sectional (mm^2) and FRP design tensile strength (MPa), respectively, ρ_f is the FRP perimeter (mm), and τ_{avg} is the average bond strength = 6.9 MPa.

Australian standards [112], in turn, proposed a formula that was mainly developed for rectangular FRP bars.

$$L_d = \frac{\pi}{2\sqrt{\frac{\tau_{max}\, L_p}{\delta_{max}\, (EA)_f}}} \tag{2.26}$$

$$\tau_{max} = (0.802 + 0.078\,\varphi)\, f_c^{0.6} \tag{2.27}$$

$$\tau_{max}\,\delta_{max} = 0.73\,\varphi^{0.5}\, f_c^{0.6} \tag{2.28}$$

$$\varphi_f = \frac{d_f}{b_f} \tag{2.29}$$

where τ_{max} and δ_{max} are the maximum bond stress (MPa) and the maximum slip (mm), respectively, L_p is the perimeter of the failure plan (mm), $(EA)_p$ is the axial stiffness of FRP plate (N), d_f and b_f are the lengths of the failure planes perpendicular and parallel to the concrete surface (mm), respectively, and f_c is the concrete compressive strength (MPa).

To sum up, several models simulating the bond behavior of both EB and NSM FRP reinforcement systems have been presented in this section. It can be seen that the developed bond models seem well suited for modeling the particular test set-up for which they were calibrated, thus made them relatively impractical for wider use. More widely versatile models are required to simulate the bond strength, as well as the bond stress-slip relationship, of concrete strengthened with FRP reinforcement. Moreover, more work is required to analytically predict the effective bonded length in the case of NSM FRP reinforcement system.

2.7 Effect of sustained load and environmental conditions

The existence of sustained loads on certain structural materials and under certain conditions may yield time-dependent increases in strain, known as creep strain, and in some cases corresponding time dependent decreases in stress (relaxation) [11]. The creep strain can be several times larger than the instantaneous strain as it highly depends on the applied sustained loading level, thus giving creep a considerable importance in the structural design. Moreover, creep can continue for a long time, and so it may be an important factor in the long-term performance of adhesive joints. It is therefore important to understand the effect of creep on stresses and strains in a joint [113].

2.7.1 Creep behavior of materials used in NSM technique

Creep is a time-dependent deformation and can be defined as the increase of the strain with time due to constant applied stress and temperature. The creep rate depends on material properties, temperature, applied load and time. The strain versus time relationship at constant stress and temperature is illustrated in Figure 2.29. It can be divided into three stages: primary creep in which the creep rate decreases, secondary creep in which the creep rate is almost constant and tertiary creep where the creep rate increases till creep rupture [113]. Creep rupture occurs due to the quick loose of strength in the tertiary creep stage in which there is an accelerating creep rate due to the accumulating damage and which may only be seen at high temperatures and stresses and in constant load machines.

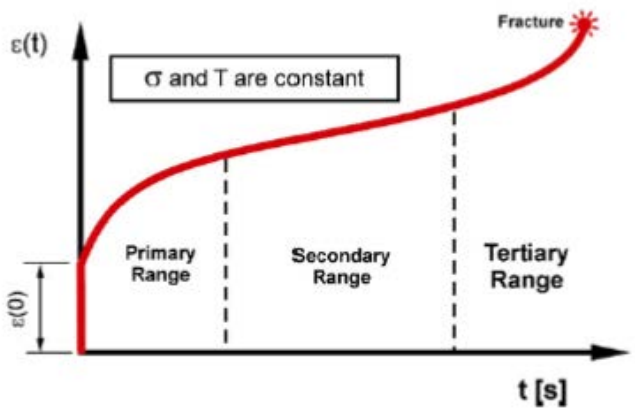

Figure 2.29: Stages of creep [113].

Creep in service is usually affected by changing conditions of loading and temperature and the number of possible stress-temperature-time combinations is infinite. While most materials are subject to creep, the creep mechanisms is often different between metals, plastics, rubber, concrete. When the applied stress is in the linear elastic region, the creep strain is a linear function of stress, which means the creep compliance is independent of applied stress levels and the material is said to be linearly viscoelastic. As the stress level increases, deviation from the linearity can be found indicating a nonlinear behavior. Additionally, the time at which the curves start to become nonlinear decreases with the increasing stress levels [114]. Temperature also is a factor of major interest as the creep rate grows with temperature, moreover, rapid heating as well as rapid cooling accelerates creep [115].

2.7.1.1 Creep of concrete

When concrete is subjected to a sustained stress, creep strain develops gradually with time, as shown in Figure 2.30. Creep increases with time at a decreasing rate. In the period immediately after initial loading, creep develops rapidly, but the rate of increase slows appreciably with time. Creep is generally thought to approach a limiting value as the time after first loading approaches infinity. About 50% of the final creep develops in the first 2-3 months and about 90% after 2-3 years. After several years under load, the rate of change of creep with time is very small [12].

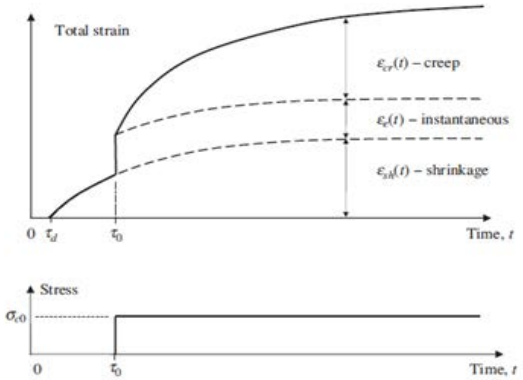

Figure 2.30: Concrete strain components under sustained load [12].

After removing the sustained load, a large amount of creep strain is not recoverable, and therefore this amount is known as residual strain/deformation. [116]. Figure 2.31 illustrates creep strain, elastic recovery, creep recovery, and irrecoverable creep. The main factors affecting the rate and ultimate values of creep of concrete include

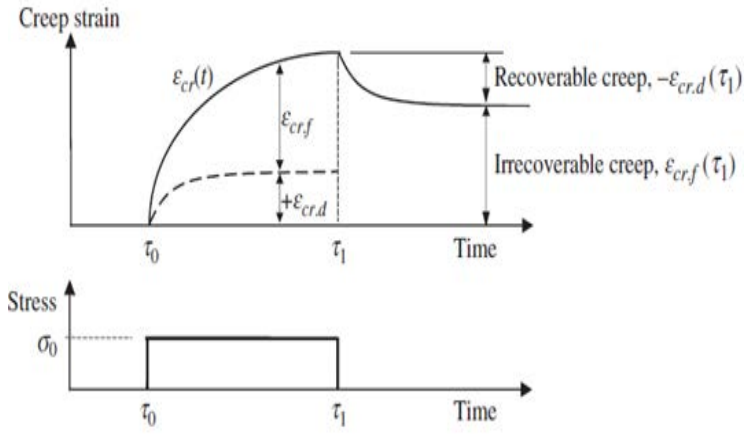

Figure 2.31: Recoverable and irrecoverable creep components [12].

its compressive strength, the stress level at which concrete is subjected to, the environmental conditions during curing and during the life of the structure, the age at loading, and the mix proportions.

Creep in concrete is caused by the rearrangement of calcium-silicate-hydrates, which are the building blocks of cement paste, at the nano-scale. Thus, creep is a function of the volumetric content of the cement paste in the concrete. Additionally, the composing aggregate is another factor that may affect the creep in concrete. Therefore, smaller creep deformation can be observed in concrete made with higher modulus aggregates [11, 117].

Some theoretical models were developed to predict the time-dependent behavior of concrete [118–120], and many codes and guidelines are available to calculate the creep strain in concrete [121–123].

2.7.1.2 Creep of FRP

Creep phenomenon is not limited only to concrete. Structural materials composed of polymers, such as FRPs and adhesives, are also vulnerable to this phenomenon. FRP materials subjected to constant loading over time can suddenly fail after a time period referred to as the endurance time. This type of failure is known as creep-rupture [6].

The creep behavior of FRP composite materials is dependent on several parameters such as the fiber reinforcement's direction, the fiber type and its volume fraction, the type of polymer matrix and the stress history, the applied sustained loading level, temperature and moisture conditions [124].

Several studies have been carried out to investigate the creep behavior of FRPs. Creep rupture tests were performed by Malvar [125] using CFRP, GFRP and AFRP bars. Experimental results revealed that glass fibers were most susceptible to the creep rupture and carbon fibers were the least.

The creep behavior of a carbon fiber/epoxy matrix composite was studied by [126]. CFRP specimens were loaded up to 77% of the ultimate tensile strength and it was observed that the carbon fiber composites were resistant to creep rupture under ambient conditions, as no creep rupture failure was observed.

A simple model, based on a linear viscoelastic approach, was suggested in [127] to predict FRP strain under sustained load. According to the model, the evolution of FRP strains reads:

$$\varepsilon = \varepsilon_0 + \varepsilon_t \, t^n \tag{2.30}$$

where ε is the total strain, ε_0 and ε_t are the immediate and time-dependent strains, respectively, and t is the time after loading in hours.

As an alternative to the previous model, the creep effect of FRP composites can be predicted using the effective modulus of elasticity, following the same approach stated in [6] for creep of concrete

$$E_f(t) = \frac{E_f}{1 + \phi_f(t)} \tag{2.31}$$

where $E_f(t)$ is the FRP modulus of elasticity (MPa) at time t after loading (hours), E_f is the initial FRP modulus of elasticity (MPa) and $\phi_f(t)$ is the creep coefficient, which can be determined through the FRP strains as follow:

$$\phi_f(t) = \frac{\varepsilon_f(t) - \varepsilon_f(t_0)}{\varepsilon_f(t_0)} \tag{2.32}$$

where $\varepsilon_f(t_0)$ and $\varepsilon_f(t)$ are the FRP immediate strain and the strain at time *t* from loading, respectively.

Holmes and Just [128] proposed an alternative approach for the FRP creep coefficient that reads

$$\phi_f(t) = \left(\frac{t}{t_0}\right)^m - 1 \tag{2.33}$$

where *t* is the time in hours after application of load t_0= 1 hour and *m* is the slope of the best fit line relating *log* ε_f(t) and *log*(*t*/t_0).

2.7.1.3 Creep of adhesive

The creep of epoxy adhesives is stress-dependent. In the linear viscoelastic region, the creep strain is a linear function of stress, which means that the creep compliance is independent of the applied stress level. As the stress level increases, the behavior normally deviates from linear to nonlinear [129].

The creep behavior of epoxy adhesive was investigated by Meshgin et al. [130]. Experimental results showed that the creep of the adhesive tested was dependent on the applied sustained stress level, and the creep coefficient (creep strain/immediate strain) increased by 187% as a results of increasing the percentage of the applied sustained stress, from 15% to 30% of its tensile strength.

In the study carried out by Majda and Skrodzewicz [131], four levels of sustained load (33%, 43%, 54%, and 65% of the tensile strength) were applied to investigate the creep behavior of an epoxy adhesive. Specimens were subjected to ambient

conditions. According to results obtained, the adhesive used showed a nonlinear viscoelastic behavior in the range of stress levels applied in the study.

Significant values of creep deformations were registered in the study carried out by Costa and Barros [132], in which epoxy specimens were subjected to different sustained load levels (20%, 40% and 60% of the ultimate load) under constant environmental conditions of 20°C of temperature and 60% of relative humidity. The registered creep strain increased up to 180% of the immediate strain at loading. Further analysis of the results revealed that up to sustained loading equal to 60% of the ultimate load, the used epoxy could be considered to behave as a linear viscoelastic/viscoplastic material.

In the study reported in [133], an epoxy adhesive was tested under tensile creep tests. Two different levels of sustained stress, equal to 30% and 40% of the ultimate stress, were applied. The testing environmental conditions were 20°C of temperature and 55% of relative humidity. Results obtained showed that a linear viscoelastic behavior was observed up to a sustained stress level equal to 40% of the tensile strength. After 80 days of loading, the registered strain increased by 140% compared to the initial strain at loading when 40% of sustained stress was applied.

The long-term creep of epoxy was investigated through an experimental program on resin specimens under three different levels of tensile stress for a period of 5.7 years [134]. According to their results, epoxy resin exhibited considerable creep and the total strains exceeded the immediate ones by 4.3 to 4.7 times, as shown in Figure 2.32. At constant high stress level (80% of the tensile strength), the behavior of structural adhesives changed significantly and failure was reached very quickly [135].

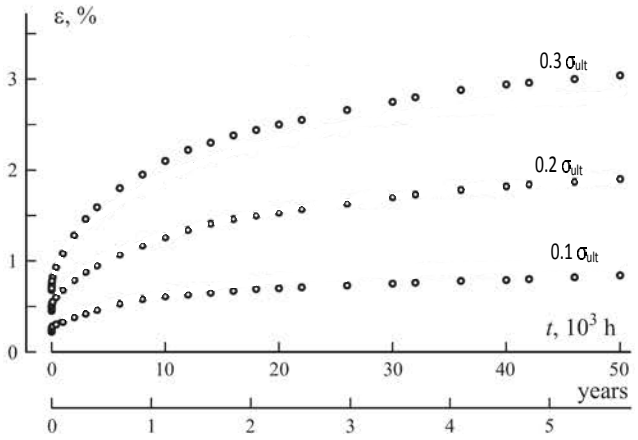

Figure 2.32: Creep strain with time at different sustained stress levels [134].

The creep behavior of epoxy adhesives can be modeled using rheological models and can be described by means of Hookean springs and Newtonian dashpots [136]. Following this approach, some analytical models to predict the creep behavior of adhesives have been suggested (see Figure 2.33).

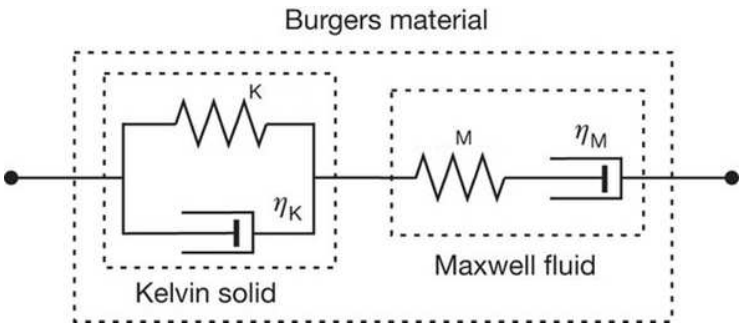

Figure 2.33: Burger's model of viscoelastic material [136].

The models are mostly based on Burger's model for viscoelastic materials. Therefore, the strain at any time t ($\varepsilon_{creep}(t)$) can be computed based on the following equation:

$$\varepsilon_{creep}(t) = \frac{\sigma}{E_M} + \frac{\sigma}{\eta_M} t + \frac{\sigma}{E_K}(1 - \exp(\frac{E_K}{\eta_K} t)) \tag{2.34}$$

where σ is the applied stress, E_M and η_M are the elastic modulus and coefficient of dynamic velocity of Maxwell's chain, E_K and η_K are the elastic modulus and coefficient of dynamic velocity of Kelvin's chain.

Feng et al. [137] proposed a model to predict the tensile creep strain of adhesive by introducing an exponential function, as shown in the following equation:

$$\varepsilon(t,T) = \frac{\sigma_0}{E_0} + \sigma_0 (\frac{1}{E_e} - \frac{1}{E_0}) (1 - \exp(-t/t^*)^{(1-n)}) \tag{2.35}$$

where σ_0 is the applied stress, E_0 is the initial young modulus, t^* is the retardation time, which corresponds to the time instant at which 63% of the Kelvin's steady-state strain is attained, n is a factor to take moisture absorption into account and E_e is the equilibrium modulus, which can be calculated by the following equation:

$$E_e = 2G_f (1 + \nu) \tag{2.36}$$

where G_f is the rubbery plateu shear modulus and ν is the Poisson's ratio.

Another model was proposed by Majda and Skrodzewicz [131] in which coefficients of dynamic viscosity, η_0 and η_1, and the elastic modulus of the relaxation response,

E_1, are defined as a function of the applied stress. According to this model, the strain at any time $\varepsilon(t)$ can be estimated by the following equations:

$$\varepsilon(t) = \frac{\sigma}{E_1} + \frac{\sigma}{\eta_1} t + \frac{\sigma}{E_2} (1 - \exp(-t/t^*)) \tag{2.37}$$

$$t^* = \frac{\eta_1}{E_1} \tag{2.38}$$

Majda and Skrodzewicz [131] followed this approach and obtained a retardation time (t^*) ranging from 3 to 24 minutes, which was extremely small compared to that previously obtained in [137].

A modification to the model proposed by Feng et al. [137] was suggested by Costa and Barros [132]. In the new model, a new parameter *n* was included with the aim at forcing the slope between experimental and numerical values to be unitary. The final proposed formula reads:

$$\varepsilon_{creep}(t) = \frac{\sigma}{E_M} + \frac{\sigma}{\eta_M} t + \frac{\sigma}{E_K} (1 - \exp(\frac{E_K}{\eta_K} t)^{1-n}) \tag{2.39}$$

In summary, the understanding of the time-dependent behavior of the materials involved in the NSM FRP system (FRPs, concrete and adhesive) becomes essential. The creep of these materials, specifically adhesives, may cause a continuous variation and time-dependent deformations in the strengthened element. Although several experimental and analytical studies investigated the creep of adhesive, much more research needs to be carried out, especially regarding the influence of the environmental conditions on the creep response.

2.7.2 Bond tests of NSM FRP reinforcement in concrete

Although many studies were carried out on the short-term bond behavior of NSM FRP, this is not the case for their long-term response. Therefore, there is still a lack of data and knowledge about their long-term bond behavior. This section presents an overview of some studies that investigated the long-term behavior of both EB and NSM FRP reinforcement systems.

Borchert and Zilch [87] carried out an experimental program, studying the effect of adhesive properties on the long-term bond behavior of concrete blocks strengthened with NSM CFRP strips (Figure 2.34) when subjected to different levels of prestressing. The main test parameters were the temperature (20°C to 50°C), the curing time (1 to 28 days) and the applied prestressing force (40% to 80% of the short-term bond capacity). The used bonded length was 100 mm.

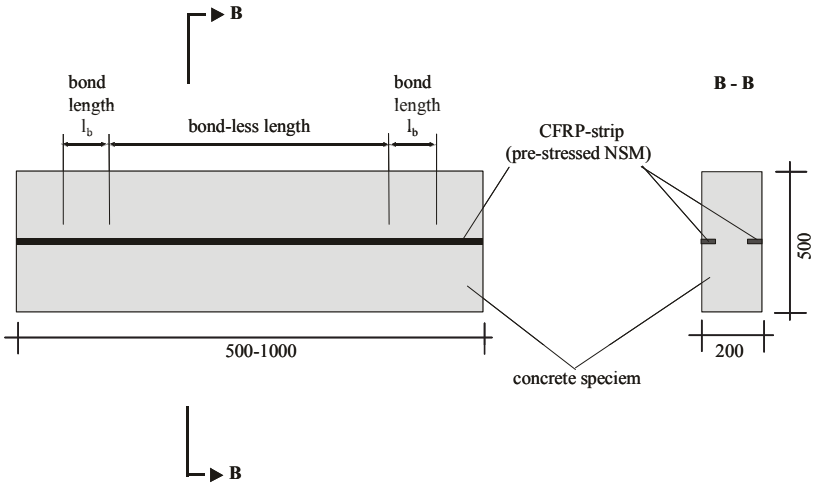

Figure 2.34: Tests specimen configuration proposed by Borchert and Zilch [87] (units in mm).

Results obtained showed that increasing the curing period reduced the creep effects, and increasing the temperature near the T_g significantly affected the system performance, causing sudden losses in the CFRP strains. In the same study, an analytical procedure to model the time-dependent bond behavior of NSM FRP strips was introduced. The proposed model assumed that the bond of NSM system is related to the adhesive bond-slip behavior. The model was based on a non-linear bond-slip law, similar to that used for bond of deformed steel bars in concrete, and was composed of four different regions (see Figure 2.35).

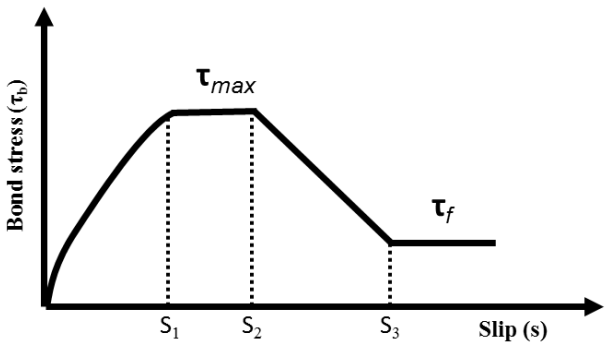

Figure 2.35: Bond stress-slip relationship for steel bars [138].

The long-term behavior was introduced by modifying the local bond stress-slip law with time, and taking into account a limit for the descending branch, following the methodology presented in [138] for long-term bond-slip behavior of steel bars in concrete (see Figure 2.36). The model was based on the reduction of τ_{max}, calculated from Mohr's material law, by using a strength factor calculated from the detailed analytical model. Although the proposed model showed good agreement with the experimental results, some limitations were observed. For example, the coefficients

are valid only for the adhesive used and their applicability shall be checked for different types of adhesives.

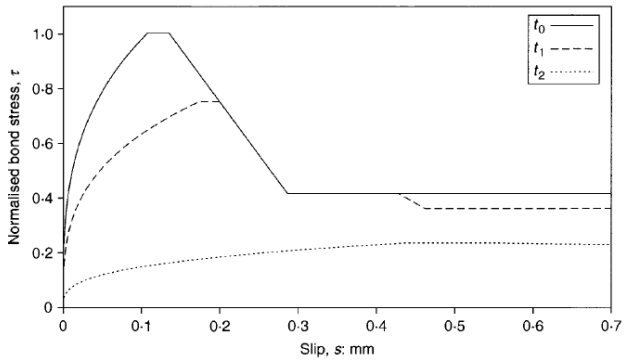

Figure 2.36: Modification of bond stress-slip relationship [87].

Silva et al. [139] performed an experimental program to study the long-term bond of concrete elements strengthened with NSM CFRP strips through beam tests (see Figure 2.37). Each specimen was composed of two equal size concrete blocks, each block having dimensions of 150 mm x 200 mm in cross-section and 385 mm length. The two blocks were connected through a steel hinge at the top and the CFRP reinforcement was installed at the bottom. In each block, five stirrups of 6 mm diameter were distributed along the length to avoid shear failure. Additional longitudinal reinforcement, 2ϕ8, was provided at the bottom and the top of each block.

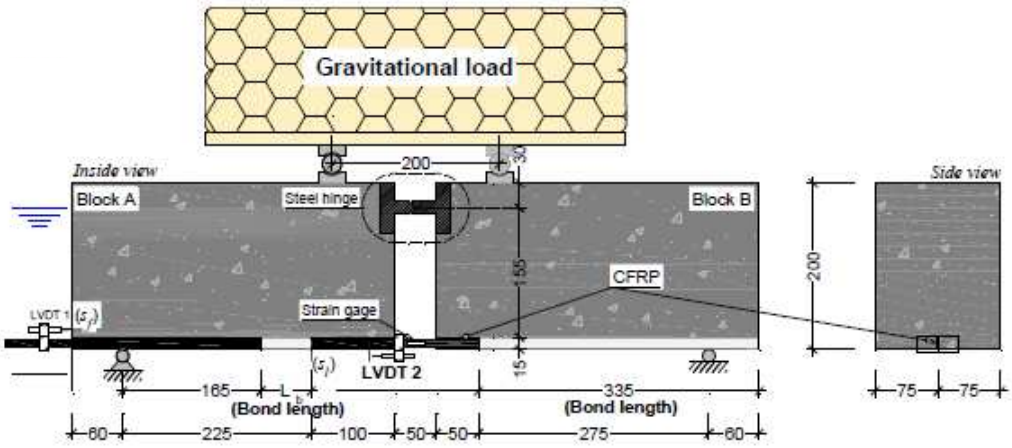

Figure 2.37: Test specimen and setup [139] (units in mm).

The CFRP strips used were 1.4 mm thickness and 10 mm width, and the bonded length and anchorage length in the reaction block were 60 mm and 335 mm, respectively. A sustained load of approximately 7 kN was applied through two steps (1.7 kN and 5.3 kN for the first and the second steps, respectively). Specimens were divided into five groups. First and second group were left unloaded and loaded, respectively, in laboratory conditions. The other three groups were loaded and

subjected to the following conditions: immersion in a water tank at 20°C with 0% of chlorides; immersion in a water tank at 20°C with 3.5% of chlorides; and exposure to wet/dry cycles with water at 20°C and 3.5% of chlorides. Results showed that the creep effect was found to be practically negligible and the loaded end slip was mainly controlled by the laboratory temperature. Besides, similar behaviors were observed in the case of specimens immersed in pure water at 20°C and those subjected to wet/dry cycles with water with 20°C and 3.5% of chlorides.

Derias et al. [140] studied the durability of nine RC beams strengthened with NSM system using GFRP strips and two types of CFRP strips. Sustained load equal to 40% of the ultimate load carrying capacity was applied. Some beams were subjected to high temperature and some other were left in room conditions. Results showed a deterioration in the epoxy-concrete interface and changes in failure modes due to the extreme environmental conditions.

Due to the rare availability in the literature of works concerning the long-term bond behavior of concrete strengthened with NSM reinforcement, and due to the possibility of applying testing methodologies used for investigating mechanical properties of EB reinforcemeny for the analysis of NSM reinforcement systems, some further studies related to EB strengthening systems are introduced in the following.

The long-term bond behavior between concrete and EB FRP plates was investigated by Mazzotti and Savoia [141]. Double shear pull-out tests were carried out in a climatic chamber, and a sustained load was applied by means of a specifically designed test frame, as shown in Figure 2.38. Two CFRP plates were bonded to opposite faces of each specimen and three different bonded lengths of 100 mm, 200 mm and 400 mm were considered. Strain profile evolutions with time along the bonded length were recorded by means of strain gauges. The results showed that a significant redistribution of shear stresses along the bonded length occurred and this was attributed to creep deformation.

To complement the experimental work, a simplified model for EB was presented by the same authors [142], in which the evolution of strain and shear stress with time along the bonded length was described. The model was developed by using the effective modulus method, and was based on a linear bond-slip law to model the FRP-concrete anchorage.

Another experimental and analytical campaign was carried out by Meshgin et al. [130], who investigated the long-term behavior of epoxy at the interface between the concrete and the EB FRP. The sustained load was applied for nine months to nine concrete specimens through a double shear pull-out test, as shown in Figure 2.39.

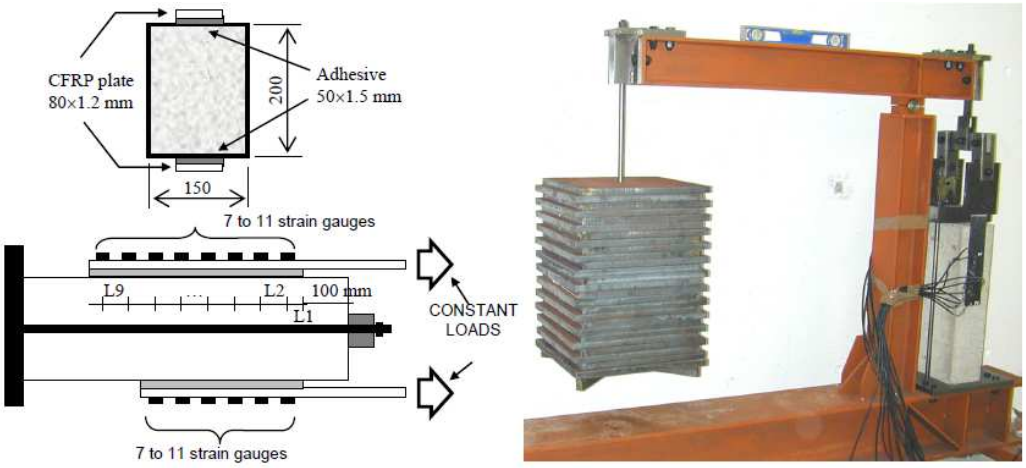

Figure 2.38: Geometry of test specimen and test setup [141].

Figure 2.39: Double-shear test setup [130].

The main parameters studied were the ratio of applied shear stress to ultimate shear strength, the epoxy thickness and the epoxy curing time before loading. From experimental results it was observed that the ratio of shear stress to ultimate shear strength and the epoxy curing time before loading could be the most critical parameters affecting creep of epoxy at the concrete-FRP interfaces. It was also found that the creep of epoxy could result in failure at the interfaces due to the combined effect of relatively high shear stress to ultimate shear strength and thick epoxy adhesive, and this may have an adverse effect on the bond performance of RC structures strengthened with FRP. Based on experimental results, a modified Maxwell model was suggested to simulate the long-term behavior of epoxy at the concrete-FRP interfaces (see Figure 2.40).

Ferrier et al. [143] studied the creep behavior of CFRP plates, externally bonded to concrete, using the double-lap shear test (see Figure 2.41). Four types of epoxy with glass transition temperatures ranging from 45 to 80°C were used for the FRP-concrete interface; the bonded joints were subjected to thermo-stimulated experiments to assess their creep behavior as a function of time and temperature under shear loading

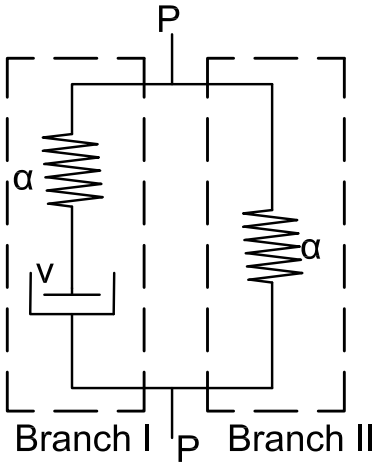

Figure 2.40: Proposed modified Maxwell model [130].

equal to 40% of the ultimate bond strength. Results revealed that increasing the temperature increased the creep strains with time; this increase was more evident when an epoxy with glass transition temperature more than 50°C was used. Besides, a decrease in the shear modulus was observed due to creep effects, with a value of 20% and 70% for high modulus and low modulus epoxy, respectively.

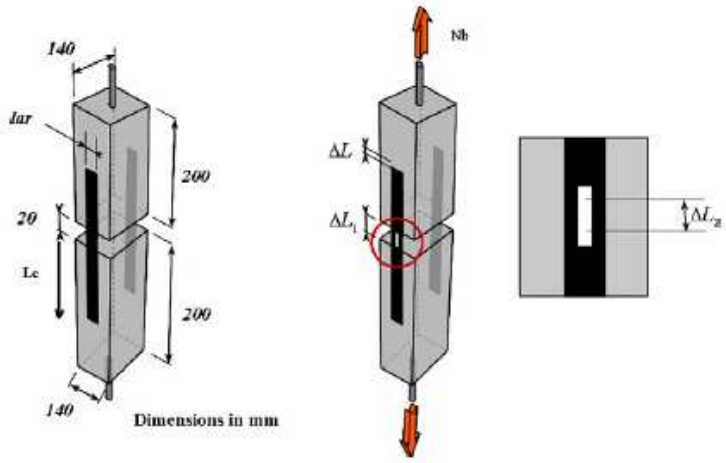

Figure 2.41: Double-shear test specimen [143].

In the same work, a rheological model to simulate the creep of an epoxy polymer was presented. The model was based on Kelvin-Voight elements connected in series (see Figure 2.42) and was calibrated based on experimental results. The application of the model allowed to determine the adhesive shear strain as a function of time, temperature, average shear stress and rheological function.

To summarize, bonding between NSM FRP and concrete is a fundamental property that can be affected by several governing parameters. Far too little attention has been paid to the time-dependent bond-slip response of RC members strengthened

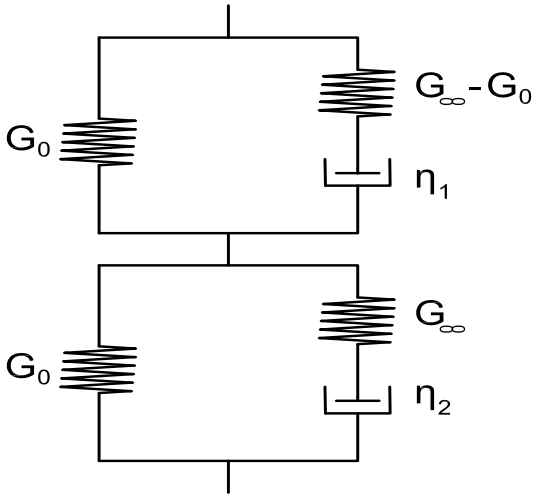

Figure 2.42: Rheological model to simulate the creep of epoxy [143].

with NSM FRP under environmental conditions and sustained loading, thus resulting in a general lack of research into this topic.

2.8 Conclusions of the literature review

Previous studies showed that NSM strengthening technique is an efficient methodology for concrete strengthening with FRP materials due to its potential advantages over the EB one. The NSM technique provides the following advantages when compared to the EB technique: (i) minimum installation time, (ii) no requirement of surface preparation except groove cutting, (iii) lower proneness to debonding failure, (iv) lesser exposure to mechanical damage, fire and vandalism as the FRP reinforcement is protected by the concrete cover, and (v) suitable to strengthen the negative moment regions of beams and slabs.

Bond between FRP reinforcement and concrete is being considered the key factor that controls the success and efficiency of the strengthening system. For the same amount of FRP reinforcement, independently of the distribution of FRP reinforcement, NSM provides higher load bearing capacity compared to EB. Introducing FRP bars/strips into grooves provides larger bond surface and improves the anchorage capacity of the FRP reinforcement.

Direct pull-out test is a reliable and practical test that can be used to determine bond capacities between FRP reinforcement and concrete. It is considered a suitable alternative to avoid disadvantages of beam pull-out test. Although different test setups and configurations have been proposed for direct pull-out test, the presence

of a standard test configuration is a critical aspect in the analysis of bond in NSM systems.

Several parameters may influence the bond behavior between NSM FRP and concrete. Some of them are related to the material properties, such as concrete strength, groove filling material and FRP reinforcement characteristics, while some others are related to the geometry of the strengthened member, such as bonded length and groove dimensions as well as its surface surface configuration. Loading conditions is another parameter that may influence the bond behavior between NSM FRP and concrete. The state of local stresses created in the zone around the reinforcement can alter the behavior of the strengthened element either in terms of bond-slip or bond capacity. This also applies for the different setups to characterize the bond behavior. The failure load, as well as the transmission of bond stresses is expected to be higher for concrete specimens subjected to compression stresses due to concrete confinement.

For the material related parameters, concrete strength plays a critical role on the bond-slip response of the NSM FRP reinforcement technique in the case of specimens with short bonded length. Moreover, epoxy adhesives provide better mechanical properties as groove filling materials when compared to cement based adhesives, although the later can be advantageous concerning fire and environmental protection. Regarding the FRP reinforcement, its characteristics such as fiber type, surface configuration, cross-sectional shape and area, have a significant influence on the bond-slip respone of NSM system in terms of the ultimate capacity and failure modes.

In the FRP NSM technique, strips have shown to be more efficient than round bars since they maximize the ratio of surface to cross-sectional area, which minimizes the bond stresses associated with a given tensile force in the FRP reinforcement. Besides, the use of strips overcomes the splitting of the epoxy cover that can occur in the case of bars, and provides more ductile global response in terms of load-displacement relationship as a result of the larger bond perimeter and the higher confinement provided by the surrounding concrete.

For the geometry related parameters, increasing the bonded length, up to the effective length, increases the ultimate pull-out load as well as the debonding resistance. In addition, rough surfaces are considered to be more realistic and provide better bond characteristics when compared to smooth surfaces. Furthermore, increasing the groove width, for a given depth and reinforcement ratio, increases the bond strength of the system.

A primary concern of NSM FRP strengthened RC structures bond performance is the long-term bond behavior under serviceability limit state conditions, which may

be affected by several parameters such as sustained loading level, bonded length, temperature and humidity level. Despite the limited number of studies available, the analysis of the literature review shows that the long-term flexural behavior, in terms of failure load and failure mode, of RC concrete members strengthened by FRP NSM system could be affected by changing temperature and humidity conditions, and the applied sustained loading level. On the other hand, the number of studies, either experimental or analytical, dealing with the effect of sustained load on the long-term bond behavior of NSM FRP reinforcement systems, combined with different temperature and humidity conditions, is relatively scarce, specially if all parameters involved are to be considered. In addition, the possible creep of materials involved in the strengthening system (mainly the adhesive) under different conditions may affect the bond between FRP reinforcement and concrete, and it is therefore a worthwhile aspect to be taken into account. Therefore, the aim of this thesis is to investigate the effect of sustained loading, bonded length, groove width, temperature and humidity on the time-dependent bond-slip response between NSM CFRP strips and concrete.

3 Tensile creep of the epoxy adhesive

3.1 Introduction

The literature review presented in Chapter 2 highlighted the lack of data currently available on the performance of NSM FRPs under different environmental conditions combined with the presence of sustained loading. Also it was reported that epoxy adhesives, which are usually used in the NSM strengthening technique, are viscoelastic materials whose properties can be highly affected under different loading and environmental conditions, thus affecting the overall behavior of the strengthened system.

Epoxy adhesives are used as the load-bearing material that connects the FRP reinforcement to concrete due to several advantages, such as the capacity of transferring stress along the bonded length without the loss of structural integrity or the ability of minimizing stress concentration through the redistribution of stresses over a large area [137]. The mechanical properties of adhesive materials highly affect the bond behavior, the load capacity and the failure mode of the strengthened system [9, 77, 82, 86–89, 144].

The long-term performance of the strengthened structures under sustained load is being considered as one of the most important aspects to ensure design safety. The time-dependent behavior of the strengthened system is mainly dependent on the performance of its composing materials. Epoxy adhesives exhibit a viscoelastic behavior under the effect of sustained loading, which may affect bond and load carrying capacity of the strengthened member over time, and cause both deformation and redistribution of stresses. On the other hand, the environmental conditions may strongly affect the mechanical behavior of the adhesives as they have a direct effect on the adhesive's internal structure.

This chapter presents an experimental program that aims to study the tensile creep behavior of the adhesive used in this work, when subjected to different conditions of temperature and humidity. The significant experimental results are presented and discussed within this chapter.

3.2 Test program

In the current study, the adhesive used was a solvent-free, thixotropic two components epoxy resin. It has the commercial name of S&P 220 epoxy resin, which is usually used for bonding CFRP laminates. This adhesive was selected as it has been used in a wide range of field applications and research projects concerning NSM reinforcement systems and therefore it is well referenced in the literature [76, 132, 133, 145, 146]. Moreover, it was provided by a company that has a wide experience in the field of concrete strengthening with FRP materials. As stated by the manufacturer [147], the package was composed of component A, which is the resin, with a light gray color, and component B, which is the hardener, with a black color. Component A contains (20%-25%) Bisphenol A and (5%-10%) Neopentyl glycol diglycidyl ether, while component B contains (20%-25%) Triethylenetetramine, (1%-2.5%) Piperazine, 3.6% diazaoctanethylenediamin and (20%-25%) Poly (oxypropylene) diamine. Both components should be mixed slowly, in a proportion of 4A:1B (in weight), until obtaining a uniformly gray color without any streaks.

The experimental program was composed of both short-term and long-term tensile tests. Standard Tensile Tests (STT), Dynamic Mechanical Analysis (DMA) and Differential Scanning Calorimetry (DSC) tests were carried out to characterize the adhesive used. Tensile creep tests were performed to investigate the creep behavior of the adhesive under varying temperatures and humidity levels. In the next sections, a description of the different tests is performed.

3.2.1 Scanning Electron Microscope (SEM)

After curing, the chemical composition and porosity of specimen were checked using a Scanning Electron Microscope (SEM). The observation was done using the Backscattered Electron (BSE) technique.

BSE technique requires a highly polished surface for optimum imaging. Therefore, the surface of the samples was prepared for observation by grinding with Silicon Carbide(SiC) paper to expose a fresh surface, and then polished using a series of successively finer grades of diamond paste.

3.2.2 Differential Scanning Calorimetry (DSC)

One of the common methods that can be used to determine the glass transition temperature (T_g) of materials, at which the material changes from rigid state to rubbery state, is the Differential Scanning Calorimetry (DSC). This test method

consists of heating or cooling the test material at a controlled heating/cooling rate in a specified purge gas supplied at a controlled flow rate. During the test, the behavior of the test material is compared to that of a reference material. To this end, either the difference in temperature or the difference in heat input between the two materials is continuously monitored with a suitable sensing device. A transition is marked by absorption or release of energy by the specimen, resulting in a corresponding endothermic or exothermic peak or baseline shift in the heating or cooling curve [148]. DSC measurements on polymers are greatly affected by the thermal history and morphology of the sample and the test specimen. It is important to ensure a preliminary heating cycle is performed and that the measurements are taken from the second heating scan [149].

In this experimental program, the DSC Q2000 equipment shown in Figure **??** was used to perform isothermal DSC tests, in which the applied heating rate was 10°C/min, using nitrogen at 50 mL/min as a purge gas. The initial and final temperatures applied were 25°C and 80°C, respectively.

3.2.3 Dynamic Mechanical Analysis (DMA)

An alternative method to determine T_g and viscoelastic properties of polymeric amorphous materials is the Dynamic Mechanical Analysis (DMA). This method is based on a frequency response analysis that uses a constant, non-destructive oscillatory strain (or stress) at selected frequencies and temperatures while recording the resulting stress (or strain) response of the material sample. In this work, tests were performed using a DMA analyzer of model METTLER TOLEDO DMA/SDTA861e in which three points bending test configuration with 45 mm distance between supports was used, as shown in Figure 3.1. The three points bending test configuration was selected among several setups available in the literature to eliminate clamping effects as the specimen is supported at both ends but not clamped [150]. The specimens were subjected to a heating rate of 2°C/min in a temperature range from 30°C to 100°C. A constant displacement amplitude of 10 μm was applied with a frequency of 1 Hz. The glass transition temperature was studied by analyzing the storage modulus $(E^{'})$, the loss modulus $(E^{''})$ and the loss factor (tanδ) as a function of temperature.

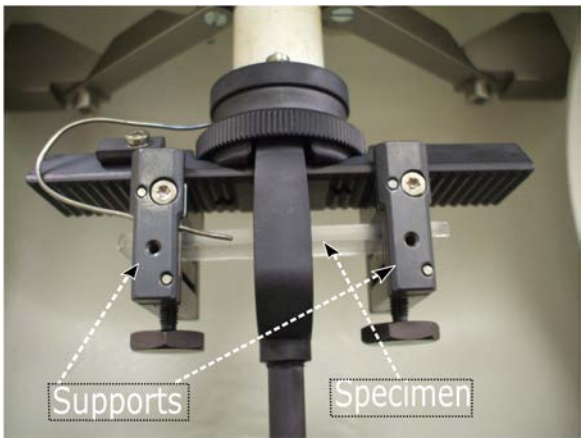

Figure 3.1: DMA test setup.

3.2.4 Standard Tensile Test (STT)

In order to determine the tensile strength and modulus of elasticity of the adhesive used, Standard Tensile Tests (STT) were carried out following ISO 527-1 specifications [151]. Dog-bone-shaped specimens were prepared according to ISO 527-2 [152] as follows:

- The two components of the epoxy were added with proportion 4A (resin):1B (hardener) by weight and mixed slowly until obtaining a uniformly gray color without any streaks.
- The epoxy paste was poured into Polytetrafluoroethylene (PTFE), usually known under the commercial name of Teflon, molds (see Figure 3.2a) and well compacted to avoid the presence of any air bubbles.
- The surface was leveled with a spatula, then covered with a Teflon sheet and pressed to have a smooth surface.
- Specimens were demolded after 24 hours and left for curing (see Figure 3.2b).

After casting, specimens were left for 10 days in laboratory conditions (20°C of temperature and 55% of relative humidity) for curing. Each specimen was instrumented with two longitudinal strain gauges glued on the center of each face. The width and thickness of the tested specimens were measured at three different positions in order to determine its average cross section. After that, tensile tests were performed using a MTS Insight electromechanical universal testing machine with a 5 kN load cell (see Figure 3.3). The specimens were tested under displacement controlled mode with a

loading rate of 1 mm/min. Load and longitudinal strains were registered during the test and then stress-strain curves were obtained.

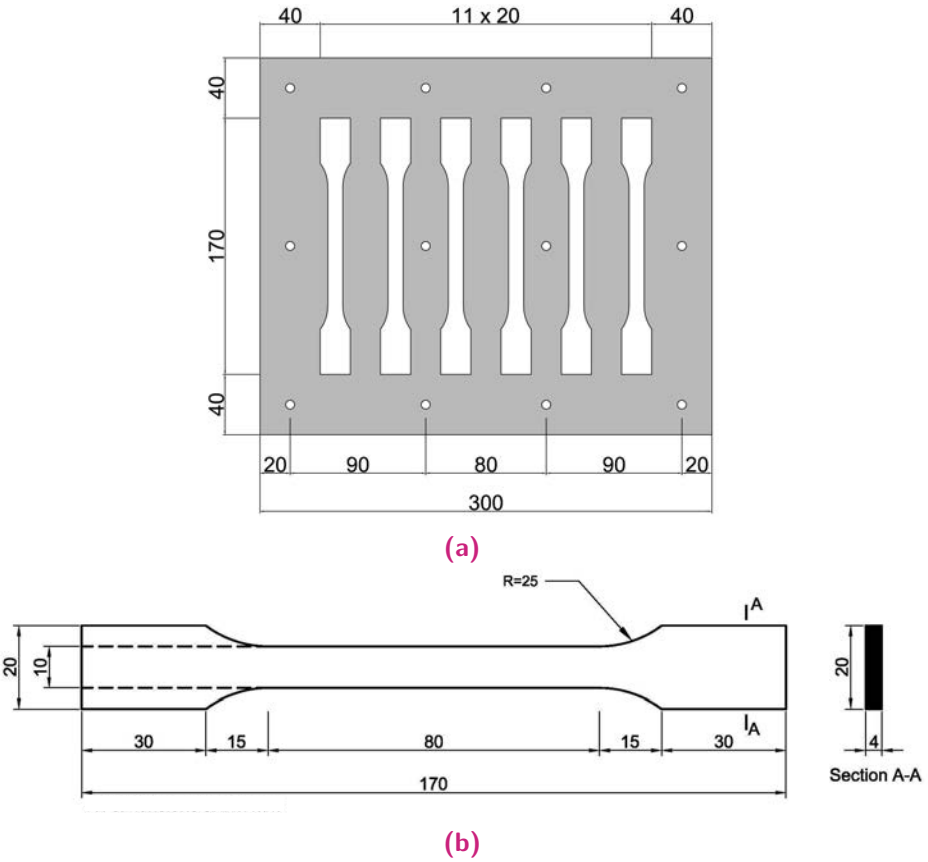

Figure 3.2: (a) PTFE mold details and (b) Test specimens (units in mm).

Figure 3.3: Tensile test setup and instrumentation.

3.2.5 Tensile creep test

An experimental campaign of four test series was carried out to study the tensile creep behavior of the epoxy adhesive under different conditions of temperature and humidity. The details of test series, specimens and parameters, are indicated in Table 3.1. The first column contains the identification of the series, while the identification of the specimens in the second column is as follows: the letter S is followed by the applied sustained stress level as a percentage of the tensile strength, then followed by the designation of the environmental conditions under which the test was carried out (C1, C2, C3 and C4) and the last character identifies the two identical specimens. The third, the fourth and the fifth columns show the applied sustained stress level as a percentage of the tensile strength, the applied temperature and the percentage of relative humidity, respectively.

For all series, three levels of sustained stress (20%, 40% and 60% of the tensile strength obtained from short-term tests) were applied to investigate the tensile creep behavior of adhesive at different environmental conditions and sustained stress levels. In the first test series (Series 1), the control one, specimens were conditioned at 20°C of temperature and 55% of relative humidity (C1). In order to study the effect of increasing the humidity level on the tensile creep behavior of the adhesive used, Series 2 was designed similarly to Series 1, keeping the temperature at 20°C, while the applied relative humidity level increased from 55% to 90% (C2). Series 3 was designed to investigate the effect of increasing the temperature on the tensile creep behavior. Specimens were tested at 40°C of temperature keeping the relative humidity level at 55% (C3) as in Series 1. Finally, the combined effect of increasing both temperature and humidity was investigated through Series 4, in which 40°C of temperature and 90% of relative humidity (C4) were applied.

Tests were carried out into a climate chamber to maintain constant conditions of temperature and humidity for each series; the specimens were introduced into the climate chamber three days before the application of sustained load. The sustained load was applied using gravity loading systems with a multiplication factor of 4 (see Figure 3.4). The specimens were instrumented with two strain gauges, glued on the center of each face, in order to register the longitudinal strain during the test period.

Table 3.1: Tensile creep test matrix.

Series	Specimen ID	Stress level (%)	Temperature(°C)	Relative humidity (%)
Series 1	S20C1a	20		
	S20C1b	20		
	S40C1a	40	20	55
	S40C1b	40		
	S60C1a	60		
	S60C1b	60		
Series 2	S20C2a	20		
	S20C2b	20		
	S40C2a	40	20	90
	S40C2b	40		
	S60C2a	60		
	S60C2b	60		
Series 3	S20C3a	20		
	S20C3b	20		
	S40C3a	40	40	55
	S40C3b	40		
	S60C3a	60		
	S60C3b	60		
Series 4	S20C4a	20		
	S20C4b	20		
	S40C4a	40	40	90
	S40C4b	40		
	S60C4a	60		
	S60C4b	60		

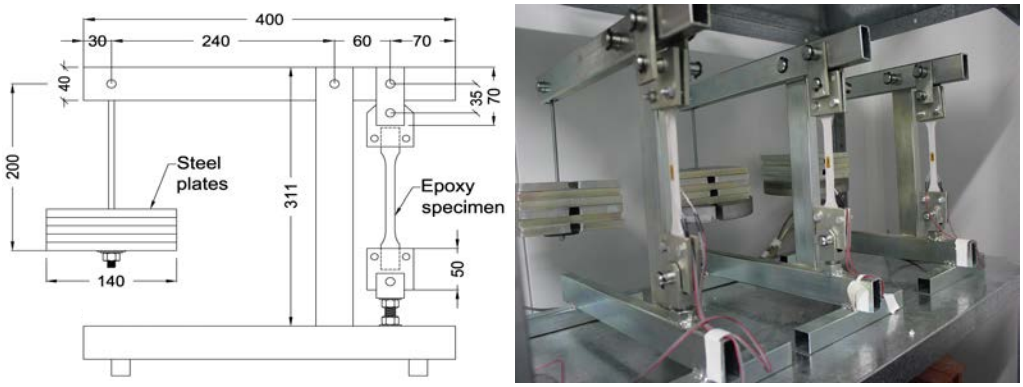

(a) (b)

Figure 3.4: Tensile creep test (a) Loading frame details (units in mm) and (b) Test setup and instrumentation.

3.3 Experimental results of adhesive tests

3.3.1 Scanning Electron Microscope (SEM) results

Results obtained from the SEM showed a high density and uniform distribution of mineral fillers (see Figure 3.5). Four main objects were identified and analyzed (see Table 3.2). A more in-depth analysis associated with the potentialities of SEM (Energy Dispersive X-Ray-EDX) allows for the identification of the components, indicating the presence of barium sulphate (sulfur, barium), titanium dioxide (titanium, oxygen), epoxy matrix (carbon, oxygen) and quartz (silicon, oxygen).

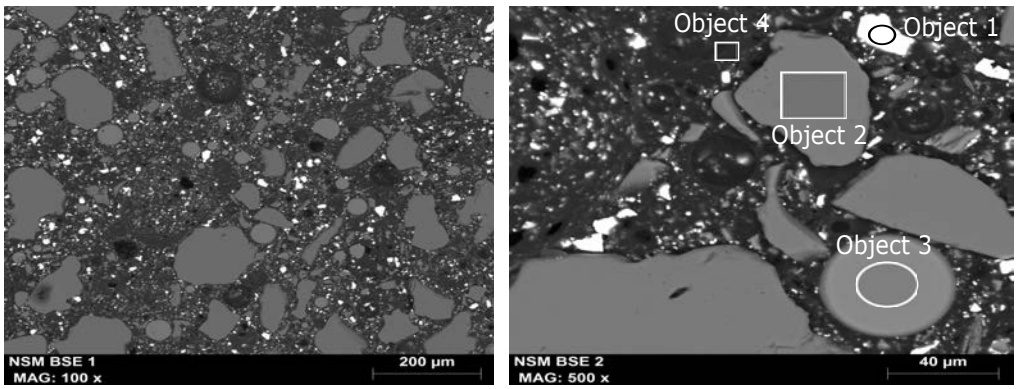

(a) (b)

Figure 3.5: SEM images (a) Particle distribution and (b) Chemical composition.

Table 3.2: Components determined by SEM.

Element	Weight (%)			
	Object 1	Object 2	Object 3	Object 4
Carbon	13.68	16.21	11.92	72.41
Oxygen	23.35	46.17	42.48	18.67
Sodium	0.26		8.06	
Magnesium			2.08	
Aluminum		0.1	0.41	0.5
Silicon	0.61	37.53	24.47	2.14
Sulfur	11.91		0.13	1.12
Potassium			0.15	
Calcium			7.31	
Barium	50.19			1.46
Chlorine				2.4
Titanium				1.31
Total	100	100	100	100

3.3.2 Glass transition temperature (T_g)

In this study, the T_g was determined through the two test methods previously indicated (DSC and DMA). In the case of DSC test, results are presented in terms of heat flow against temperature, and T_g can be obtained by measuring three temperatures as follows: (i) the extrapolated onset temperature T_{eig}, (ii) the mid-point temperature T_{mg} and (iii) the extrapolated end temperature T_{efg} (see Figure 3.6). According to standards [148, 149], the T_{mg} temperature is considered the most meaningful and may be designated as the T_g for most applications.

In the case of DMA, values of T_g can be found through the analysis of three different parameters provided by the test. Results obtained from the DMA tests are shown in Figure 3.7 in which the elastic part is represented by the storage modulus curve $(E^{'})$, which provides the stiffness of the viscoelastic material and it is proportional to the energy stored during a loading cycle. The viscous part is represented through the loss modulus curve $(E^{''})$, which is proportional to the energy dissipated during one loading cycle. Finally, the loss factor ($\tan\delta$) curve represents the relative contribution of the viscous versus elastic properties and it is a measure of the energy lost, expressed in terms of the recoverable energy, which can be calculated as the ratio of loss modulus to storage modulus. According to this, three distinct methods were used to calculate the T_g of the adhesive used in this study: (i) the

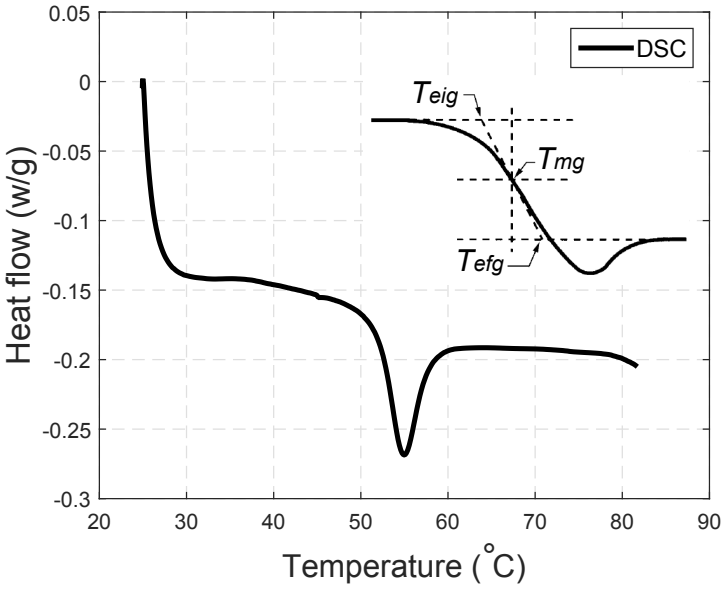

Figure 3.6: DSC test results.

onset of the storage modulus curve drop, (ii) the peak value of loss modulus curves and (iii) the loss factor (tanδ) peak. Table 3.3 presents T_g values obtained with both

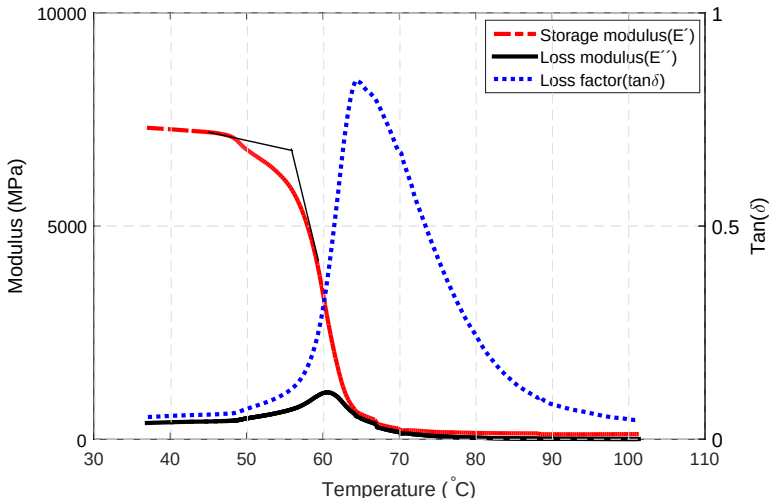

Figure 3.7: DMA test results.

DSC and DMA techniques. The analysis of the results obtained supports that T_g cannot be considered as a unique temperature, but it should rather be considered as a range of temperatures [146]. It should be mentioned that temperature transitions are more easily detected with DMA than with DSC [153], as mechanical changes are more dramatic than variations in heat capacity. DMA is able to detect short range motion before the glass transition range is attained and thus to identify the onset of the main chain motion. Measurements on materials with low moisture contents may

also present problems when tested by DSC because of indistinguishable transitions and limited accuracy [154], and this may be the reason why values of T_g obtained from DSC and DMA differ.

Table 3.3: T_g measurements from the different methods (°C).

Methodology	DSC			DMA		
	T_{eig}	T_{mg}	T_{efg}	Onset point of storage modulus($E^{'}$)	Loss modulus($E^{''}$)	tan(δ)
T_g (°C)	51.8	52.2	52.5	56.2	60.5	64.3

3.3.3 Standard Tensile Test (STT) results

Data obtained from the tensile tests are presented in Figure 3.8 showing an average tensile strength of 20 MPa and an average failure strain of 3375 $\mu\epsilon$.

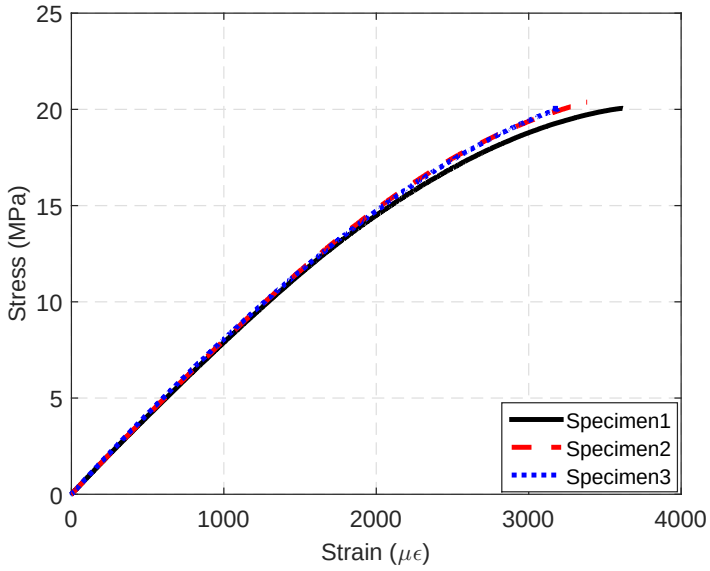

Figure 3.8: Stress versus strain results.

According to ISO 527-1 [151], the average modulus of elasticity was calculated as the slope of the secant line in the stress-strain diagram between 0.05% and 0.25% strains obtaining an average value of 6600 MPa. Results obtained are consistent with the findings reported in [49], in which the same adhesive type was tested after three days of curing at 22°C.

3.3.4 Tensile creep test results

3.3.4.1 Instantaneous behavior

Figure 3.9 represents the initial instantaneous strains registered after the application of the sustained load, for each specimen after conditioning. The lines indicate the evolution of initial strains with respect to applied sustained stresses for each series. Results show that almost linear increase in the initial instantaneous strain was observed due to the increase of the sustained loading level.

For the first series, the initial instantaneous strain increased by 110% and 192% when the sustained load level changed from 20% to 40% and to 60%, respectively. For the second series, the increments were of 104% and 176%, and they changed to 109% and 197% in the third series. Finally, the increases were of 110% and 186% in the fourth series.

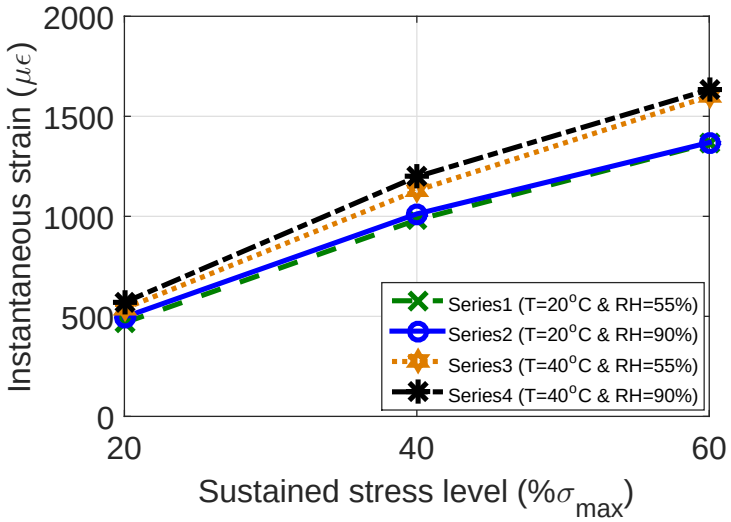

Figure 3.9: Instantaneous strain values.

At sustained load equal to 20% of the epoxy tensile strength, the influence on instantaneous strains of changing the environmental conditions was the lowest in all series. Initial strain values of 468 $\mu\varepsilon$, 496 $\mu\varepsilon$, 539 $\mu\varepsilon$ and 570 $\mu\varepsilon$ were obtained for Series 1, Series 2, Series 3 and Series 4, respectively. An increment of 6% in the strain was observed due to the increase in humidity from 55% to 90% (Series 1 versus Series 2), while this increase was 15% in case of changing only the temperature from 20°C to 40°C (Series 1 versus Series 3). Maximum increment of 22% was observed in the case of changing both temperature and humidity (Series 1 versus Series 4). Values of these increases for tests at the medium level of sustained load (i.e. at 40% of the tensile strength) read 3% when changing only the humidity from 55% to

90%, 15% when changing only the temperature from 20°C to 40°C and 22% when increasing both temperature and humidity. Finally, when a sustained load equal to 60% of the tensile strength was applied, increments of 0.3%, 17% and 20% were obtained for the same changes of environmental parameters indicated previously.

In general, the increase in the instantaneous strain due to changes in humidity conditions from 55% to 90%, for both 20°C to 40°C, seemed to be very low (less than 6%). Additionally, it can be observed that, by increasing the sustained load level, the percentages of increase in the instantaneous initial strain were rather constant with average increments of 3%, 16% and 21% for Series 2, Series 3 and Series 4, respectively, compared to Series 1. Conditioning of the specimens tested prior to the application of sustained load allowed the environmental conditions to have an effect on the adhesive, showing that increasing the temperature increased the instantaneous strains 2.5 times the increase in case of increasing the humidity level. As shown in Figures 3.6 and 3.7, 40°C is a value of temperature relatively close to the T_g of the resin which may be the reason for the higher variations.

3.3.4.2 Long-term behavior

The evolution of longitudinal strain with time was registered for each specimen for 1000 hours, following ISO and ASTM standards [155, 156], thus allowing obtaining the creep strain and the creep compliance curves with time over the testing period. Creep compliances were calculated through the following equation:

$$J_c(t) = \frac{\epsilon(t)}{\sigma_0} \tag{3.1}$$

where $J_c(t)$ is the creep compliance at time t, and $\epsilon(t)$ and σ_0 are the strain at time t and the applied sustained stress, respectively. On the other hand, creep coefficients were calculated as follows:

$$\phi(t) = \frac{\epsilon(t) - \epsilon(t_0)}{\epsilon(t_0)} \tag{3.2}$$

where $\phi(t)$ is the creep coefficient at time t, and $\epsilon(t)$ and $\epsilon(t_0)$ are the strain at time t and the instantaneous strain, respectively. Values of creep compliance and creep coefficient for the different series, at the end of the testing period, are summarized in Table 3.4.

The progress of both strain and creep compliance with time for Series 1 (20°C and 55% RH), when subjected to different levels of sustained loading, is shown in Figure 3.10. In this series, it can be seen that similar curves of creep compliance versus time were obtained at all the applied sustained loading levels. Up to sustained loading

Table 3.4: Creep coefficients and creep compliances after 1000 hours.

Series	Specimen ID	Creep coefficient	Creep compliance (1/MPa)	Time to failure (hrs.)
Series 1	S20C1	2.20	375	—
	S40C1	2.26	400	—
	S60C1	3.02	457	—
Series 2	S20C2	2.81	472	—
	S40C2	2.92	496	—
	S60C2	*	*	60
Series 3	S20C3	10.88	1601	—
	S40C3	*	*	346
	S60C3	*	*	30
Series 4	S20C4	*	*	113
	S40C4	*	*	1
	S60C4	*	*	0.5

*: specimen failed

level equal to 60% of the tensile strength, the creep compliance was found to be relatively independent of the stress levels. This can be an evidence of the exhibited linear viscoelastic behavior of the material up to sustained loading equal to 60% of its tensile strength. Increasing the applied sustained load level increased the creep rate and creep strain values. By the end of the testing period (i.e. 1000 hours), the obtained creep coefficients of specimens S40C1 and S60C1 were found to be 2.6% and 37%, respectively, higher than that of specimen S20C1. All specimens tested within this series lasted till the end of the test period without failure.

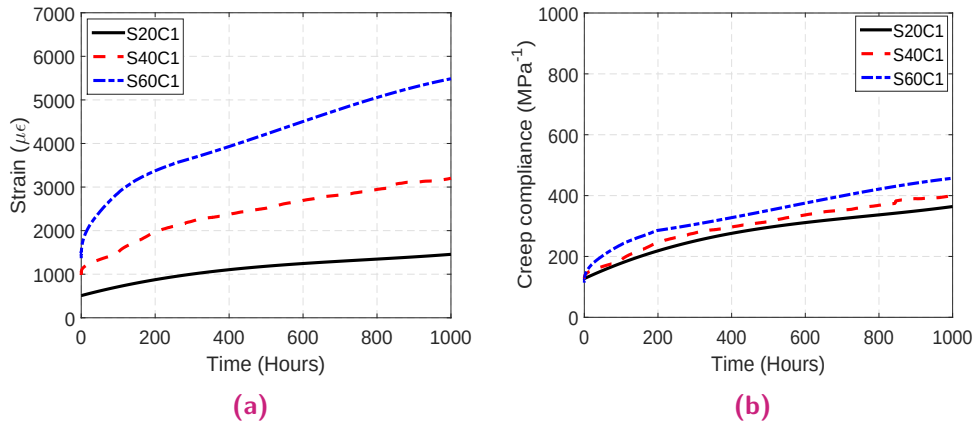

Figure 3.10: Series 1 (a) Tensile strain with time and (b) Creep compliance with time.

The progress of both strain and creep compliance with time for Series 2 (20°C and 90% RH), when subjected to different levels of sustained loading, is shown in Figure 3.11. Results show that specimens subjected to sustained loading level less or equal to 40% exhibited a linear viscoelastic behavior within the new environmental

conditions applied, as similar creep compliance evolution with time was observed. Unlike Series 1, the linearity in the viscoelastic behavior did not exist in the case of specimen S60C2 subjected to sustained loading equal to 60% as a result of increasing the humidity from 55% to 90%. This also caused a premature failure of the same specimen after 60 hours of loading.

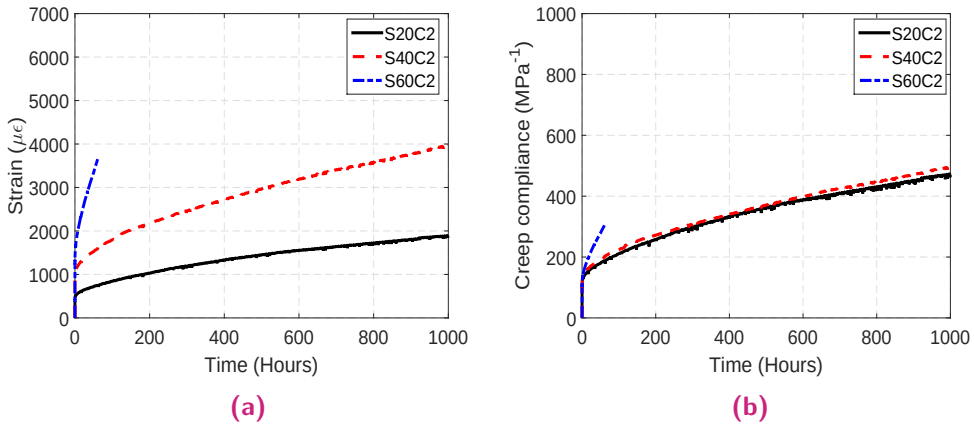

(a) (b)

Figure 3.11: Series 2 (a) Tensile strain with time and (b) Creep compliance with time.

After 1000 hours of loading, the creep coefficient of specimen S40C2 was 4% higher than that of specimen S20C2. Compared to the first test series, the creep coefficient increased by 27% and 29% for specimens under sustained load levels of 20% and 40%, respectively, and higher creep strain values were registered with time. In this test series, the application of a 90% of humidity resulted in an increase in water absorption, leading to plasticization effects and chemical modifications of the epoxy resin as well as changes in its mechanical properties and behavior [157, 158].

The progress of both strain and creep compliance with time for Series 3 (40°C and 55% RH), when subjected to different levels of sustained loading, is shown in Figure 3.12.

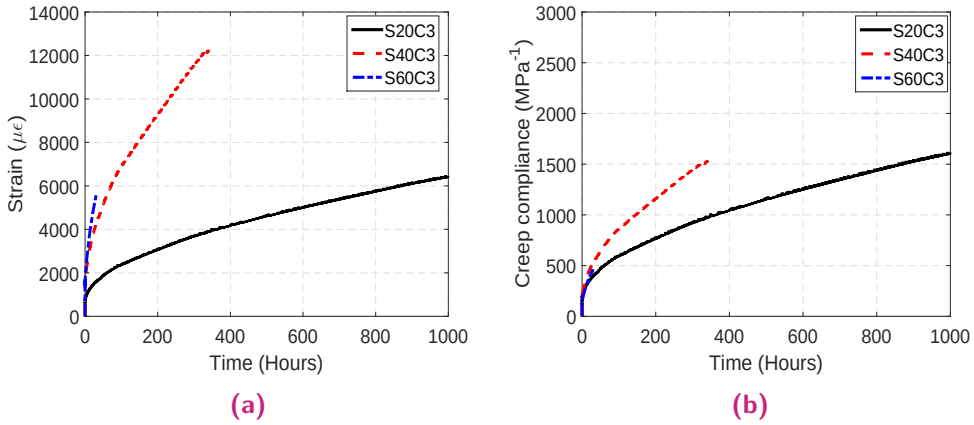

(a) (b)

Figure 3.12: Series 3 (a) Tensile strain with time and (b) Creep compliance with time.

It is evident from the different creep compliance evolutions obtained and presented in in Figure 3.12 that the viscoelastic behavior of the adhesive was significantly affected by increasing the temperature level. Specimens S40C3 and S60C3 failed after 346 hours and 30 hours, respectively, from loading. On the other hand, no failure was observed in the case of specimen S20C3, loaded at 20% of the tensile strength. In addition, specimen S20C3 showed a high value of creep coefficient (10.88) which was 394% higher than that of the first test series. In this test series, the application of a relatively high temperature (40°C) resulted in higher strain values and early failure. These results are consistent with those of other studies [133, 146] and suggest that applying a temperature level near to glass transition range resulted in rapid and dramatic changes in the stiffness and strength of the epoxy resin.

The progress of both strain and creep compliance with time for Series 4 (40°C and 90% RH), when subjected to different levels of sustained loading, is shown in Figure 3.13. In this test series, all specimens failed before reaching the end of the testing period, and shorter failure times were observed; specimens S20C4, S40C4 and S60C4 failed at 113 hours, 1 hour and 0.5 hour, respectively. Compared to previous series tested in this experimental campaign, higher creep strains, creep rates and creep compliance values were obtained. The combined effect of increasing both temperature and humidity was the main cause of this behavior. The application of 90% of humidity resulted in a dramatic degradation in both the strength and the stiffness of the adhesive, and a reduction in the T_g [159]. Moreover, more degradation in the stiffness and strength was present due to the exposure to 40°C, as the resin started to enter the rubbery stage [160].

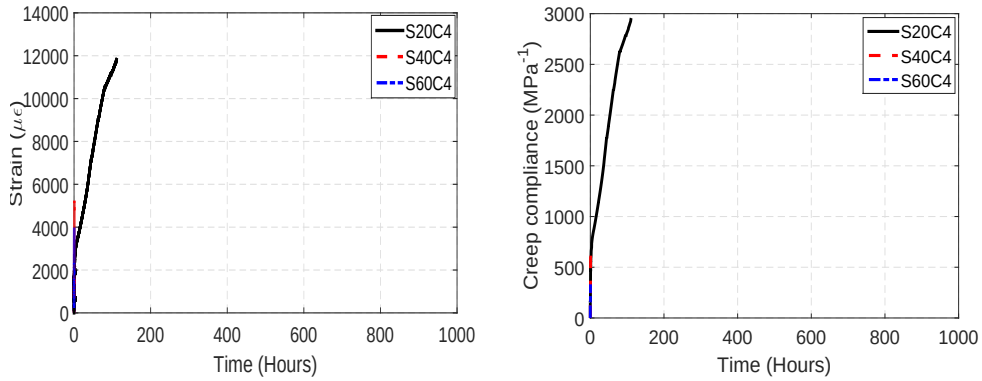

Figure 3.13: Series 4 (a) Tensile strain with time and (b) Creep compliance with time.

3.4 Summary of results

In this chapter, an experimental program to study the tensile creep behavior of a commercially sold structural epoxy adhesive used in concrete strengthening applications with FRPs has been carried out. The program comprised four test series in which sustained stress levels, temperature and humidity were the main parameters studied. The results obtained can summarized as follows:

- The average increase of instantaneous strain, for all test series, was 108% and 188% when the sustained loading level changed from 20% to 40% and to 60%, respectively.

- Increasing the humidity level to 90% at 20°C did not significantly affect the instantaneous initial strain for a specific sustained loading level.

- Changing the environmental conditions (temperature from 20°C to 40°C and humidity from 55% to 90%) affected the instantaneous initial strain only in the cases of medium and high levels of sustained loading (i.e. 40% and 60%), while almost no effect was observed at low level of sustained loading (i.e. 20%).

- The linear viscoelastic behavior of the adhesive was present up to sustained loading level equal to 60% under 20°C and humidity level equal to 55%. This limit started to decrease when the environmental conditions were changed.

- Increasing the humidity level increased creep rates and creep coefficient. Increasing the humidity level up to 90% increased the creep coefficient by 27% and 29% in case of sustained loading level equal to 20% and 40%, respectively.

- At 90% humidity with normal temperature conditions, failure was observed after 60 hours of loading in the case of specimens subjected to sustained loading equal to 60% of the tensile strength.

- At 40°C and 55% humidity, higher creep coefficients and creep strains were obtained and shorter times to failure were observed. The registered times were 346 hours and 30 hours at sustained loading levels of 40% and 60%, respectively.

- Under the combined effect of high temperature (40°C) and humidity (90%), no specimen lasted until the end of the test period and shorter times to failure were observed due to rapid degradation in the adhesive's strength and the

stiffness. The registered times to failure were 113 hours, 1 hour and 0.5 hour at sustained loading levels of 20%, 40% and 60%, respectively.

- High levels of temperature and humidity caused a rapid increase in the creep behavior.

- Temperature, compared to that of humidity, showed greater effect on the instantaneous strain, creep coefficient and time to failure.

4 Long-term pull-out experimental program and experimental results

4.1 Introduction

In both RC strengthening techniques (EB and NSM), bond behavior has a great influence on the ultimate capacity of the strengthened element, as well as on its serviceability features, such as crack width and crack spacing. In this sense, the effectiveness of any strengthening system relies upon the possibility to transfer stresses between the reinforcement and the surrounding concrete. In this regard, it should be taken into account that two interfaces exist in the NSM FRP technique, the bar-epoxy one and the concrete-epoxy one, in which adequate bond has to be achieved.

A primary concern of strengthened RC structures performance is its long-term bond behavior under serviceability conditions, which may be affected by several parameters in case of NSM systems. The literature review presented in Chapter 2 highlighted the lack of data currently available on the long-term performance of NSM FRPs in concrete. Specifically, the bond behavior between NSM FRP and concrete, which may be affected by the possible creep of materials involved in the NSM system, under sustained loading and environmental conditions.

The direct pull-out test is one of the most common tests used in the assessment of bond performance due to its simplicity and the advantages it provides [9]. Due to the absence of a standard test configuration, several pull-out test setups, specimens and configurations have been studied in the literature under short-term conditions [18, 64].

In the current study, an experimental program concerning the long-term bond behavior of NSM CFRP laminates in concrete was performed. Direct pull-out tests have been carried out under both short-term and long-term conditions. Test setup, specimens and conditions have been selected based on the available literature. Among several different direct pull-out test specimens and configurations reported in the literature, a simple pull-out specimen was selected and its dimensions were adapted for this work. Apart from its inherent greater constructive simplicity, the

simple pull-out setup provides an easier manipulation and easiness of inspection of the tested area. A detailed description of the experimental program including the characterization of materials used, the choice of the study parameters, specimen's preparation procedures, the experimental test setup, testing conditions, testing procedures and experimental results are presented and discussed in this chapter.

4.2 Experimental program

4.2.1 Parameters of the study

Limited literature concerning the long-term bond performance between NSM FRP and concrete is available. Therefore, the study parameters of this experimental program have been selected based on the literature on the short-term bond performance.

In this sense, bonded length has been found to have an influence on the short-term bond behavior, and therefore it is selected as the only parameter to be considered in the short-term tests of this experimental program (L_b=60, 90 and 120 mm).

The objectives of this work included to study the bond between NSM FRP and concrete under sustained loading combined with different environmental conditions. Therefore, in addition to bonded length, sustained load level (25% and 50% of the instantaneous load capacity), temperature and humidity have been also selected to be the study parameters covered in the long-term tests of this experimental program.

4.2.2 Materials

This section presents the properties of the materials used in the experimental program (i.e concrete, a two components epoxy adhesive and CFRP laminates). Material properties and its characterization tests are presented and discussed in detail in the following sections to better understand the behavior of NSM strengthening system. It should be mentioned, however, that characterization of the epoxy adhesive used in this study was already presented and discussed in Chapter 3.

4.2.2.1 Concrete

In this study concrete specimens were cast with ready mixed concrete, with a maximum aggregate size of 12 mm, prepared by a local company with the mix composition illustrated in Table 4.1. For each concrete batch, the instantaneous mechanical properties were characterized by using cylinders of 150 mm diameter and 300 mm height, that were prepared according to ISO 1920-3 [161].

The compressive strength, the modulus of elasticity and the tensile strength were determined (28 days after casting) according to ISO 1920-4 [162] and ISO 1920-10 [163] (see Figure 4.1). Each property was determined as the average value of three characterization cylinders tested. The average compressive strength obtained was 32 MPa, and the average tensile strength and modulus of elasticity were 3 MPa and 31 GPa, respectively.

Table 4.1: Concrete mix composition.

Component	Unit	Quantity
Water	kg/m^3	185
Cement 42.5	kg/m^3	320
W/C ratio		0.58
Fine aggregate	kg/m^3	880
Coarse aggregate	kg/m^3	875
Target compressive strength	MPa	30

(a) (b) (c)

Figure 4.1: Concrete characterization tests (a) Compression, (b) Elasticity modulus and (c) Indirect tensile.

Regarding the long-term characterization, concrete cylinders of 150 mm diameter and 450 mm height were tested, according to ISO 1920-9 [164], under sustained

loading equal to 40% of the compressive strength and different environmental conditions (see Figure 4.2a). In these tests, embedded strain gauges were used to register the time-dependent deformations. Additional unloaded specimens were also instrumented under the same conditions to register shrinkage deformations over time (see Figure 4.2b).

(a) (b)

Figure 4.2: (a) Concrete creep test setup and (b) Unloaded specimens with embedded strain gauges.

4.2.2.2 CFRP Laminates

CFRP laminates under the commercial name *S&P laminates CFK 150/2000* were obtained from S&P Clever Reinforcement Ibérica Lda. The CFRP laminates were provided in rolls and composed of unidirectional carbon fibers. The laminates were 1.4 mm thickness and 10 mm width. This CFRP laminates were selected due to their wide spread in the field applications and research projects concerning NSM reinforcement systems [27, 76, 145].

In this experimental program, specimens for CFRP laminate characterization were prepared according to ISO 527-5 Standards [165] as follows:

- Laminates were cut to the required length (350 mm), the thickness was measured at different locations, and then the surface was well cleaned with acetone.

- Four tabs, made of GFRP, with 10 mm width, 100 mm length and 2 mm thickness were glued to the laminate (see Figure 4.3a).

- Two longitudinal strain gauges were glued on the center of the laminate, one on each side.

- The specimen was connected to the testing machine through two steel plates, specially built to act as a gripping system. These two plates had the dimensions of 100 mm x 40 mm and 10 mm thickness, and were connected together by means of steel screws.

Tensile tests were carried out, on three CFRP specimens using a servo-hydraulic testing machine of model Servosis MUE 60 with a capacity of 600 kN. The specimen was positioned across the two cross-heads of the machine and aligned with the axis of the machine grips. Tests were performed in a displacement controlled mode and the load was applied at a rate of 2 mm/min up to failure (see Figure 4.3b). The load was registered with a 10 kN load cell and the axial strain was registered with strain gauges. Both the load cell and strain gauges were connected to a data acquisition system to monitor and save the data.

(a) (b)

Figure 4.3: CFRP tensile test (a) CFRP specimens and (b) Test setup.

After testing, stress versus strain curves were plotted and analyzed. A linear elastic behavior up to failure was observed in all specimens (see Figure 4.4), being the failure mode FRP rupture in the middle part of the laminate (see Figure 4.5).

Based on the stress versus strain plots, the modulus of elasticity was calculated as the slope of the secant line in the stress-strain diagram between 0.05% and 0.25% strains [165]. The average tensile strength and modulus of elasticity were 2.4 GPa and 160 GPa, respectively.

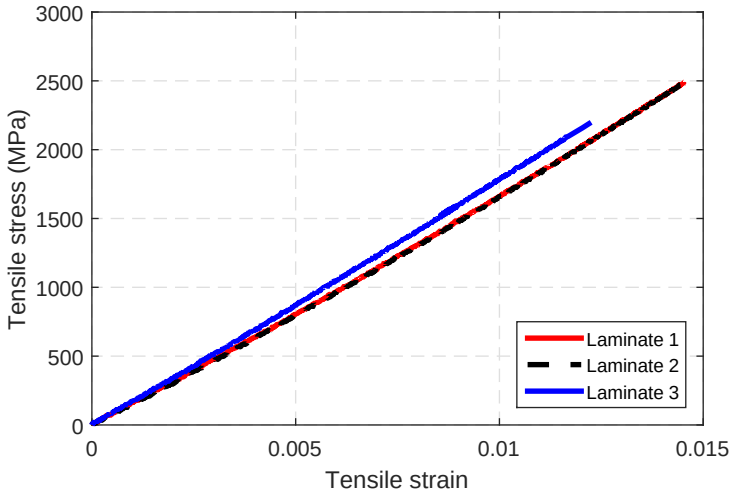

Figure 4.4: CFRP tensile test results (stress versus strain relationship).

Figure 4.5: FRP rupture failure mode of CFRP laminates.

4.2.3 Specimens preparation

4.2.3.1 Molds preparation, casting and curing procedures

Concrete specimens were cast in molds made of protected wood, as shown in Figure 4.6. Before casting, the inner surface of the mold was coated with a thin film of oil to make easier the demolding of concrete specimens. The specimens were cast in the Structural Engineering laboratory at the University of Girona using concrete supplied by a local ready-mixed concrete company. The mix was specified to have a 28-day target compressive strength of 30 MPa. Tests were performed prior to placing the concrete to ensure that the slump was satisfactory, following ISO 1920-2 standards [166]. During casting, specimens were vibrated using an electrical vibrator and

given a smooth troweled finish. The specimens were covered with plastic drop sheets and allowed to moist cure for three days before being stripped from the formwork and stored in ambient conditions in the laboratory for three weeks. The specimens dimensions were 200 mm x 200 mm x 250 mm (see Figure 4.7).

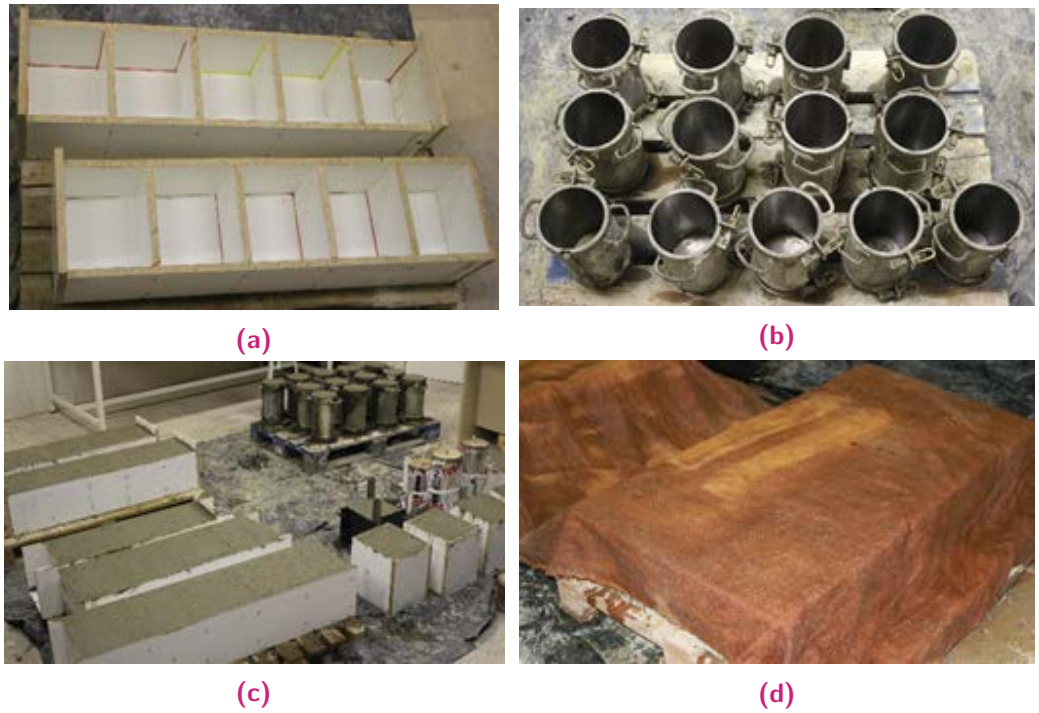

Figure 4.6: Moulds preparation and casting (a) Specimens' moulds, (b) Moulds for cylinder specimens, (c) Already cast concrete and (d) Specimens in moist curing.

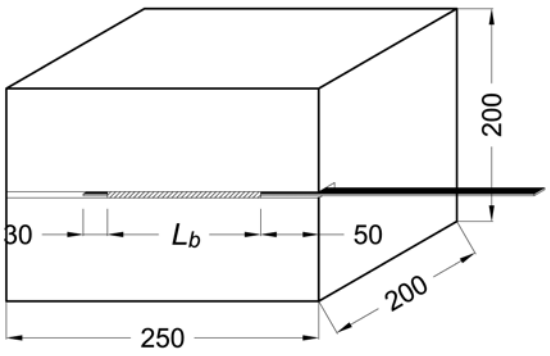

Figure 4.7: Test specimen configuration (units in mm).

4.2.3.2 Groove preparation and CFRP bonding procedures

NSM grooves of 5 mm wide and 15 mm deep were cut into one face of each specimen using a saw cut. A steel guide was specially designed to guide the saw along a straight line while keeping the blade perpendicular to the surface of the tensile face of the specimen. After cutting, the groove surfaces were ground and cleaned with compressed air to provide a sound surface for the bond of the adhesive. Thereafter, plastic tabs were glued beside the groove edges to keep the specimen clean during the preparation process (see Figure 4.8a). Before installing FRP laminates, they were cut from the continuous roll to the required length by an electrical saw to, thereafter, glue two metallic pieces, which limited the bonded length and helped in measuring the loaded and unloaded-end slips during the test (see Figure 4.8b). Prior to the installation of the CFRP in the groove, foam strips were laid into the groove on either side to provide a seal and prevent the adhesive from flowing out of the groove.

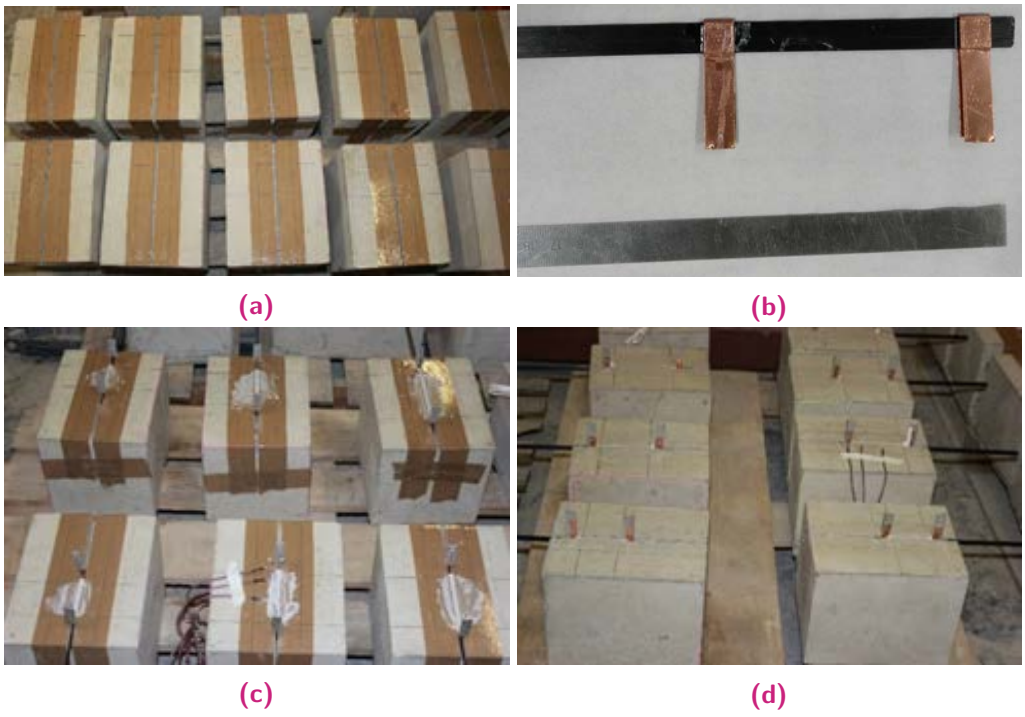

Figure 4.8: Specimens preparation (a) Specimens with plastic tabs, (b) CFRP laminates with metallic pieces, (c) CFRP laminates glued to concrete and (d) Curing of resin.

The two parts of S&P 220 epoxy adhesive, composed of a clear resin and a black hardener, were mixed by a ratio 4:1 by weight, and then hand stirred for five minutes as recommended by the manufacturer. The adhesive was carefully poured into the NSM groove at the bonded zone and the CFRP laminate was coated with a thin layer of resin and inserted into the groove (see Figure 4.8c). Finally, the exceed resin was removed, the surface was leveled, the plastic tabs were removed and the specimens were left 10 days for the curing of the resin before testing (see Figure 4.8d).

4.2.4 Short-term pull-out tests

Bonded length was the unique parameter considered in short-term pull-out tests of this experimental program. According to the literature review of previous experimental works [145], the effective bonded length of pull-out specimens similar to those of this work (see Figure 4.7) is within the range of 80 to 90 mm. Therefore, with the aim at analyzing the effect of bonded length on the bond performance, three different bonded lengths were selected (60 mm, 90 mm and 120 mm) representing to be lower than, equal to and larger than the effective bonded length, respectively. Information of short-term pull-out tests (i.e. failure mode and failure load) was thereafter used to determine the sustained load to be applied in long-term pull-out tests. For every bonded length, three identical specimens were tested, thus making a total of nine single shear pull-out specimens.

4.2.4.1 Test setup, instrumentation and procedures

The test setup for short-term pull-out test is shown in Figure 4.9a. The concrete block was fixed at the testing machine by a steel plate with 20 mm thickness placed at the top of the specimen. The plate was fixed to the testing machine by four steel bars of 15 mm diameter as seen in Figure 4.9b. The top steel plate had a groove of 30 mm $\times$ 30 mm allowing the CFRP laminate to pass through. The CFRP laminate was attached to the loading machine by two steel plates that functioned as a gripping system. These two plates had the dimensions of 100 mm $\times$ 40 mm and 10 mm thickness and were connected together by means of steel screws.

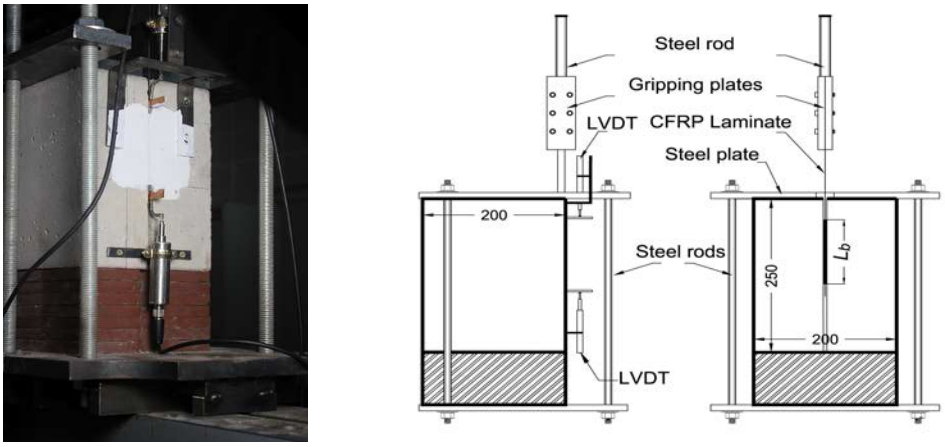

Figure 4.9: (a) Short-term test setup and (b) Sketch of short-term setup (units in mm).

Two displacement transducers (LVDTs), connected to the concrete block, were used to measure both the loaded and unloaded-end slips. The load was applied using

a servo-hydraulic testing machine (of model Servosis MUE 60 with a capacity of 600 kN) with a displacement controlled rate of 0.2 mm/min up to failure. The experimental data from both LVDTs and the machine load cell were recorded using an automatic data acquisition system.

4.2.5 Long-term pull-out tests

With the aim to investigate the long-term bond behavior of NSM CFRP laminates in concrete, twenty-seven single shear pull-out specimens, as those shown in Figure 4.7 were tested under sustained loading conditions. Same bonded lengths as those of short-term tests were selected (i.e. 60 mm, 90 mm and 120 mm). For every bonded length, two different sustained loads were applied (25% and 50% of the failure load of short-term tests). Additionally, two values for the groove width were selected (5 and 10 mm) to study the effect of increasing the adhesive volume. All tests were carried out inside a climatic chamber under four different combinations of temperature and humidity.

4.2.5.1 Test setup, instrumentation and procedures

Long-term pull-out tests were carried out using a specially designed steel frame having a magnification factor of 8.3 (see Figure 4.10). With the aim to use the same configuration as that of short-term tests, a steel plate was placed on the top of the concrete block connecting it to the testing frame by four steel rods attached to another steel plate that was welded to the loading frame. The laminate was connected to the loading frame with the same gripping system as that described in the previous section.

As for the short-term pull-out test, both loaded-end and unloaded-end deformations were measured by means of displacement transducers (LVDTs) connected to the concrete block (see Figure 4.11). Specimens were introduced inside the climate chamber three days before the application of the sustained load. The load was applied by means of small concrete blocks and specimens were kept loaded inside the chamber for 1000 hours.

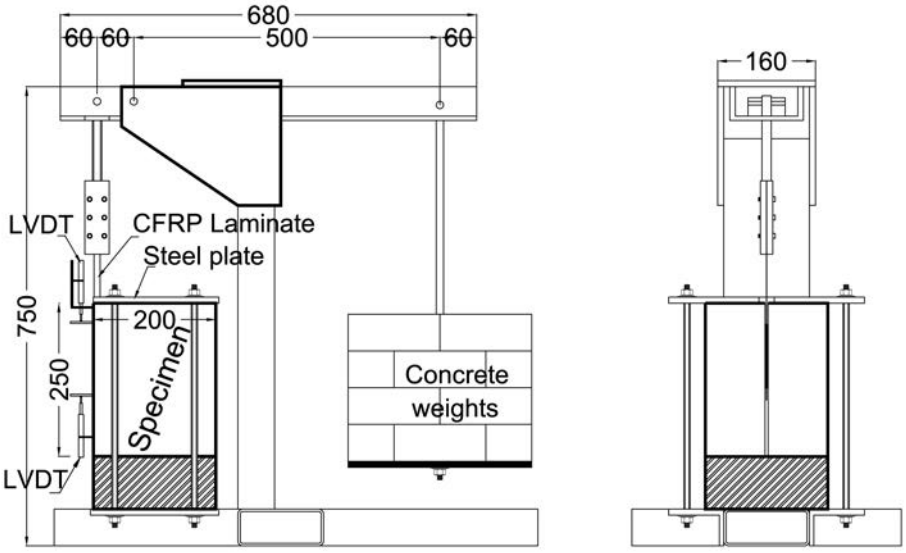

Figure 4.10: Long-term pull-out frame details (units are in mm).

Figure 4.11: Long-term pull-out setup.

4.2.5.2 Test matrix

Table 4.2 presents the long-term pull-out test matrix including specimens' configurations and test conditions. The first column of the table contains the identification of the test series, while the identification of the specimens in the second column is as follows: the letter L is followed by the used bonded length (60 mm, 90 mm and 120 mm); then the letter S is followed by the applied level of sustained load, defined as a percentage of the corresponding failure load of short-term test; the identification follows with the environmental conditions under which the test was carried out (C1, C2, C3 and C4). To conclude the identification, the letter G is followed by the groove width (5 mm or 10 mm). The third, the fourth, the fifth, the sixth and the seventh columns of the table show the bonded length, the applied sustained load level as a percentage of the failure load, the groove width, the applied temperature and the percentage of relative humidity, respectively. The temperature and humidity applied for the four environmental conditions were: 20°C of temperature and 55% of relative humidity for C1, 20°C of temperature and 90% of relative humidity for C2, 40°C of temperature and 55% of relative humidity for C3 and 40°C of temperature and 90% of relative humidity for C4.

Series S1 was designed to investigate the effect of the applied sustained stress level and the bonded length on the bond performance at normal conditions of temperature and humidity (20°C and 55% RH).

As in series S1, the same sustained loading levels and bonded lengths were applied in series S2, S3 and S4; the difference consists in the environmental conditions under which the tests were conducted. To investigate the effect of humidity on the long-term bond performance between NSM FRP and concrete, specimens of series S2 were subjected to relative humidity level equal to 90% while the temperature was kept equal to 20°C. Unlike series S2, specimens of series S3 were subjected to 40°C, while the humidity level was kept equal to 55%, to investigate the effect of temperature on the long-term bond performance. On the other hand, series S4 was designed to study the long-term bond performance under the combined effect of high levels of temperature and humidity. Therefore, specimens in series S4 were subjected to 40°C and 90% RH. Finally, series S5 was designed to investigate the effect of increasing the groove width under conditions of temperature and humidity as those applied for series S1. Unlike previous series, a unique level of sustained load (equal to 50% of the ultimate load) was applied in this latter series.

Table 4.2: Long-term pull-out test matrix.

Series	Specimen ID	Bond length (mm)	Load level (%)	Groove width (mm)	Temperature (°C)	Relative humidity (%)
S1	L60S25C1G5	60	25			
	L90S25C1G5	90	25			
	L120S25C1G5	120	25	5	20	55
	L60S50C1G5	60	50			
	L90S50C1G5	90	50			
	L120S50C1G5	120	50			
S2	L60S25C2G5	60	25			
	L90S25C2G5	90	25			
	L120S25C2G5	120	25	5	20	90
	L60S50C2G5	60	50			
	L90S50C2G5	90	50			
	L120S50C2G5	120	50			
S3	L60S25C3G5	60	25			
	L90S25C3G5	90	25			
	L120S25C3G5	120	25	5	40	55
	L60S50C3G5	60	50			
	L90S50C3G5	90	50			
	L120S50C3G5	120	50			
S4	L60S25C4G5	60	25			
	L90S25C4G5	90	25			
	L120S25C4G5	120	25	5	40	90
	L60S50C4G5	60	50			
	L90S50C4G5	90	50			
	L120S50C4G5	120	50			
S5	L60S50C1G10	60	50			
	L90S50C1G10	90	50	10	20	55
	L120S50C1G10	120	50			

4.3 Experimental results

4.3.1 Short-term results

Figure 4.12 shows the experimental load-slip curves for the direct short-term pull-out tests. Each curve was obtained from average results of three specimens tested for each bonded length (60, 90 and 120 mm). In all cases, an initial linear branch was observed, which corresponds to the bond stiffness of each specimen. Stiffness reduces with further loading, especially for specimens with shorter bonded length (i.e. 60 mm). The average load capacities were 25 kN for specimens with L_b equal to 60 mm and 30 kN for specimens with L_b equal to 90 mm and 120 mm. Specimens with L_b equal to 60 mm failed by concrete failure, while specimens with L_b equal to

90 and 120 mm showed similar behavior and both failed by FRP rupture (see Figure 4.13), indicating that increasing the bonded length beyond the effective one, which according to previous experiments is within the range of 80 mm to 90 mm [145], had no effect on the load capacity as well as the failure mode of specimens tested.

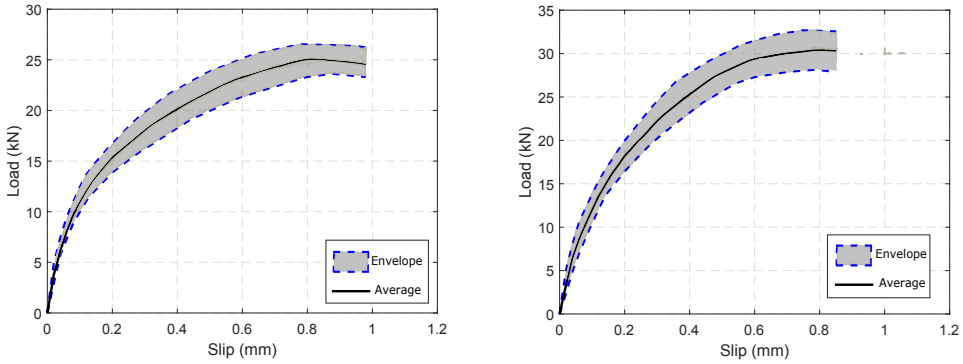

Figure 4.12: Load versus loaded-end slip for short-term tests (a) L_b=60 mm and (b) L_b=90 and 120 mm..

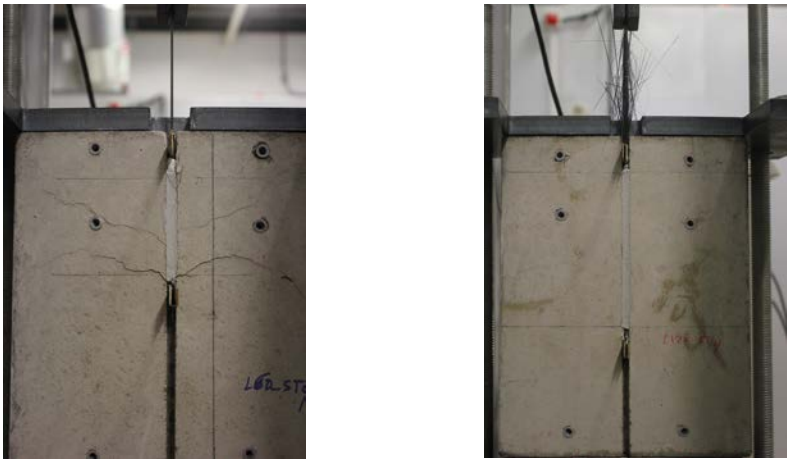

Figure 4.13: Failure modes (a) Concrete failure and (b) CFRP rupture.

4.3.2 Long-term results

The total slip values due to sustained loading were registered along the testing period (i.e. 1000 hours) for each specimen. The total slip includes both the instantaneous (just after the application of load) and time-dependent slips due to the application of the sustained loading.

The loaded-end slip evolution with time for specimens with L_b equal to 60, 90 and 120 mm tested under sustained loading and different environmental conditions is shown in Figures 4.14, 4.15 and 4.16, respectively.

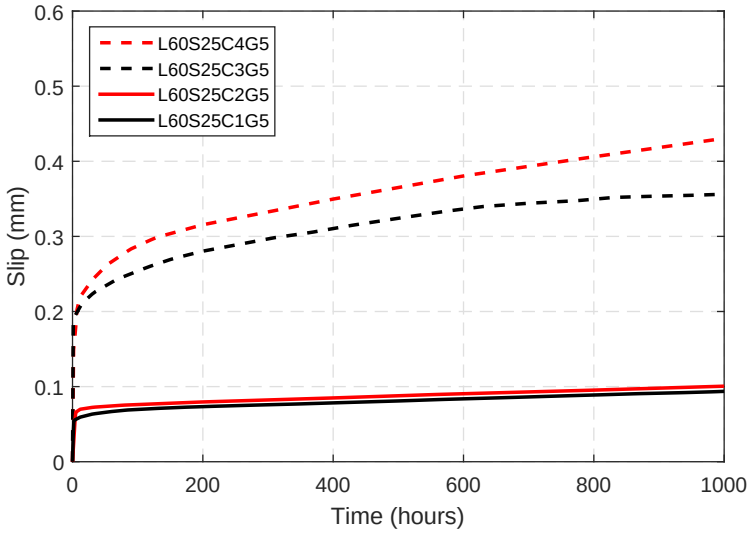

(a)

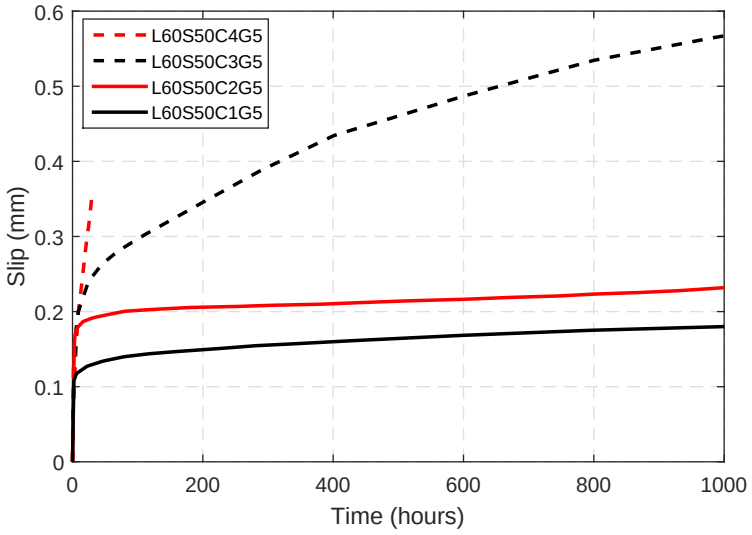

(b)

Figure 4.14: Total loaded-end slip evolution with time for specimens with L_b=60 mm (a) sustained loading equal to 25% and (b) sustained loading equal to 50%.

Results presented in Figure 4.14a show that for specimens at 20°C subjected to a sustained loading level equal to 25% of the load capacity, increasing the humidity level from 55% to 90% (conditions C1 versus C2 in Table 4.2) had no significant effect on the total slip during the testing period in terms of slip values and shape of the slip versus time curve. On the other hand, increasing the humidity level from 55% to 90% at 40°C (C3 versus C4) resulted in an increase in the total slip with time (20% after 1000 hours) with a minor change in the shape of the slip versus time evolution. Similarly, increasing the humidity level in the case of specimens with L_b equal to 90 mm (Figure 4.15a) and specimens with L_b equal to 120 mm (Figure 4.16a) had an analogous effect on the total slip evolution with time as it did for

specimens with L_b equal to 60 mm under the same temperature conditions (Figure 4.14a).

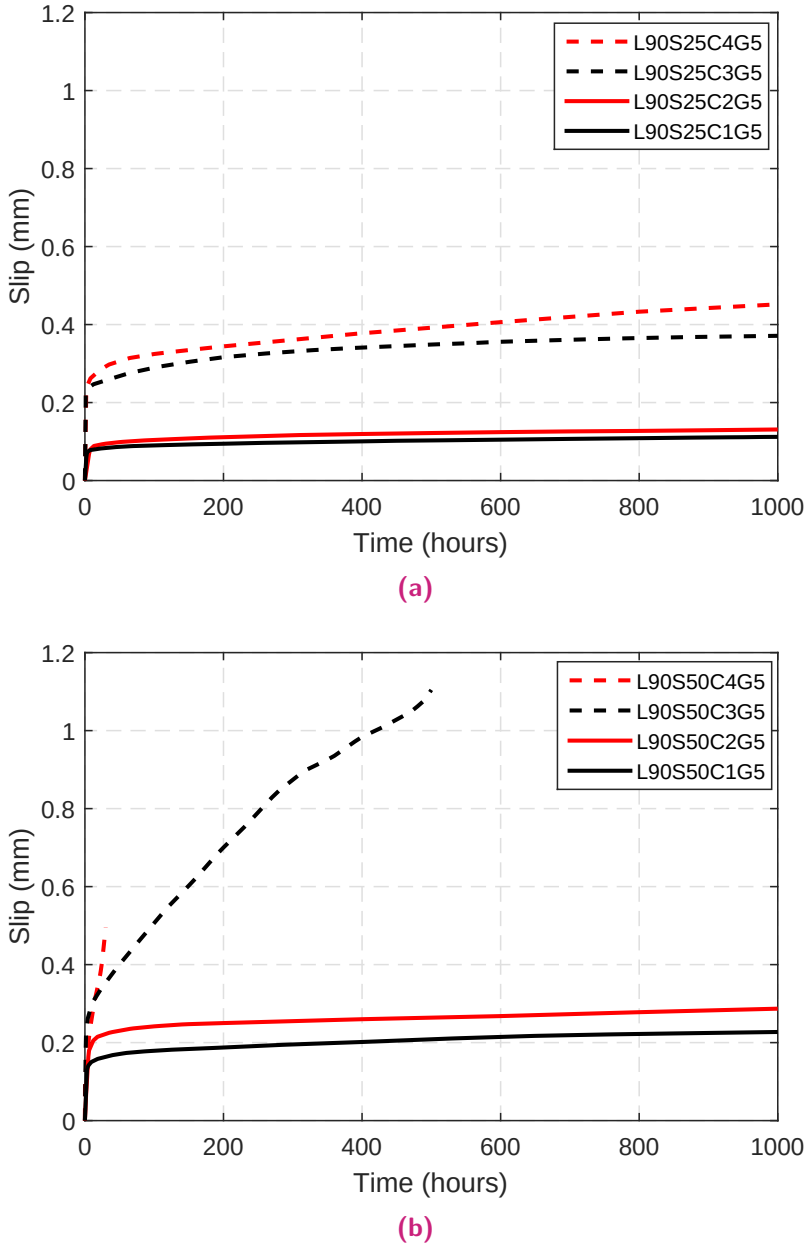

Figure 4.15: Total loaded-end slip evolution with time for specimens with L_b=90 mm (a) sustained loading equal to 25% and (b) sustained loading equal to 50%.

For all the bonded lengths used, when a sustained loading level equal to 50% of the load capacity was applied (Figures 4.14b, 4.15b and 4.16b), increasing the humidity level from 55% to 90% (C1 versus C2) at 20°C increased the total slip with time. The ratio of increase in the total slip was similar for all bonded lengths with values of 1.28, 1.23 and 1.28 observed for specimens with L_b equal to 60, 90 and 120 mm, respectively. Applying the same increase in the humidity at 40°C resulted in greater deformation in the adhesive layer, leading to a dramatic increase of slip with

time and the early failure of specimens L60S50C4G5 (Figure 4.14b), L90S50C4G5 (Figure 4.15b) and L120S50C4G5(Figure 4.16b). The times to failure observed were 40, 30 and 130 hours after the initiation of the test, respectively.

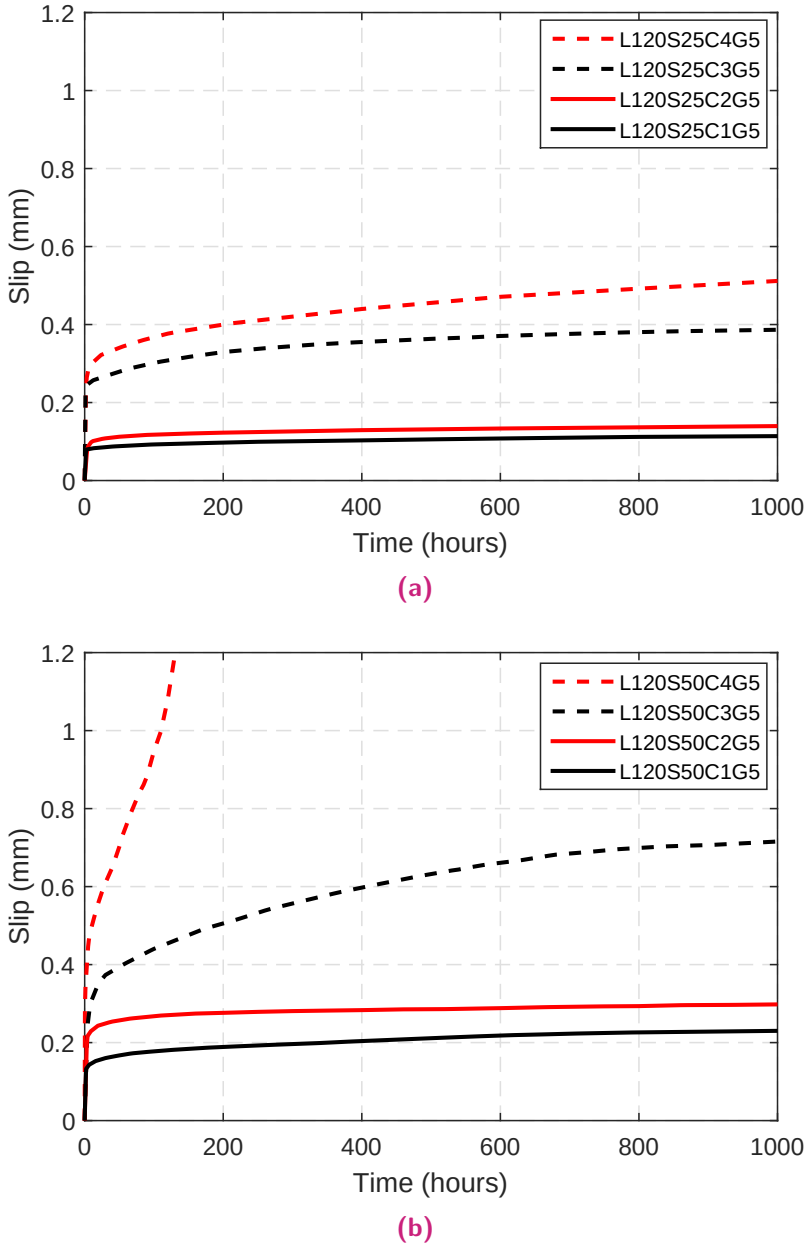

Figure 4.16: Total loaded-end slip evolution with time for specimens with L_b=120 mm (a) sustained loading equal to 25% and (b) sustained loading equal to 50%.

In the case of specimens subjected to a sustained loading of 25% (Figures 4.14a, 4.15a and 4.16a) and a humidity of 55% RH, increasing the temperature from 20°C to 40°C (C1 versus C3) increased both the instantaneous and time-dependent slips for all bonded lengths used. Higher increases in terms of total slip were observed when the temperature increased from 20°C to 40°C at 90% RH (C2 versus C4).

For both aforementioned cases, the shape of the total slip curve started to slightly change with time as more slip developed due to the increase in the temperature.

Increasing the temperature from 20°C to 40°C at sustained loading of 50% resulted in a greater increase in the slip values with time and, therefore, a larger increase in the ratios of the total slip to the instantaneous slip, hereafter referred to as R, when 55% RH was applied (see Table 4.3). Moreover at 90% RH, the increase in temperature led to the early failure of all the specimens.

Specimen L90S50C3G5, tested at a sustained loading of 50% and subjected to 40°C and 55% RH, failed after 500 hours from loading (See Figure 4.15b). Although the results clearly indicate the influence that temperature has on all the specimens, this specific element seemed to exhibit an anomalous behavior since no failure was observed in the case of the specimens with either shorter or longer lengths (i.e. 60 mm and 120 mm). A little misalignment detected between FRP and loading frame might explain this unexpected failure.

For a testing temperature of 20°C, doubling the sustained loading level (from 25% to 50%), almost doubled the total slip values over the testing period. The observed average ratios of increase in the slip with time were 1.9, 2.1 and 2.1 for specimens subjected to 55% RH with L_b equal to 60, 90 and 120 mm, respectively (condition C1). These ratios were 2.3, 2.2 and 2.1 for specimens subjected to 90% RH with L_b equal to 60, 90 and 120 mm, respectively (condition C2). Greater increase in the slip was observed when the sustained loading was doubled as in the case of conditions C3 and C4.

Whatever the environmental conditions and the level of sustained load applied, similar behaviors, in terms of slip evolution with time, were observed for specimens with L_b equal to 90 and 120 mm. This indicates that increasing the bonded length beyond the effective one had minor effects on the slip evolution with time, irrespective of the level of sustained load and environmental conditions applied. The specimens with L_b equal to 60 mm exhibited lower slip values over time as a lower value of sustained loading was applied according to the percentage of the failure load.

Figure 4.17 illustrates the total slip with time when sustained loading equal to 50% was applied, for the case of specimens with groove width equal 10 mm. Results show that, whatever the bonded length used L_b (60, 90 and 120 mm), increasing the groove width from 5 to 10 mm resulted in a lower total slip values. The increase in the groove width caused an increase in the adhesive volume that might allow more redistribution of stresses along the bonded length, leading to less deformation. In the case of specimens having L_b equal to 90 mm and 120 mm similar tendencies were observed (see Figure 4.17) as for previous series. The average reduction in the

total slip was 0.82, 0.91 and 0.93 for specimen with L_b equal to 60, 90 and 120 mm, respectively.

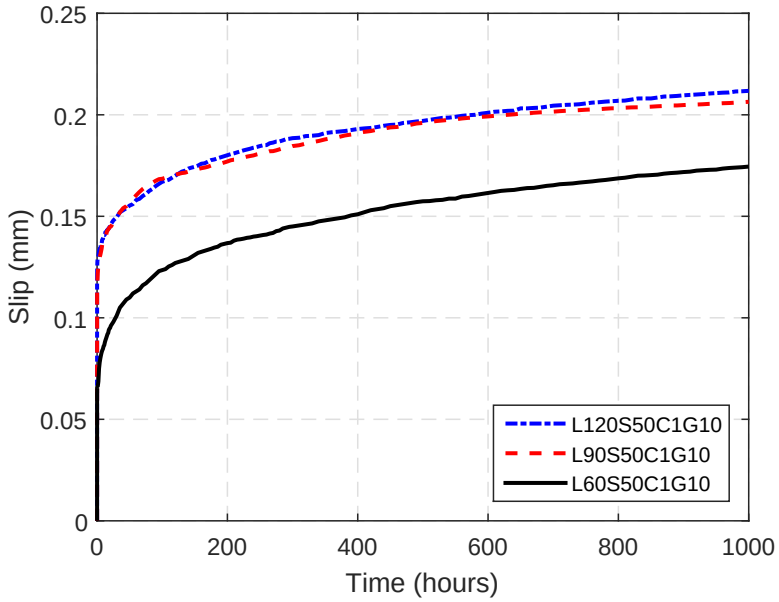

Figure 4.17: Total loaded-end slip with time at 50% of sustained loading (Series 5).

Table 4.3 shows the ratio between total slip and instantaneous slip (R) at different times from loading. For specimens from series S1 and S2, the observed values of R were found to be almost constant (the average ratio was 1.77) whatever the bonded length used and the sustained loading level applied. Specimens from series S3 (loaded at 25%) exhibited higher values for R (with an average of 1.91), when compared with those in series S1 and S2. More significant increases in these ratios were observed for specimens from series S3 loaded at 50% of the maximum load (the average ratio was 3.24). The highest ratios at sustained loading equal to 25% (with an average of 2.21) were observed in the case of specimens subjected to 40°C and 90% RH (series S4). In general, increasing the sustained load level within the S3 and S4 conditions increased the ratio R, while it was almost constant within the conditions for S1 and S2.

Table 4.3: Ratio between total slip and instantaneous slip (R) at different times from loading.

Series	Specimen ID	Time since loading (hours)			
		50	100	500	1000
S1	L60S25C1G5	1.25	1.32	1.53	1.75
	L90S25C1G5	1.29	1.43	1.63	1.75
	L120S25C1G5	1.28	1.44	1.63	1.74
	L60S50C1G5	1.29	1.46	1.59	1.75
	L90S50C1G5	1.30	1.49	1.68	1.76
	L120S50C1G5	1.30	1.48	1.67	1.74
S2	L60S25C2G5	1.31	1.34	1.55	1.77
	L90S25C2G5	1.34	1.41	1.62	1.77
	L120S25C2G5	1.44	1.51	1.67	1.79
	L60S50C2G5	1.49	1.55	1.64	1.78
	L90S50C2G5	1.50	1.51	1.65	1.79
	L120S50C2G5	1.54	1.61	1.72	1.81
S3	L60S25C3G5	1.31	1.39	1.79	1.90
	L90S25C3G5	1.38	1.49	1.80	1.91
	L120S25C3G5	1.37	1.48	1.80	1.91
	L60S50C3G5	1.52	1.68	2.73	3.44
	L90S50C3G5	1.70	2.22	4.78	*
	L120S50C3G5	1.69	1.87	2.77	3.05
S4	L60S25C4G5	1.36	1.50	1.88	2.23
	L90S25C4G5	1.46	1.55	1.90	2.20
	L120S25C4G5	1.48	1.61	2.00	2.22
	L60S50C4G5	*	*	*	*
	L90S50C4G5	*	*	*	*
	L120S50C4G5	2.33	3.33	*	*
S5	L60S50C1G10	1.57	1.76	2.24	2.43
	L90S50C1G10	1.43	1.54	1.78	1.82
	L120S50C1G10	1.30	1.40	1.64	1.75

∗: specimen failed

4.4 Summary of results

The results of an experimental program investigating the long-term bond behavior, in terms of slip evolution with time, between NSM CFRP laminates and concrete

when subjected to sustained loading and different environmental regimes have been presented. Sustained load levels of 25% and 50% of the load capacity obtained from short-term tests, bonded lengths of 60, 90 and 120 mm, combined with different levels of temperature (20°C and 40°C) and relative humidity (55% and 90%) were the main parameters of the study. Based on the results obtained the following summary can be highlighted:

- At 20°C, increasing the humidity had no significant effect on the slip evolution with time when sustained loading level equal to 25% was applied. Meanwhile, a significant effect was observed at sustained loading level equal to 50% within the same test conditions.

- The effect of increasing humidity was more evident in the case of specimens tested at 40°C than in those tested at 20°C.

- For all bonded lengths used, increasing the sustained loading level from 25% to 50% (within S1 and S2 conditions) increased the total slip by almost the double at any time along the testing period.

- Whatever the environmental conditions and the level of sustained load applied, similar behaviors, in terms of slip evolution with time, were observed for specimens with L_b equal to 90 and 120 mm.

- The application of sustained loading equal to 50% combined with the most severe environmental regimes (40°C and 90% RH) led to the early failure of all specimens. The observed times to failure were 40, 30, and 130 hours for specimens with L_b equal to 60, 90 and 120 mm, respectively.

- For specimens of series S1 and S2, the ratio between the total slip after 1000 hours to the instantaneous one was almost constant, whatever the bonded length used and the sustained loading level applied. This ratio was increased with the increase in the sustained loading level applied within series S3 and S4.

- When the groove width increased from 5 to 10 mm, the total slip values reduced for all bonded lengths. The average reduction was 0.82, 0.91 and 0.93 for specimen with L_b equal to 60, 90 and 120 mm, respectively.

5 Analytical modeling

5.1 Introduction

A number of analytical models have been developed to simulate the short-term bond behavior of NSM FRP bonded to concrete, but existing work on long-term models has been rather limited. In this chapter, a simplified procedure to simulate the long-term behavior, under non-aggressive serviceability conditions and sustained loading, of the NSM joint is proposed. First the governing equations for short-term bond behavior between NSM CFRP strips and concrete are described, and then the simulation of the long-term behavior is introduced. Finally, the predicted slip variation versus time is compared to experimental results.

5.2 Short-term bond behavior

In a monotonic pull-out test, forces are transferred from reinforcement to concrete through the adhesive by means of shear stresses that developed at their interfaces. Figure 5.1 shows an infinitesimal element of CFRP strip of length *dx*, showing the shear stresses at the interface and tensile stresses at the transversal section (of dimensions $h_f \times t_f$).

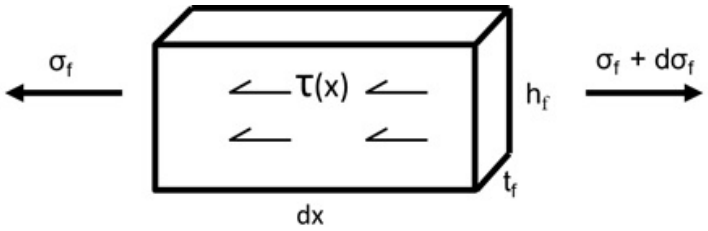

Figure 5.1: Stresses acting on an infinitesimal element of NSM strip.

Equilibrium equation of this infinitesimal element, along with the assumption that the CFRP strip has a linear elastic behavior and the CFRP-concrete joint is at the elastic stage, allows obtaining the differential equation governing the stress transfer process (Equation 5.1):

$$\frac{d\sigma_f}{dx} = \frac{\tau(x)}{t_{eq}} \tag{5.1}$$

$$t_{eq} = A_f / L_p \tag{5.2}$$

$$L_p = (t_f + t_a) + 2\,(h_f + t_a) \tag{5.3}$$

where σ_f is the tensile stress in the FRP, τ is the shear stress, t_{eq} is the ratio between the FRP cross-sectional area (A_f) and the intermediate perimeter in the adhesive layer (L_p), t_a is the thickness of the adhesive layer, and t_f and h_f are the thickness and the width of the FRP strip, respectively (see Figure 5.2).

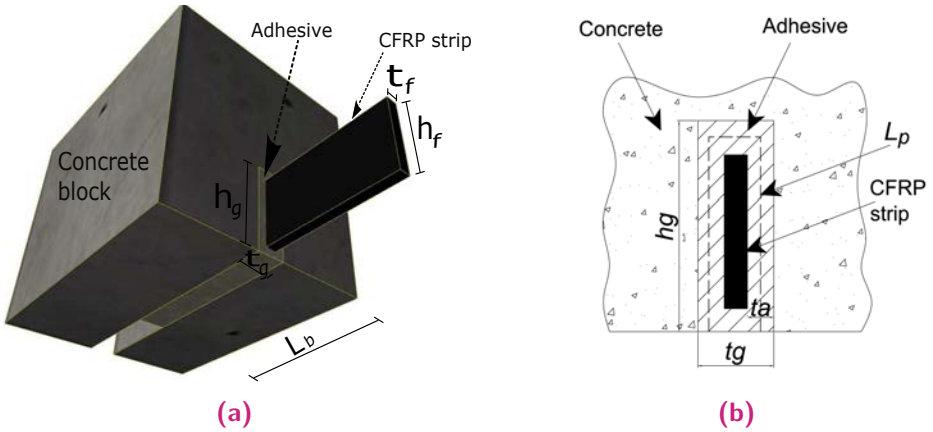

Figure 5.2: (a) NSM system and (b) Details of cross section.

According to the literature [9, 64, 103, 107, 108, 142, 167–171], the bond-slip behavior of elements strengthened with FRP reinforcement can be satisfactorily simulated by using a local bilinear law as that shown in Figure 5.3 and described by Equation 5.4.

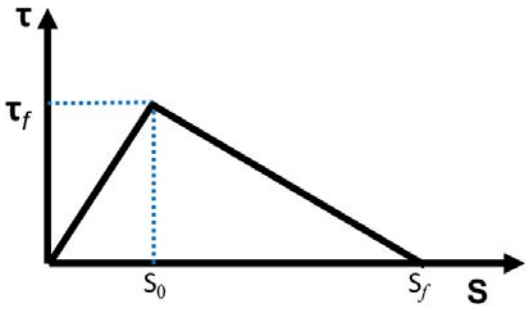

Figure 5.3: Bi-linear bond-slip.

$$\tau = \begin{cases} \frac{\tau_f}{s_0} s & for \quad 0 < s \leq s_0 \\ \frac{\tau_f}{s_f - s_0}(s_f - s) & for \quad s_0 < s \leq s_f \\ 0 & for \quad s > s_f \end{cases} \tag{5.4}$$

where τ and s are the interfacial shear stress and its corresponding slip, respectively, τ_f is the maximum interfacial shear stress, s_0 is the slip at τ_f and s_f is the maximum slip of the τ-s relationship.

This study aims to simulate the effects of sustained loading under serviceability conditions. For this purpose, it is assumed that the slip between CFRP and concrete can be represented by a local bond-slip law applied to the adhesive layer, that the deformability of the concrete can be neglected, and that the adhesive is subjected to pure shear [104, 108, 142, 168, 171–173]. The interfacial shear stress in the ascending branch of the bilinear bond-slip law can be obtained by:

$$\tau = K_e \, s \tag{5.5}$$

where s is the slip of the CFRP strip and K_e is the stiffness of the τ-s relationship, that can be described as:

$$K_e = \frac{\tau_f}{s_0} \tag{5.6}$$

being τ_f and s_0 the maximum interfacial bond stress in the τ-s relationship and its corresponding slip, respectively.

The first derivative of Equation 5.5 yields to:

$$\frac{d\tau}{dx} = K_e \, \varepsilon_f \tag{5.7}$$

where ε_f is the strain in FRP strip.

By using Equations 5.7 and 5.1, the following differential equation can be obtained:

$$\frac{d^2\sigma_f}{dx^2} - \alpha^2 \sigma_f = 0 \tag{5.8}$$

where

$$\alpha^2 = \frac{K_e}{E_f \, t_{eq}} \tag{5.9}$$

being E_f the modulus of elasticity of the FRP.

Equation 5.8 can be solved applying the following boundary conditions: at $x = 0$ (unloaded-end), $\sigma_f = 0$ and at $x = L$ (loaded-end), $\sigma = \sigma_0$ (the applied stress in the FRP). After solving, the distribution of the axial FRP stress, shear stress and the slip along the bonded length (at any distance x from the unloaded-end) are given by:

$$\sigma_f(x) = \sigma_0 \frac{\sinh(\alpha x)}{\sinh(\alpha L_b)} \tag{5.10}$$

$$\tau(x) = t_{eq}\,\alpha\,\sigma_0\,\frac{\cosh(\alpha x)}{\sinh(\alpha L_b)} \tag{5.11}$$

$$s(x) = \frac{t_{eq}}{K_e}\,\alpha\,\sigma_0\,\frac{\cosh(\alpha x)}{\sinh(\alpha L_b)} \tag{5.12}$$

5.3 Bond behavior under sustained loading

The bases of the approach presented in [138] for modeling the long-term bond behavior of steel bars in concrete have been followed in this work, with the difference that the creep effects are introduced here into the bilinear bond-slip model for short-term behavior of the NSM system previously described (Figure 5.3). According to this approach, the evolution of the local bond-slip with time can be estimated based on the initial local bond-slip law and the creep function of the joint, in such a way that slip at any time can be described by:

$$s(t) = s_0(1 + \phi(t, t_0)) \tag{5.13}$$

where *s(t)* and *s(t_0)* are the slip values at time *t* and t_0 from loading, respectively, and $\phi(t, t_0)$ is the creep function of the joint between times *t* and t_0.

The application of this assumption to the short-term bond-slip model (Figure 5.3) would cause a shift on the right of the curve for t_0, resulting in a set of curves for different times as that indicated in Figure 5.4. This increment of area under the curves would represent an unrealistic increment in the available energy under long-term loading. To avoid this inconsistency the use of the bond-slip law at time t_0 as an envelope is proposed in [138], and this way the maximum available energy corresponds to that of the short-term bond law. Therefore the final set of curves for long-term would correspond to the modified ascending branches for each time *t* intersecting with the descending branch for short-term as indicated in Figure 5.4 (the path for ascending and descending branches at time *t* is given by the arrows). This assumption was shown to be adequate in previous works using a non-linear bond-slip law composed of four zones, similar to that used for deformed steel bars in concrete [87].

The practical application of this methodology can be carried out by using the so-called Effective Modulus Method (EMM) in which an effective stiffness $K_e(t)$ [142] for the ascending branch is used as follows:

$$K_e(t) = \frac{K_e(t_0)}{(1 + \phi(t, t_0))} \tag{5.14}$$

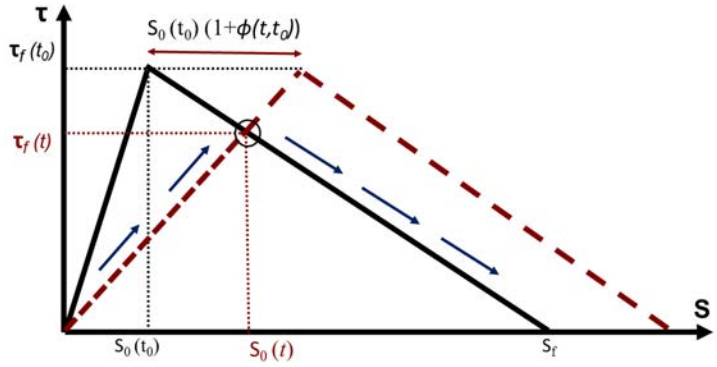

Figure 5.4: Bond-slip evolution with time (arrows show the new bond-slip law at time t).

$$\tau_f(t) = K_e(t)\, s_0(t) \tag{5.15}$$

where $K_e(t_0)$ and $K_e(t)$ are the stiffnesses of the ascending branch at times t_0 and t, respectively, $\tau_f(t)$ and ϕ(t,t_0) are the maximum interfacial shear stress and the creep coefficient at time t, respectively, and $s_0(t)$ is the slip corresponding to $\tau_f(t)$.

This is represented in Figure 5.4 through the reduction in the slope of the ascending branch of the bond-slip relationship at time t ($t > t_0$). With this reasoning, the time-dependent behavior can be introduced in the analytical equations describing the short-term bond problem (Equations 5.9-5.12) just by changing the stiffness K_e by the stiffness with time ($K_e(t)$).

The evolution of bond-slip law with time presented in Figure 5.4 is mainly dependent on the adhesive's properties. These properties can be determined through a tensile creep test that allows for creep coefficients at different times ($\phi(t)$) to be obtained, and therefore, for bond-slip relationships at any time to be determined. Through this procedure, the analytical equations describing the distribution of the axial CFRP stress, the shear stress and the slip along the bonded length with time read:

$$\alpha^2(t) = \frac{K_e(t)}{E_f\, t_{eq}} \tag{5.16}$$

$$\sigma_f(x,t) = \sigma_0\, \frac{\sinh(\alpha(t)\, x)}{\sinh(\alpha(t)\, L_b)} \tag{5.17}$$

$$\tau(x,t) = t_{eq}\, \alpha(t)\, \sigma_0\, \frac{\cosh(\alpha(t)\, x)}{\sinh(\alpha(t)\, L_b)} \tag{5.18}$$

$$s(x,t) = \frac{t_{eq}}{K_e(t)}\,\alpha(t)\,\sigma_0\,\frac{\cosh(\alpha(t)\,x)}{\sinh(\alpha(t)\,L_b)} \tag{5.19}$$

From the equations above it is seen that the creep developed in the joint with time under the effects of sustained loading leads to a reduction in the effective stiffness and consequently more slip takes place along the bonded length as well as more bonded length is activated. Furthermore, this effect leads to a redistribution of stresses resulting in a decrease of the maximum shear and local concrete stresses.

5.4 Comparison between analytical and experimental results

The experimental results in non-aggressive environmental conditions (i.e Series S1) obtained in the current work are used to check the presented analytical model.

Assuming a short-term load-slip curve as that shown in Figure 5.5 and that the axial stiffness of the FRP strip is much smaller than that of the concrete, the maximum bond-stress at time t_0 ($\tau_f(t_0)$) can be obtained as [108, 142]:

$$\tau_f(t_0) = \frac{P_{max}^2}{L_p\,A_f\,E_f\,s_f} \tag{5.20}$$

where P_{max} and s_f are the load and slip values at the peak point of the load-slip curve (i.e. point B) at which the interface shear stress reaches its maximum value, and s_0 is the slip at the end of the linear-elastic part of the curve (point A).

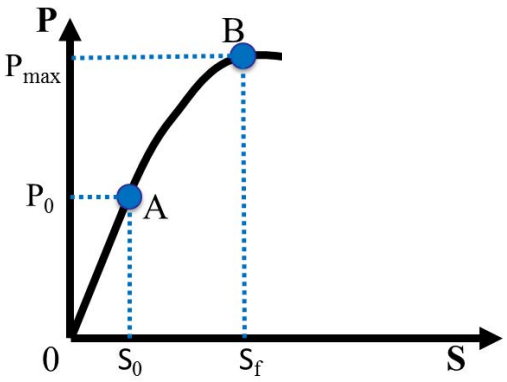

Figure 5.5: Load versus slip relationship under monotonic loading.

The adhesive's creep coefficients were obtained from the tensile creep test carried in Chapter 3 at the same environmental conditions as the pull-out tests and with the same batch of epoxy resin. Experimental values of creep coefficients and the

corresponding equivalent stiffnesses are presented in the second and third columns of Table 5.1, respectively, while the bond-slip parameters ($\tau_f(t)$ and $s_0(t)$ in Figure 5.4) for the long-term equivalent curves at different times are indicated in the fourth and fifth columns, respectively.

Table 5.1: Bond-slip parameters at different times.

Time (hours)	ϕ(t)	K_e(t) (N/mm^3)	τ_f(t) (MPa)	s_0(t) (mm)
0	0	229	18.35	0.08
10	0.21	189	18.04	0.10
50	0.45	158	17.71	0.11
100	0.67	137	17.41	0.13
500	1.66	86	16.20	0.19
1000	2.40	68	15.42	0.23

Once the equivalent stiffness ($K_e(t)$) has been obtained, analytical predictions of the evolution of slip with time (Equation 5.19) are compared to experimental values of the experimental program and presented in Figures 5.6-5.8, for specimens with bonded length of 60, 90 and 120 mm, respectively. As it can be seen, good agreement is in general observed for the analyzed cases, thus indicating that the proposed methodology predicts reasonably well the slip evolution with time.

Table 5.2 presents a summary of the experimental and predicted values for the loaded-end slips at loading (t=0 hours) and at the end of the testing period (t=1000 hours). The ratios between experimental and predicted slip values are also shown along with the mean and the standard deviation showing good correlation between experimental and analytical results.

Table 5.2: Comparison between experimental and analytical long-term predictions.

Specimen ID	loaded-end slip at t= 0 hours (mm)			loaded-end slip at t= 1000 hours (mm)		
	$s_{exp.}$	s_{model}	$s_{model}/s_{exp.}$	$s_{exp.}$	s_{model}	$s_{model}/s_{exp.}$
L60S25C1G5	0.053	0.052	0.98	0.094	0.103	1.10
L60S50C1G5	0.103	0.104	1.01	0.180	0.201	1.10
L90S25C1G5	0.063	0.064	1.02	0.112	0.122	1.09
L90S50C1G5	0.131	0.132	1.01	0.230	0.241	1.04
L120S25C1G5	0.063	0.064	1.02	0.109	0.119	1.09
L120S50C1G5	0.132	0.131	0.99	0.231	0.241	1.04
Mean			1.01			1.06
Standard deviation			0.01			0.04

$s_{exp.}$: experimental value
s_{model}: analytical value

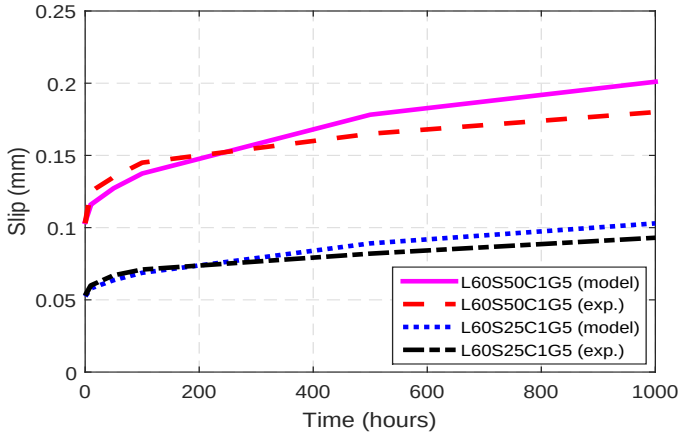

Figure 5.6: Comparison of analytical and experimental evolution of slip with time for specimens with L_b=60 mm.

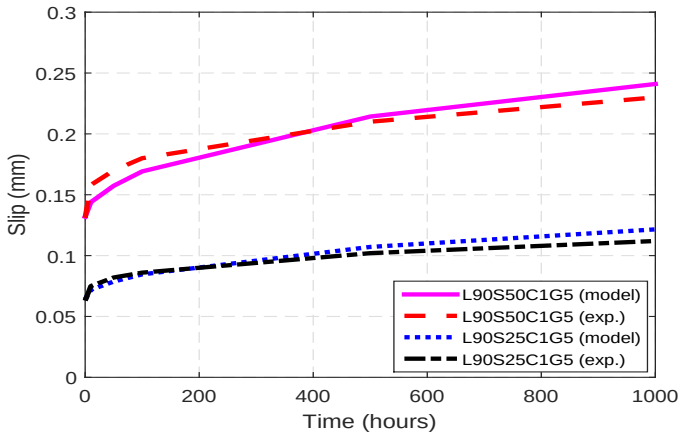

Figure 5.7: Comparison of analytical and experimental evolution of slip with time for specimens with L_b=90 mm.

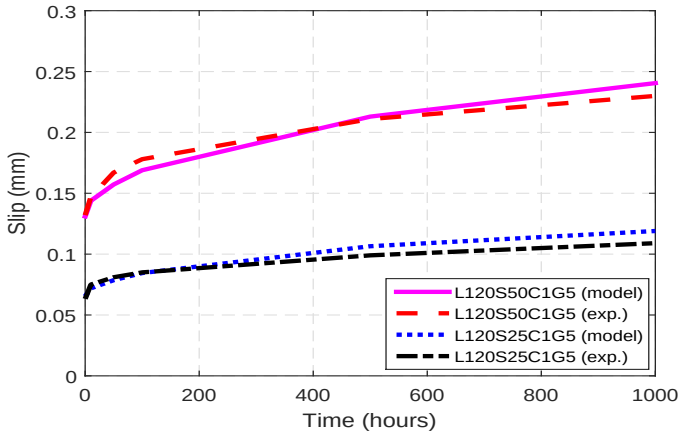

Figure 5.8: Comparison of analytical and experimental evolution of slip with time for specimens with L_b=120 mm.

5.5 Conclusions

A simplified analytical methodology was developed, based on a bi-linear interface model, using the EMM to simulate the long-term behavior of NSM CFRP laminates in concrete under sustained loading and serviceability conditions. In the presented methodology it was assumed that the slip between CFRP and concrete can be represented by a local bond-slip law applied to the adhesive layer, the deformability of the concrete can be neglected and the adhesive is subjected to pure shear. The long-term behavior was introduced by shifting the bond-slip law with respect to time but maintaining the initial one as an envelope. The parameters of the bond-slip model were calculated by using results of the experimental program previously carried out in this thesis. Good agreement in terms of total slip evolution with time was observed between analytical and experimental results, thus indicating the adequacy of the model and assumptions used. Furthermore, the proposed experimental procedure is acceptable and recommended for constitutive modeling of bond mechanics of NSM strips in elements subjected for long-term loading.

6 Conclusions and future work

6.1 Summary

The use of FRP materials as NSM reinforcement has become an attractive technique for strengthening and preserving RC structures. Despite of the popularity of the traditional EB technique, there has been an increasing interest in the NSM technique due to several potential advantages it provides. The bond behavior of NSM system, which affects the success and efficiency of the strengthening system, may be influenced by different parameters. Investigations on the bond behavior of NSM CFRP strips in concrete have been mainly concentrated on short-term behavior while studies on the long-term behavior, as well as available experimental data about it, are still scarce. Furthermore, the durability and performance during the service life of the structure are aspects of main importance that are strongly related to the long-term behavior of the structural system. Therefore, there is an urgent need of extending the knowledge and information about this crucial issue in order to provide understanding that could contribute to the improvement of design.

In the present work, the long-term bond behavior, in terms of bond strength and bond-slip response, of NSM CFRP strips in concrete has been investigated both analytically and experimentally. Firstly, an experimental program to characterize the tensile creep behavior of the adhesive used in the study has been carried out. Sustained load level and different conditions of temperature and humidity have been considered. The experimental instantaneous and long-term tensile strains with time have been reported and discussed.

Secondly, an experimental program has been carried out to study the main variables involved in time-dependent bond-slip response of NSM CFRP strips in concrete. Direct pull-out tests have been carried out under both short-term and long-term conditions. Different sustained load levels, bonded lengths, as well as temperature and humidity conditions have been considered. A specific setup for the application of sustained gravity loads based on a lever arm system has been designed. The experimental instantaneous and long-term deformations have been reported and discussed.

Furthermore, a rational methodology that maintains simplicity has been proposed by using the general principles of the EMM. The proposed methodology simulates the time-dependent bond-slip response of NSM CFRP strips in concrete. Finally, the predictions obtained with the proposed analytical method have been compared to the experimental results obtained from the present work showing a general good agreement.

6.2 Creep of adhesive

The most relevant conclusions from the experimental studies performed in Chapter 3 can be summarized as follows:

- Increasing temperature and humidity caused a rapid increase in the creep behavior. Temperature, compared to that of humidity, showed a greater effect on the instantaneous strain, creep coefficient and time to failure.

- The adhesive showed a linear viscoelastic creep behavior up to a sustained loading level equal to 60% under 20°C and humidity level equal to 55%. The creep compliance was almost constant. This level of load for linear creep behavior started to decrease when the environmental conditions were changed to more extreme conditions.

- Increasing the sustained loading level of the adhesive (up to 60% of its ultimate strength) resulted in almost linear increase in the instantaneous initial strain values. Changes in temperature and humidity conditions did not affect this behavior.

- Whatever the sustained loading level applied, changing the humidity from low level to high level did not significantly affect the instantaneous initial strain.

- At low level of sustained loading, increasing temperature combined with high humidity level almost had no effect on the instantaneous initial strain. On the other hand, the instantaneous initial strain increased at medium and high levels of sustained loading

- Increasing the humidity level increased both creep rates and creep coefficient and caused early failure of specimens when combined with high levels of sustained loading.

- Increasing the temperature increased both creep coefficients and creep strains and resulted in shorter times to failure in case of medium and high levels of sustained loading.

- Increasing both temperature and humidity resulted in shorter times to failure for all specimens due to the rapid degradation in the adhesive's strength and the stiffness.

6.3 Bond behavior

The most relevant conclusions from the experimental and analytical studies carried out in Chapters 4 and 5 can be summarized as follows:

- The innovative equipment adopted in this experimental program for the long-term pull-out tests appears to be an efficient protocol for investigation of time-dependent bond-slip response of NSM FRP reinforcement in concrete. It gives reliable data while maintaining a manageable specimen size.

- The proposed experimental procedure is acceptable and recommended for constitutive modeling of bond mechanics of NSM strips in elements subjected for long-term loading.

- The time-dependent bond-slip response of the adhesively bonded joint was found to be influenced by the adhesive.

- Temperature seemed to have greater effect, compared to that of humidity, on the time-dependent bond-slip response of NSM CFRP laminates in concrete; however, the combination of high temperature and humidity levels led to the early failure of all specimens subjected to sustained loading level equal to 50%.

- Whatever the environmental conditions and the level of sustained load applied, similar behaviors, in terms of slip evolution with time, were observed for specimens with L_b equal to 90 and 120 mm.

- At 20°C, increasing the humidity had no significant effect on the slip evolution with time when sustained loading level equal to 25% was applied. Meanwhile, a significant effect was observed at sustained loading level equal to 50% within the same test conditions.

- The effect of increasing humidity was more evident in the case of specimens tested at high temperature than in those tested at normal temperature (20°C).

- Whatever the bonded lengths used at 20°C, increasing the sustained loading level from 25% to 50% increased the total slip by almost the double at any time along the testing period.

- At 20°C, the bonded length as well as the applied sustained loading level had almost no effect on the the ratio between the total slip after 1000 hours to the instantaneous one. On the other hand, This ratio was increased with the increase in the sustained loading level applied for specimens tested at higher temperature.

- Increasing the groove width from 5 to 10 mm reduced the total slip values for all bonded lengths.

- A simplified analytical methodology has been developed, based on a bi-linear interface model, using the effective modulus method. Good agreement is observed between analytical and experimental results.

6.4 Future work

Based on the results of this research and the conducted literature review, the following topics are proposed as future work:

- To extend the experimental work regarding the long-term bond behavior of NSM CFRP strips in concrete under levels of sustained loading corresponding to serviceability conditions, in conjunction with different combinations of environmental conditions, constant and variable.

- To study the effect of additional parameters that may affect the long-term bond-slip response of the NSM FRP strengthened elements, as for example: FRP shape, FRP material, type of adhesive, type of concrete and specimen's configuration.

- To extend the experimental work regarding the long-term bond-slip response of NSM CFRP strips in concrete under environmental adversities such as freeze-thaw cycles and elevated temperatures.

- To study the effect of long-term loading on the ultimate load of the NSM FRP RC systems to properly estimate the reliability of structures subject to significant permanent loads during their life.

- To perform a numerical study using finite element method in order to analyze the long-term effects for different combinations of influencing parameters. Different bond-slip laws, jointly with nonlinear material modeling of materials and time-dependent analysis shall be considered.

- To extend the analytical methodology for the case of different conditions of temperature and humidity. A parametric study and further experimental tests should be carried out for its validation.

Bibliography

[1] FIB Bulletin 14. *Externally bonded* FRP *reinforcement for* RC *structures. Design and use of externally bonded fibre reinforced polymer reinforcement* (FRP EBR) *for reinforced concrete structures*. fib Task Group 9.3 FRP reinforcement for concrete structures, the International Federation for Structural Concrete. Lausanne, Switzerland, 2001.

[2] B. Täljsten, A. Carolin, and H. Nordin. "Concrete structures strengthened with near surface mounted reinforcement of CFRP". In: *Advances in structural engineering* 6.3 (2003), pp. 201–213.

[3] U. Meier. "Carbon fiber-reinforced polymers: modern materials in bridge engineering". In: *Structural Engineering International* 2.1 (1992), pp. 7–12.

[4] J. Teng, J.-F. Chen, S. T. Smith, and L Lam. "FRP: strengthened RC structures". In: *Frontiers in Physics* (2002), p. 266.

[5] L. C. Bank. *Composites for construction: structural design with FRP materials*. John Wiley & Sons, 2006.

[6] ACI 440.2.R-17. *Guide for the Design and Construction of Externally Bonded* FRP *Systems for Strengthening of Concrete Structures*. ACI Committee 440, American Concrete Institute. Farmington Hills, Michigan, USA, 2017.

[7] P. Balaguru, A. Nanni, and J. Giancaspro. FRP *composites for reinforced and prestressed concrete structures: A guide to fundamentals and design for repair and retrofit*. CRC Press, 2008.

[8] R. Parretti and A. Nanni. "Strengthening of RC members using near-surface mounted FRP composites: Design overview". In: *Advances in Structural Engineering* 7.6 (2004), pp. 469–483.

[9] L. De Lorenzis and J. Teng. "Near-surface mounted FRP reinforcement: An emerging technique for strengthening structures". In: *Composites Part B: Engineering* 38.2 (2007), pp. 119–143.

[10] L. De Lorenzis and A. Nanni. "Bond between Near-Surface Mounted Fiber-Reinforced Polymer Rods and Concrete in Structural Strengthenings". In: *ACI Structural Journal* 99.2 (2002), pp. 123–132.

[11] A. M. Neville. *Properties of concrete*. Vol. 4. Longman London, 1995.

[12] R. I. Gilbert and G. Ranzi. *Time-dependent behaviour of concrete structures*. CRC Press, 2010.

[13] H. V. GangaRao, N. Taly, and P. Vijay. *Reinforced concrete design with FRP composites*. CRC press, 2006.

[14] D. A. Hensher. *Fiber-reinforced-plastic (FRP) reinforcement for concrete structures: properties and applications*. Vol. 42. Elsevier, 2016.

[15] R. M. Jones. M*echanics of composite materials*. 2nd ed. Taylor and Francis, 1999.

[16] L. C. Hollaway and J.-G. Teng. *Strengthening and rehabilitation of civil infrastructures using fibre-reinforced polymer (FRP) composites*. Elsevier, 2008.

[17] R. Fangueiro. *Fibrous and composite materials for civil engineering applications*. Elsevier, 2011.

[18] Z. K. Szabó. "Bond characteristics of NSM reinforcements based on advanced test method". PhD thesis. Budapest, Hungary: Budapest University of Technology and Economics, 2013.

[19] K. Pilakoutas, Z. Achillides, and P. Waldron. "Non-ferrous reinforcement in concrete structures". In: *Topping, E.M.L.&.B., Centenary Conference on Innovation in Civil and Structural Engineering. Civil-Comp Ltd*. Topping, E.M.L.&.B., Centenary Conference on Innovation in Civil and Structural Engineering. Civil-Comp Ltd. 1997, pp. 47–58.

[20] J. Y. Sheikh-Ahmad. *Machining of polymer composites*. Springer, 2009.

[21] L. Bisby and J Fitzwilliam. "An introduction to FRP composites for construction". In: *ISIS education module, Manitoba, Canada* (2006).

[22] P. K. Mallick. *Fiber-reinforced composites: materials, manufacturing, and design*. CRC press, 2007.

[23] A. Carolin. "Carbon fibre reinforced polymers for strengthening of structural elements". PhD thesis. Luleå tekniska universitet, 2003.

[24] G. Akovali. *Handbook of composite fabrication*. iSmithers Rapra Publishing, 2001.

[25] R. El-Hacha and S. H. Rizkalla. "Near-surface-mounted fiber-reinforced polymer reinforcements for flexural strengthening of concrete structures". In: *Structural Journal* 101.5 (2004), pp. 717–726.

[26] M. Blaschko and K. Zilch. "Rehabilitation of concrete structures with CFRP strips glued into slits". In: *Proceedings of the twelfth international conference of composite materials, ICCM*. Vol. 12. 1999.

[27] J. M. de Sena Cruz and J. A. Oliveira de Barros. "Bond between near-surface mounted carbon-fiber-reinforced polymer laminate strips and concrete". In: *Journal of Composites for Construction* 8.6 (2004), pp. 519–527.

[28] J. Teng, L De Lorenzis, B. Wang, R. Li, T. Wong, and L. Lam. "Debonding failures of RC beams strengthened with near surface mounted CFRP strips". In: *Journal of Composites for Construction* 10.2 (2006), pp. 92–105.

[29] M. Baena. "Study of bond behaviour between FRP reinforcement and concrete". ISBN: 978-84-694-2484-1. PhD thesis. Girona, Spain: University of Girona, 2010.

[30] B. Täljsten. "The importance of bonding: A historic overview and future possibilities". In: *Advances in Structural Engineering* 9.6 (2006), pp. 721–736.

[31] S. Ebnesajjad and A. H. Landrock. *Adhesives technology handbook*. William Andrew, 2014.

[32] A. Pizzi and K. L. Mittal. *Handbook of adhesive technology, revised and expanded*. CRC press, 2003.

[33] L. De Lorenzis, A. Rizzo, and A. La Tegola. "A modified pull-out test for bond of near-surface mounted FRP rods in concrete". In: *Composites Part B: Engineering* 33.8 (2002), pp. 589–603.

[34] R. El-Hacha and K. Soudki. "Prestressed near-surface mounted fibre reinforced polymer reinforcement for concrete structures: A review". In: *Canadian Journal of Civil Engineering* 40.11 (2013), pp. 1127–1139.

[35] A. Nanni. "Concrete repair with externally bonded FRP reinforcement". In: *Concrete International* 17.6 (1995), pp. 22–26.

[36] A. Khalifa, W. J. Gold, A. Nanni, and A. A. MI. "Contribution of externally bonded FRP to shear capacity of RC flexural members". In: *Journal of composites for construction* 2.4 (1998), pp. 195–202.

[37] T. C. Triantafillou. "Shear strengthening of reinforced concrete beams using epoxy-bonded FRP composites". In: *Structural Journal* 95.2 (1998), pp. 107–115.

[38] J. Chen and J. Teng. "Shear capacity of FRP-strengthened RC beams: FRP debonding". In: *Construction and Building Materials* 17.1 (2003), pp. 27–41.

[39] E. Oller Ibars, D. Cobo del Arco, and A. R. Mari Bernat. "Interface Behavior in Fiber-Reinforced Polymer-Strengthened Beams Subjected to Transverse Loads: Maximum Transferred Force". In: *Journal of Composites for Construction* 13.1 (2009), pp. 35–44.

[40] A. De Diego, A. Arteaga, J. Fernández, R. Perera, and D. Cisneros. "Behaviour of FRP confined concrete in square columns". In: *Materiales de Construcción* 65.320 (2015), p. 069.

[41] V. Gribniak, A. K. Arnautov, A. Norkus, V. Tamulenas, E. Gudonis, and A. Sokolov. "Experimental Investigation of the Capacity of Steel Fibers to Ensure the Structural Integrity of Reinforced Concrete Specimens Coated with CFRP Sheets". In: *Mechanics of Composite Materials* 52.3 (2016), pp. 401–410.

[42] V. Gribniak, V. Tamulenas, P.-L. Ng, A. K. Arnautov, E. Gudonis, and I. Misiunaite. "Mechanical Behavior of Steel Fiber-Reinforced Concrete Beams Bonded with External Carbon Fiber Sheets". In: *Materials* 10.6 (2017), pp. 666–684.

[43] P. Mukhopadhyaya and N. Swamy. "Interface shear stress: a new design criterion for plate debonding". In: *Journal of Composites for Construction* 5.1 (2001), pp. 35–43.

[44] J. Sena-Cruz, J. Barros, V. Bianco, A. Bilotta, D. Bournas, F. Ceroni, G. Dalfré, R. Kotynia, G. Monti, E. Nigro, et al. "NSM systems". In: *Design Procedures for the Use of Composites in Strengthening of Reinforced Concrete Structures*. Springer, 2016, pp. 303–348.

[45] N. Kishi, H. Mikami, Y. Kurihashi, and S. Sawada. "Flexural behaviour of RC beams reinforced with NSM AFRP rods". In: *Proceedings of the International Symposium on Bond Behaviour of FRP in structures (BBFS 2005)*. 2005, pp. 337–342.

[46] J. G. Tumialan, M. Vatovec, and P. L. Kelley. “Case study: strengthening of parking garage decks with near-surface-mounted CFRP bars”. In: *Journal of Composites for Construction* 11.5 (2007), pp. 523–530.

[47] R. Parretti and A. Nanni. “Strengthening of RC members using near-surface mounted FRP composites: Design overview”. In: *Advances in Structural Engineering* 7.6 (2004), pp. 469–483.

[48] R. El-Hacha, R. Wight, and M. Green. “Prestressed fibre-reinforced polymer laminates for strengthening structures”. In: *Progress in Structural Engineering and Materials* 3.2 (2001), pp. 111–121.

[49] J. Michels, J. Sena-Cruz, C. Czaderski, and M. Motavalli. “Structural strengthening with prestressed CFRP strips with gradient anchorage”. In: *Journal of Composites for Construction* 17.5 (2013), pp. 651–661.

[50] R. Kotynia, K. Lasek, and M. Staskiewicz. “Flexural behavior of preloaded RC slabs strengthened with prestressed CFRP laminates”. In: *Journal of Composites for Construction* 18.3 (2013), A4013004–11.

[51] M. Rezazadeh, I. Costa, and J. Barros. “Influence of prestress level on NSM CFRP laminates for the flexural strengthening of RC beams”. In: *Composite Structures* 116 (2014), pp. 489–500.

[52] M. M. Hosseini, S. J. Dias, and J. A. Barros. “Effectiveness of prestressed NSM CFRP laminates for the flexural strengthening of RC slabs”. In: *Composite Structures* 111 (2014), pp. 249–258.

[53] J. Michels, M. Staśkiewicz, C. Czaderski, R. Kotynia, Y. E. Harmanci, and M. Motavalli. “Prestressed CFRP strips for concrete bridge girder retrofitting: application and static loading test”. In: *Journal of Bridge Engineering* 21.5 (2016), pp. 04016003–14.

[54] H. Nordin and B. Täljsten. “Concrete beams strengthened with prestressed near surface mounted CFRP”. In: *Journal of composites for construction* 10.1 (2006), pp. 60–68.

[55] D. M. Nguyen, T. K. Chan, and H. K. Cheong. “Brittle failure and bond development length of CFRP-concrete beams”. In: *Journal of Composites for Construction* 5.1 (2001), pp. 12–17.

[56] E. Oller Ibars, D. Cobo del Arco, and A. R. Mari Bernat. “Laminate debonding process of FRP-strengthened beams”. In: *Structure and Infrastructure Engineering* 7.1-2 (2011), pp. 131–146.

[57] H Toutanji and P Balaguru. “Durability characteristics of concrete columns wrapped with FRP tow sheets”. In: *Journal of materials in civil engineering* 10.1 (1998), pp. 52–57.

[58] Z. K. Szabó and G. L. Balázs. “Near surface mounted FRP reinforcement for strengthening of concrete structures”. In: *Periodica Polytechnica. Civil Engineering* 51.1 (2007), pp. 33–38.

[59] A. Bilotta, F. Ceroni, M. Di Ludovico, E. Nigro, M. Pecce, and G. Manfredi. “Bond efficiency of EBR and NSM FRP systems for strengthening concrete members”. In: *Journal of Composites for Construction* 15.5 (2011), pp. 757–772.

[60] J. A. Barros, S. J. Dias, and J. L. Lima. “Efficacy of CFRP-based techniques for the flexural and shear strengthening of concrete beams”. In: *Cement and Concrete Composites* 29.3 (2007), pp. 203–217.

[61] D. Lim. “Shear behaviour of RC beams strengthened with NSM and EB CFRP strips”. In: *Magazine of Concrete Research* 62.3 (2010), pp. 211–220.

[62] S.-Y. Seo, L. Feo, and D. Hui. “Bond strength of near surface-mounted FRP plate for retrofit of concrete structures”. In: *Composite Structures* 95 (2013), pp. 719–727.

[63] T. Hassan and s. Rizkalla. “Investigation of bond in concrete structures strengthened with near surface mounted carbon fiber reinforced polymer strips”. In: *Journal of composites for construction* 7.3 (2003), pp. 248–257.

[64] M. R. Coelho, J. M. Sena-Cruz, and L. A. Neves. “A review on the bond behavior of FRP NSM systems in concrete”. In: *Construction and Building Materials* 93 (2015), pp. 1157–1169.

[65] L. De Lorenzis and A. Nanni. “Characterization of FRP rods as near-surface mounted reinforcement”. In: *Journal of Composites for Construction* 5.2 (2001), pp. 114–121.

[66] M. Blaschko. “Bond behaviour of CFRP strips glued into slits”. In: *Proceedings of Sixth International Symposyum on FRP Reinforcement for Concrete Structures. Singapore: World Scientific, Singapore*. 2003, pp. 205–14.

[67] L. De Lorenzis. “Strengthening of RC structures with near surface mounted FRP rods”. PhD thesis. University of Missouri-Rolla, United States, 2001.

[68] R. Perera, A. Recuero, A. De Diego, and C. López. “Adherence analysis of fiber-reinforced polymer strengthened RC beams”. In: *Computers & structures* 82.23 (2004), pp. 1865–1873.

[69] D. Galati and L. De Lorenzis. “Effect of construction details on the bond performance of NSM FRP bars in concrete”. In: *Advances in Structural Engineering* 12.5 (2009), pp. 683–700.

[70] F. Ceroni, M. Pecce, A. Bilotta, and E. Nigro. “Bond behavior of FRP NSM systems in concrete elements”. In: *Composites Part B: Engineering* 43.2 (2012), pp. 99–109.

[71] D. Lee, L. Cheng, and J. Yan-Gee Hui. “Bond characteristics of various NSM FRP reinforcements in concrete”. In: *Journal of Composites for Construction* 17.1 (2012), pp. 117–129.

[72] W. Kalupahana, T. Ibell, and A. Darby. “Bond characteristics of near surface mounted CFRP bars”. In: *Construction and Building Materials* 43 (2013), pp. 58–68.

[73] J. Sena-Cruz. “Strengthening of concrete structures with near-surface mounted CFRP laminate strips”. PhD thesis. Guimarães, Portugal: Universidade do Minho, 2004.

[74] F. Al-Mahmoud, A. Castel, R. François, and C. Tourneur. “Anchorage and tension-stiffening effect between near-surface-mounted CFRP rods and concrete”. In: *Cement and Concrete Composites* 33.2 (2011), pp. 346–352.

[75] A. Merdas, B. Firio, and N. Chikh. “Bond behavior of carbon laminate strips and rods into concrete by pullout-bending tests”. In: *Bond in Concrete. Brescia, Italy.* 2012, pp. 1087–1092.

[76] J. M. Sena Cruz, J. A. Barros, R. Gettu, and A. F. Azevedo. “Bond behavior of near-surface mounted CFRP laminate strips under monotonic and cyclic loading”. In: *Journal of Composites for Construction* 10.4 (2006), pp. 295–303.

[77] R. Seracino, N. M. Jones, M. Ali, M. W. Page, and D. J. Oehlers. “Bond strength of near-surface mounted FRP strip-to-concrete joints”. In: *Journal of Composites for Construction* 11.4 (2007), pp. 401–409.

[78] I. Sharaky. “A study of the bond and flexural behaviour of reinforced concrete elements strengthened with near surface mounted (NSM) FRP reinforcement”. PhD thesis. Girona, Spain: Universitat de Girona, 2013.

[79] T. Hassan and s. Rizkalla. “Bond mechanism of NSM FRP bars for flexural strengthening of concrete structures”. In: *ACI Structural Journal* 101.6 (2004), pp. 830–839.

[80] L. De Lorenzis, K. Lundgren, and A. Rizzo. “Anchorage Length of Near-Surface Mounted Fiber-Reinforced Polymer Bars for Concrete Strengthening - Experimental Investigation and Numerical Modeling”. In: *ACI Structural Journal* 101.2 (2004), pp. 269–278.

[81] D. Novidis, S. Pantazopoulou, and E. Tentolouris. “Experimental study of bond of NSM-FRP reinforcement”. In: *Construction and Building Materials* 21.8 (2007), pp. 1760–1770.

[82] I. Sharaky, L Torres, M Baena, and C Miàs. “An experimental study of different factors affecting the bond of NSM FRP bars in concrete”. In: *Composite Structures* 99 (2013), pp. 350–365.

[83] I. Sharaky, L Torres, M Baena, and I Vilanova. “Effect of different material and construction details on the bond behaviour of NSM FRP bars in concrete”. In: *Construction and Building Materials* 38 (2013), pp. 890–902.

[84] D. Galati and L. De Lorenzis. “Experimental Study on the Local Bond Behavior of NSM-FRP Bars to Concrete”. In: *Proceedings of Third International Conference on FRP Composites in Civil Engineering (CICE 2006)*. 2006, pp. 95–98.

[85] M. A. Blaschko. “Mechanical behaviour of concrete structures with CFRP strips glued into slits (Zum Tragverhalten von Betonbauteilen mit Schlitze eingeklebten CFK-Lamellen)”. PhD thesis. Technical University München, Berichte aus dem Konstructiven Inginieurbau (In German), 2001.

[86] S. M. Soliman, E. El-Salakawy, and B. Benmokrane. “Bond performance of near-surface-mounted FRP bars”. In: *Journal of Composites for Construction* 15.1 (2010), pp. 103–111.

[87] K. Borchert and K. Zilch. “Bond behaviour of NSM FRP strips in service”. In: *Structural Concrete* 9.3 (2008), pp. 127–142.

[88] L. Torres, I. A. Sharaky, C. Barris, and M. Baena. “Experimental study of the influence of adhesive properties and bond length on the bond behaviour of NSM FRP bars in concrete”. In: *Journal of Civil Engineering and Management* 22.6 (2016), pp. 808–817.

[89] K. Borchert and K. Zilch. “A general bond stress-slip relationship for NSM FRP strips”. In: *Proceedings of the FRPRCS-8 International Symposium*. 2007, pp. 8–1.

[90] I. Costa and J. Barros. “Critical Analysis of Fibre-Reinforced Polymer Near-Surface Mounted Double-shear Pull-out Tests”. In: *Strain* 49.4 (2013), pp. 299–312.

[91] A. Palmieri, S. Matthys, J. A. Barros, I. Costa, A. Bilotta, E. Nigro, F. Ceroni, Z. Szambo, and G. Balazs. “Bond of NSM FRP strengthened concrete: round robin test initiative”. In: *CICE 2012 6th International Conference on FRP Composites in Civil Engineering*. CICE 2012 6th International Conference on FRP Composites in Civil Engineering. 2012, pp. 1–8.

[92] F. Al-Mahmoud, A. Castel, R. François, and C. Tourneur. “Effect of surface pre-conditioning on bond of carbon fibre reinforced polymer rods to concrete”. In: *Cement and Concrete Composites* 29.9 (2007), pp. 677 –689.

[93] A. Bilotta, F. Ceroni, J. A. Barros, I. Costa, A. Palmieri, Z. K. Szabó, E. Nigro, S. Matthys, G. L. Balazs, and M. Pecce. “Bond of NSM FRP-strengthened concrete: Round robin test initiative”. In: *Journal of Composites for Construction* 20.1 (2015), p. 04015026.

[94] F. Ceroni, J. A. Barros, M. Pecce, and M. Ianniciello. “Assessment of nonlinear bond laws for near-surface-mounted systems in concrete elements”. In: *Composites Part B: Engineering* 45.1 (2013), pp. 666–681.

[95] J. A. Barros and J. Sena-Cruz. “Bond behavior of carbon laminate strips into concrete by pullout-bending tests”. In: *Bond in concrete: from research to standards: proceedings of the third International Symposium on Bond in Concrete*. 2002, pp. 614–621.

[96] FIB Bulletin 10. B*ond of Reinforcement in Concrete*. State-of-the-art report, Technical report, the International Federation for Structural Concrete. Lausanne, Switzerland, 2000.

[97] M. G. Alexander, H.-D. Beushausen, F. Dehn, and P. Moyo. *Concrete Repair, Rehabilitation and Retrofitting III: 3rd International Conference on Concrete Repair, Rehabilitation and Retrofitting, ICCRRR-3, 3-5 September 2012, Cape Town, South Africa*. CRC Press, 2012.

[98] R. Kotynia. “Bond between FRP and concrete in reinforced concrete beams strengthened with near surface mounted and externally bonded reinforcement”. In: *Construction and Building Materials* 32 (2012), pp. 41–54.

[99] X. Yan, B. Miller, A. Nanni, and C. Bakis. “Characterization of CFRP rods used as near surface mounted reinforcement”. In: *8th International conference on structural faults and repair*. 1999.

[100] S. El-Gamal, Y. Al-Salloum, S. Alsayed, and M. Aqel. “Performance of near surface mounted glass fiber reinforced polymer bars in concrete”. In: *Journal of Reinforced Plastics and Composites* 31.22 (2012), pp. 1501–1515.

[101] Z. K. Szabó and G. L. Balázs. “Experimental evaluation of bond strength for near surface mounted reinforcements”. In: *6th International Conference of Analytical Models and New Concepts in Concrete and Masonry Structures (AMCM,2008), June 9-11, Lodz, Poland*. 2008.

[102] D. Cisnerios, I. Sharaky, M. Baena, L. Torres, A. Arteaga, A. De Diego, and R. Perera. "Comparative Study of Beam-test and Pull-out Test to Investigate Bond of NSM FRP Bars in Concrete". In: *Proceedings of the 11th International Symposium on Fiber Reinforced Polymer Reinforcement for Reinforced Concrete Structures FRPRCS-11 Guimaraes, (eds. Barros, Cruz) Portugal, pp. 103-104*. 2013.

[103] R. Seracino, M. Raizal Saifulnaz, and D. Oehlers. "Generic debonding resistance of EB and NSM plate-to-concrete joints". In: *Journal of Composites for Construction* 11.1 (2007), pp. 62–70.

[104] J. S. Sena Cruz and J. Barros. "Modeling of bond between near-surface mounted CFRP laminate strips and concrete". In: *Computers & Structures* 82.17 (2004), pp. 1513–1521.

[105] A. M. Malek, H. Saadatmanesh, and M. R. Ehsani. "Prediction of failure load of R/C beams strengthened with FRP plate due to stress concentration at the plate end". In: *ACI structural Journal* 95 (1998), pp. 142–152.

[106] T. Kanakubo, T. Furuta, and H. Fukuyama. "Bond strength between fiber-reinforced polymer laminates and concrete". In: *Proceedings of 6th International Symposium on FRP Reinforcement for Concrete Structures*. Vol. 1. 2003, pp. 133–142.

[107] M. M. Ali, D. Oehlers, M. Griffith, and R Seracino. "Interfacial stress transfer of near surface-mounted FRP-to-concrete joints". In: *Engineering Structures* 30.7 (2008), pp. 1861–1868.

[108] H. Yuan, J. Teng, R. Seracino, Z. Wu, and J. Yao. "Full-range behavior of FRP-to-concrete bonded joints". In: *Engineering structures* 26.5 (2004), pp. 553–565.

[109] S. Zhang, J.-G. Teng, and T. Yu. "Bond strength model for CFRP strips near-surface mounted to concrete". In: *Journal of Composites for Construction* 18.3 (2013), A4014003.

[110] S. Zhang, J. Teng, and T. Yu. "Bond–slip model for CFRP strips near-surface mounted to concrete". In: *Engineering structures* 56 (2013), pp. 945–953.

[111] J. Teng, S. T. Smith, J Yao, and J. F. Chen. "Intermediate crack-induced debonding in RC beams and slabs". In: *Construction and building materials* 17.6 (2003), pp. 447–462.

[112] SA. *Design handbook for RC structures retrofitted with FRP and metal plates: beams and slabs*. HB 305-2008. Standards Australia GPO Box 476, Sydney, NSW 2001, Australia, 2008, p. 76.

[113] K. Naumenko and H. Altenbach. *Modeling of creep for structural analysis*. Springer Science & Business Media, 2007.

[114] W. N. Findley and F. A. Davis. *Creep and relaxation of nonlinear viscoelastic materials*. Courier Corporation, 2013.

[115] Z. P. Bazant. "Theory of creep and shrinkage in concrete structures: A precis of recent developments". In: *Mechanics today* 2 (1975), pp. 1–93.

[116] A. M. Neville. "Properties of Concrete, 4th". In: *London: Pitman Publishing* 687 (2011), p. 331.

[117] P. Mitchell. "Freeze-thaw and sustained load durability of near surface mounted FRP strengthened concrete". PhD thesis. 2010.

[118] Z. P. Bazant and R. L'Hermite. *Mathematical modeling of creep and shrinkage of concrete*. Wiley New York, 1988.

[119] R. I. Gilbert. "Time effects in concrete structures". In: *Developments in civil engineering* 23 (1988).

[120] K. T. Chong, S. J. Foster, and R. I. Gilbert. "Time-dependent modelling of RC structures using the cracked membrane model and solidification theory". In: *Computers & Structures* 86.11 (2008), pp. 1305–1317.

[121] ACI 209R. *Prediction of Creep, Shrinkage, and Temperature Effects in Concrete Structures*. ACI Committee 209, American Concrete Institute, 1992.

[122] FIB Bulletin 65 & 66. *Model Code 2010 Final Draft*. Vol. 65&66. ISBN 987-2-88394-106-9. International Federation for Structural Concrete. Lausanne, Switzerland, 2012.

[123] ACI 318-14. *Building Code Requirements for Structural Concrete and C*. ACI Committee 318, American Concrete Institute. Farmington Hills, Michigan, USA, 2014.

[124] L. C. Hollaway and M. Leeming. *Strengthening of reinforced concrete structures: Using externally-bonded FRP composites in structural and civil engineering*. Elsevier, 1999.

[125] L. Malvar. "Durability of composites in reinforced concrete". In: *Proceedings of the first international conference on durability of composites for construction*. 1998, pp. 361–372.

[126] W. K. Goertzen and M. Kessler. "Creep behavior of carbon fiber/epoxy matrix composites". In: *Materials Science and Engineering: A* 421.1 (2006), pp. 217–225.

[127] W. Findley. "Mechanism and mechanics of creep of plastics". In: *SPE journal* 16.1 (1960), pp. 57–65.

[128] M. Holmes and D. Just. "GRP in Structural Engineering.(Retroactive Coverage)". In: *Applied Science Publishers Ltd., 1983,* (1983), p. 298.

[129] C.-W. Feng. "Prediction of long-term creep behavior of epoxy adhesives for structural applications". MA thesis. Texas A&M University., 2004.

[130] P. Meshgin, K.-K. Choi, and M. M. R. Taha. "Experimental and analytical investigations of creep of epoxy adhesive at the concrete–FRP interfaces". In: *International Journal of Adhesion and Adhesives* 29.1 (2009), pp. 56–66.

[131] P. Majda and J. Skrodzewicz. "A modified creep model of epoxy adhesive at ambient temperature". In: *International Journal of Adhesion and Adhesives* 29.4 (2009), pp. 396–404.

[132] I. Costa and J. Barros. "Tensile creep of a structural epoxy adhesive: Experimental and analytical characterization". In: *International Journal of Adhesion and Adhesives* 59 (2015), pp. 115–124.

[133] P. Silva, T. Valente, M. Azenha, J. Sena-Cruz, and J. Barros. "Viscoelastic response of an epoxy adhesive for construction since its early ages: Experiments and modelling". In: *Composites Part B: Engineering* 116 (2017), pp. 266–277.

[134] R. Maksimov and E Plume. "Long-term creep of hybrid aramid/glass-fiber-reinforced plastics". In: *Mechanics of composite materials* 37.4 (2001), pp. 271–280.

[135] M. Miravalles and I. Dharmawan. “The creep behaviour of adhesives. A numerical and experimental investigation”. In: *Master Thesis, Department of Structural Engineering, Chalmers University of Technology, Göteborg, Sweden* (2007).

[136] H. BRINSON and L. C. Brinson. *Polymer engineering science and viscoelasticity*. Springer, 2016.

[137] C.-W. Feng, C.-W. Keong, Y.-P. Hsueh, Y.-Y. Wang, and H.-J. Sue. “Modeling of long-term creep behavior of structural epoxy adhesives”. In: *International journal of adhesion and adhesives* 25.5 (2005), pp. 427–436.

[138] CEB-Serviceability Models-Behavior. *Modeling in Serviceability Limit States Including Repeated and Sustained Loads*. Comite Euro-International Du Beton. Lausanne, Switzerland, 1997.

[139] P. Silva, P. M. G. Fernandes, J. Sena-Cruz, M. Azenha, and J. A. Barros. “Creep behavior and durability of concrete elements strengthened with NSM CFRP strips”. In: *7th International Conference on Fiber Reinforced Polymer (FRP) Composites in Civil Engineering (CICE 2014)*. 2014, pp. 1–6.

[140] M. Derias, R. El-Hacha, and S. Rizkalla. “Durability of NSM FRP strengthening systems for RC flexural members”. In: *4th International Conference on Fiber Reinforced Polymer (FRP) Composites in Civil Engineering (CICE 2008), Zurich, Switzerland*. 2008.

[141] C. Mazzotti and M. Savoia. “Long term properties of bond between concrete and FRP”. In: *Proc int sympo on bond behavior of FRP in structures* (2005), pp. 539–45.

[142] C. Mazzotti and M. Savoia. “Stress redistribution along the interface between concrete and FRP subject to long-term loading”. In: *Advances in Structural Engineering* 12.5 (2009), pp. 651–661.

[143] E. Ferrier, L. Michel, B. Jurkiewiez, and P. Hamelin. “Creep behavior of adhesives used for external FRP strengthening of RC structures”. In: *Construction and Building Materials* 25.2 (2011), pp. 461–467.

[144] A. Rizzo and L. De Lorenzis. “Behavior and capacity of RC beams strengthened in shear with NSM FRP reinforcement”. In: *Construction and Building Materials* 23.4 (2009), pp. 1555–1567.

[145] P. M. Fernandes, P. M. Silva, and J. Sena-Cruz. “Bond and flexural behavior of concrete elements strengthened with NSM CFRP laminate strips under fatigue loading”. In: *Engineering Structures* 84 (2015), pp. 350–361.

[146] J. Michels, R. Widmann, C. Czaderski, R. Allahvirdizadeh, and M. Motavalli. “Glass transition evaluation of commercially available epoxy resins used for civil engineering applications”. In: *Composites Part B: Engineering* 77 (2015), pp. 484–493.

[147] S&P220. *220 epoxy adhesive:Two-component epoxy resin-based adhesive for S&P* FRP *Systems*. 2013.

[148] ASTM D3418. *Standard Test Methods of Polymers by Differential Scanning Calorimetry*. American Society for Testing and Materials. West Conshohocken, PA, 1999.

[149] ISO 11357-2. *Plastics - Differential Scanning Calorimetry - Part 2: Determination of glass transition temperature*. International Organization for Standardization. Geneva, Switzerland, 1999.

[150] K. P. Menard. *Dynamic mechanical analysis: a practical introduction*. CRC press, 2008.

[151] ISO 527-1. *Plastics - Determination of tensile properties - Part 1: General principles*. International Organization for Standardization. Geneva, Switzerland, 2012.

[152] ISO 527-2. *Plastics - Determination of tensile properties - Part 2: Test conditions for moulding and extrusion plastics*. International Organization for Standardization. Geneva, Switzerland, 2012.

[153] M. G. Abiad, O. H. Campanella, and M. T. Carvajal. "Assessment of thermal transitions by dynamic mechanical analysis DSC using a novel disposable powder holder". In: *Pharmaceutics* 2.2 (2010), pp. 78–90.

[154] M. Kalichevsky, E. Jaroszkiewicz, S Ablett, J. Blanshard, and P. Lillford. "The glass transition of amylopectin measured by DSC, DMTA and NMR". In: *Carbohydrate Polymers* 18.2 (1992), pp. 77–88.

[155] ISO 899-1. *Plastics - Determination of creep behaviour - Part 1: Tensile creep*. International Organization for Standardization. Geneva, Switzerland, 2003.

[156] ASTM D2290. *Standard Test Methods for Tensile, Compressive, and Flexural Creep and Creep-Rupture of Plastics*. American Society for Testing and Materials. Pennsylvania, US, 2001.

[157] B. De Neve and M. Shanahan. "Effects of humidity on an epoxy adhesive". In: *International Journal of Adhesion and Adhesives* 12.3 (1992), pp. 191–196.

[158] M. Lettieri and M. Frigione. "Effects of humid environment on thermal and mechanical properties of a cold-curing structural epoxy adhesive". In: *Construction and Building Materials* 30 (2012), pp. 753–760.

[159] B. De'Nève and M. Shanahan. "Water absorption by an epoxy resin and its effect on the mechanical properties and infra-red spectra". In: *Polymer* 34.24 (1993), pp. 5099–5105.

[160] L. F. Da Silva and R. Adams. "Measurement of the mechanical properties of structural adhesives in tension and shear over a wide range of temperatures". In: *Journal of Adhesion Science and Technology* 19.2 (2005), pp. 109–141.

[161] ISO 1920-3. *Testing of concrete – Part 3: Making and curing test specimens*. Technical Committee: ISO/TC 71/SC 1, International Organization for Standardization. Geneva, Switzerland, 2004.

[162] ISO 1920-4. *Testing of concrete – Part 4: Strength of hardened concrete*. Technical Committee: ISO/TC 71/SC 1, International Organization for Standardization. Geneva, Switzerland, 2005.

[163] ISO 1920-10. *Testing of concrete – Part 10: Determination of static modulus of elasticity in compression*. Technical Committee: ISO/TC 71/SC 1, International Organization for Standardization. Geneva, Switzerland, 2005.

[164] ISO 1920-9. *Testing of concrete – Part 9: Determination of creep of concrete cylinders in compression*. Technical Committee: ISO/TC 71/SC 1, International Organization for Standardization. Geneva, Switzerland, 2005.

[165] ISO 527-5. *Plastics - Determination of tensile properties - Part 5: Test conditions for unidirectional fibre-reinforced plastic composites*. International Organization for Standardization. Geneva, Switzerland, 1997.

[166] ISO 1920-2. *Testing of concrete – Part 3: Properties of fresh concrete*. Technical Committee: ISO/TC 71/SC 1, International Organization for Standardization. Geneva, Switzerland, 2010.

[167] G. Monti, M. Renzelli, and P. Luciani. "FRP adhesion in uncracked and cracked concrete zones". In: *Fibre-Reinforced Polymer Reinforcement for Concrete Structures: (In 2 Volumes)*. World Scientific, 2003, pp. 183–192.

[168] X. Lu, J. Teng, L. Ye, and J. Jiang. "Bond–slip models for FRP sheets/plates bonded to concrete". In: *Engineering structures* 27.6 (2005), pp. 920–937.

[169] A. Bilotta, C. Faella, E. Martinelli, and E. Nigro. "Indirect identification method of bilinear interface laws for FRP bonded on a concrete substrate". In: *Journal of Composites for Construction* 16.2 (2011), pp. 171–184.

[170] H. Ko, S. Matthys, A. Palmieri, and Y. Sato. "Development of a simplified bond stress–slip model for bonded FRP–concrete interfaces". In: *Construction and Building Materials* 68 (2014), pp. 142–157.

[171] L. De Lorenzis, B. Miller, and A. Nanni. "Bond of fiber-reinforced polymer laminates to concrete". In: *ACI Materials Journal* 98 (2001), pp. 256–264.

[172] R. Capozucca. "On the strengthening of RC beams with near surface mounted GFRP rods". In: *Composite Structures* 117 (2014), pp. 143–155.

[173] J. Pan and Y.-F. Wu. "Analytical modeling of bond behavior between FRP plate and concrete". In: *Composites Part B: Engineering* 61 (2014), pp. 17–25.